

The Influence of Morphology on Barrier Island Recovery Following Storms: Insights
from the Virginia Barrier Islands, Mid-Atlantic Bight, USA

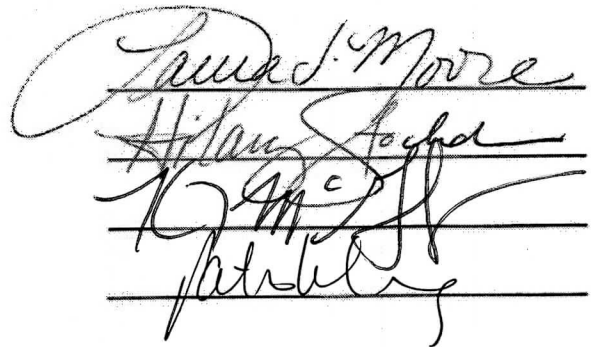
Dana Jean Oster
Mercer Island, Washington

B.S., Bates College, 2009

A Thesis Presented to the Graduate Faculty
Of the University of Virginia in Candidacy for the Degree of
Master of Science

Department of Environmental Sciences

University of Virginia
May, 2012


The image shows four handwritten signatures, each written on a horizontal line. From top to bottom, the signatures are: 1. A cursive signature that appears to read 'Laura J. Moore'. 2. A cursive signature that appears to read 'Hilary Stach'. 3. A cursive signature that appears to read 'G. M. Stach'. 4. A cursive signature that appears to read 'Patrick'. The lines are evenly spaced and extend across the width of the signatures.

ABSTRACT

Barrier island storm response and recovery patterns vary alongshore because they are a direct reflection of island morphology, which is also spatially variable. To provide a measure of barrier island recovery, we define recovery as the change in overwash probability between two points in time—the first immediately following Hurricane Bonnie in 1998 and the second 2 years following a subsequent storm event in 2005. We then explore how barrier island recovery varies with morphologic characteristics along two islands (Metompkin and Smith Island), both located on the U.S. mid-Atlantic coast within the Virginia Coast Reserve (VCR).

Results of continuous wavelet transforms show both recovery and morphologic characteristics all vary alongshore at spatial scales of ~1-6 km. Wavelet coherence analysis indicate that where beaches are relatively narrow and the shoreline is eroding, (e.g., northern Smith Island and southern and northern Metompkin Island) areas of greatest recovery are influenced primarily by dune recovery processes and patterns. The initial dune structure (i.e. continuous, discontinuous, or overwash terraces) and overwash distribution control dune recovery patterns and thus recovery alongshore. Along areas where the beach is wide and dissipative and the shoreline is accreting (e.g., southern Smith Island, and the middle of Metompkin Island), recovery is closely linked with foreshore recovery processes. Narrow intermediate beaches are typically more susceptible to overwash events which in part may be contributing to the significance of dune recovery processes to recovery, while along wider dissipative beaches storm impact is primarily confined to the foreshore, which is also the zone most critical to recovery.

ACKNOWLEDGEMENTS

First, I would like to thank my advisor, Laura Moore, for her critical support and guidance throughout the formation and development of this work. The invaluable feedback from my committee members, Pat Wiberg, Karen McGlathery, and Hilary Stockdon, truly elevated this project. Without the generosity of the USGS Coastal Change Hazards group, particularly Kara Doran, Hilary Stockdon (again!), and Abby Sallenger, I would have had no lidar data, no Matlab code, and no clue what to do. Additionally I would like to thank Todd Scanlon, Brad Murray, and Matt O'Connell for sharing their wavelet expertise. I am also grateful to Dave Carr for taking the time to work with me through spatial autocorrelation and SAS code. I would also like to acknowledge John Porter for his technical support and providing me with a digital tour of Smith Island which I could not visit in person.

I am very grateful to my wonderful labmates, Cat Wolner, Amy Grady, and Owen Brenner for years of feedback, editing, and moral support. Finally I would like to thank my friends and family for their encouragement and editing.

Continuous wavelet transform and wavelet coherence software were provided by © Aslak Grinsted 2002-2004 (<http://www.pol.ac.uk/home/research/wavelets/>). This research was supported by the U.S. Department of Energy's Office of Science (BER) through the Coastal Center of the National Institute for Climatic Change Research at Tulane University. Additional support provided by Virginia Coast Reserve Long-Term Ecological Research (VCR LTER), and the Department of Environmental Sciences at the University of Virginia.

TABLE OF CONTENTS

Abstract.....	ii
Acknowledgements.....	iii
Table of contents.....	iv
List of figures.....	v
1. Introduction.....	1
Background.....	1
Study site	6
2. Methods	11
Extracting morphologic characteristics.....	11
Quantifying recovery	13
Wavelet analysis	15
3. Results and interpretations	19
Metompkin Island.....	19
Recovery	19
Morphologic characteristics	22
Coherence and interpretations	25
Smith Island.....	31
Recovery	31
Morphologic characteristics	34
Coherence and interpretations	37
4. Discussion.....	42
5. Conclusions.....	49
References.....	52
Appendix 1: Methods.....	57
1.1 Feature extraction procedures	57
1.2 Overwash probabilities	61
1.3 Wavelet analysis parameters.....	62
1.4 Surf similarity index	63

Appendix 2: Supplementary data.....	64
2.1 VCR recovery	64
2.2 Metompkin Island.....	66
Morphologic summary tables	66
Additional signals	67
Continuous wavelet transforms.....	68
Wavelet coherence analyses	70
2.3 Smith Island.....	85
Morphologic summary tables	85
Additional signals	86
Continuous wavelet transforms.....	87
Wavelet coherence analyses	89

LIST OF FIGURES AND TABLES

Figure 1.1	Storm impact regimes.....	5
Figure 1.2	Foredune geometry and wave runup parameters.....	5
Figure 1.3	Map of the Eastern Shore of Virginia.....	8
Figure 1.4	Orthorectified and oblique images of Smith Island.....	9
Figure 1.5	Orthorectified and oblique images of Metompkin Island.....	10
Figure 2.1	Cross-section of lidar data and morphologic feature selection.....	12
Figure 3.1	Recovery on Metompkin Island	21
Figure 3.2	Metompkin Island spatial series of 1998 and 2005 morphology.....	23
Figure 3.3	Metompkin Island spatial series of change in morphology	24
Figure 3.4	Wavelet coherence analysis for Metompkin Island.....	30
Figure 3.5	Recovery on Smith Island.....	33
Figure 3.6	Smith Island spatial series of 1998 and 2005 morphology.....	35
Figure 3.7	Smith Island spatial series of change in morphology	36
Figure 3.8	Wavelet coherence analysis for Smith Island.....	41
Figure 5.1	Summary of dune and foreshore characteristics important to recovery	51
Table 3.1	Coherence of recovery and morphologic signals on Metompkin Island.....	29
Table 3.2	Coherence of recovery and morphologic signals on Smith Island.....	40

1. INTRODUCTION

Background

Acting as the mainland's first line of defense from storms, barrier islands are dynamic landscapes, highly sensitive to fluctuations in environmental conditions (FitzGerald et al., 2008). Storm severity is directly reflected in the morphologic response of barrier systems; at the same time, alongshore topographic variations in the landscape promote an array of morphologic responses to storm events (Stockdon et al., 2007). The effects of accelerated sea level rise rates (Church and White, 2006; IPCC, 2007) and potential increases in storm intensity (Webster et al., 2005; Emanuel, 2005; Knutson et al., 2010) could amplify the frequency of storms capable of causing extreme morphological change.

During storm conditions, elevated wave and water levels combine allowing waves to overtop dunes and deposit sediment on the island interior in a process known as overwash (e.g., Leatherman et al., 1977; Leatherman and Zaremba, 1987; Morton and Sallenger, 2003; Donnelly et al., 2006). This process plays an essential role in the long-term evolution of barrier islands as they respond to rising sea level (e.g., Hayden et al., 1980; Morton and Sallenger, 2003). Given sufficient sand supply, sand transferred from the foreshore to the backshore by overwash allows islands to migrate (Moore et al., 2010) and therefore maintain their elevation above sea level. Under conditions of insufficient sediment supply or if sea level rises too quickly, barrier islands may become submerged or disintegrate entirely (Moore et al., 2010).

The likelihood that overwash will occur during a storm is directly related to interactions between beachface morphology and swash-zone dynamics (Sallenger, 2000). During storms, the seaward-most dune often limits the landward extent of wave impacts. However, if maximum wave run-up exceeds the elevation of the dune, overwash may occur. The ‘Storm Impact Scale’ presented by Sallenger (2000) classifies barrier vulnerability to individual storm events based on the relationship between the elevation of the foredune crest and toe relative to the elevation of maximum wave runup (Figure 1.1). Here, “vulnerability” is defined as the probability that beach profile response to a storm will fall into one of four categories under maximum runup (R_{high}) conditions: swash, collision, overwash, and inundation (Sallenger, 2000).

In previous studies, the Storm Impact Scale has been used as a general tool for making alongshore predictions of storm impact regimes from pre-storm lidar data, which have then been compared with observed impact regimes from post-storm lidar data (Judge et al., 2003; Stockdon et al., 2007). The accuracy with which a storm impact regime can be predicted—although variable for individual storms, depending upon storm characteristics (e.g., duration)—is highest for the overwash regime (Judge et al., 2003; Stockdon et al., 2007). For example, Stockdon et al. (2007) were able to predict overwash occurrence along a series of transects in the Outer Banks of North Carolina during Hurricane Bonnie (1998) with an accuracy of 84.2% (Stockdon et al., 2007). Here, we will use the Storm Impact Scale—and specifically overwash vulnerability—to measure the change in overwash vulnerability between two lidar surveys. The difference in

vulnerability will serve as a proxy for beachface recovery, and therefore barrier island recovery following storms.

Following a storm event, barrier island recovery minimizes the effects of subsequent storms. Recovery processes include restoration of beach width, dune height, shoreline position and beach/dune volume to pre-storm conditions, and re-colonization of dune vegetation; however, not all recovery processes occur in concert with one another (Morton et al., 1994; Houser and Hamilton, 2009). Complete barrier island recovery following a storm can take more than a decade (Zhang et al., 2002) or only a few years (Morton et al., 1994), depending upon environmental conditions and morphology (e.g., Houser and Hamilton, 2009; Priestas and Fagherazzi, 2010) or may not occur at all (Morton et al., 1994; Houser and Hamilton, 2009). Recovery patterns and processes, although strongly influenced by island initial storm response, also depend on storm intensity, storm sequencing (the order of occurrence and frequency of storms having different intensities) and antecedent conditions.

Houser and Hamilton (2009) demonstrate the importance of antecedent conditions by identifying localized coherence between the volume of beachface recovered and post storm island width, nearshore bathymetry, initial dune structure, post-storm vegetation presence, and overwash occurrence in the Florida Panhandle. They found that areas of greatest foreshore volume loss during storms typically coincided with areas that regained foreshore volume, and that areas with the least amount of overwash penetration occurred where an island was widest. Furthermore, they observed that alongshore recovery patterns varied widely within a single barrier island (Houser and Hamilton, 2009).

We hypothesize that the spatially variable rate and degree of local barrier island recovery is likely coherent with the alongshore variability of local morphologic characteristics. By assessing the scaling properties and spatial relationships between morphologic characteristics and post-storm barrier recovery patterns, we seek to better understand why some locations and/or barrier islands recover more than others.

To evaluate our hypothesis that barrier island recovery and morphologic characteristics covary at various spatial scales alongshore and to develop a better understanding of the mechanisms that are likely to be important in determining barrier island recovery, we explore two representative islands within the undeveloped Virginia Coast Reserve (VCR) located within the Mid-Atlantic Bight of the U.S. East Coast. Using lidar data and wavelet analysis we 1) quantify barrier island recovery alongshore, 2) investigate alongshore variations in barrier island recovery including how this measure varies in space and in scale, 3) investigate alongshore variations in morphological characteristics including how they vary in space and in scale, and 4) examine the spatial covariance between barrier island recovery and morphological characteristics.

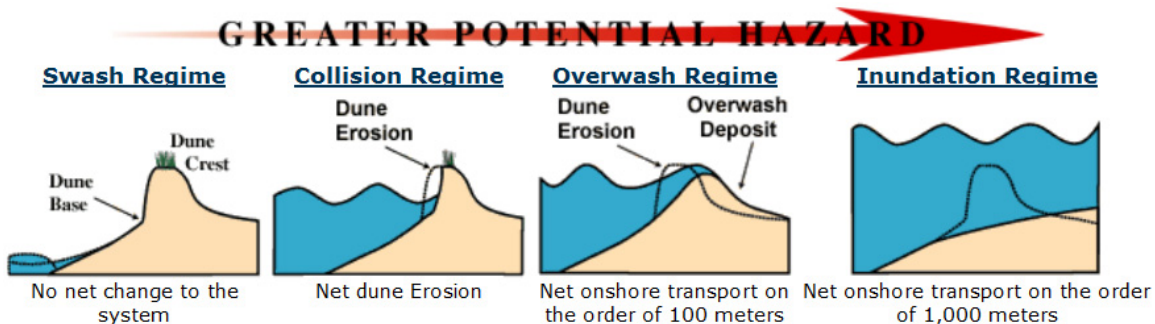


Figure 1.1: The four storm impact regimes. The net sediment change before (black line) and after (beige) storm event and maximum runoff extent on the shoreface is shown. From USGS Coastal Change Hazards, 2010 (<http://coastal.er.usgs.gov/hurricane/impact-scale/index.php>).

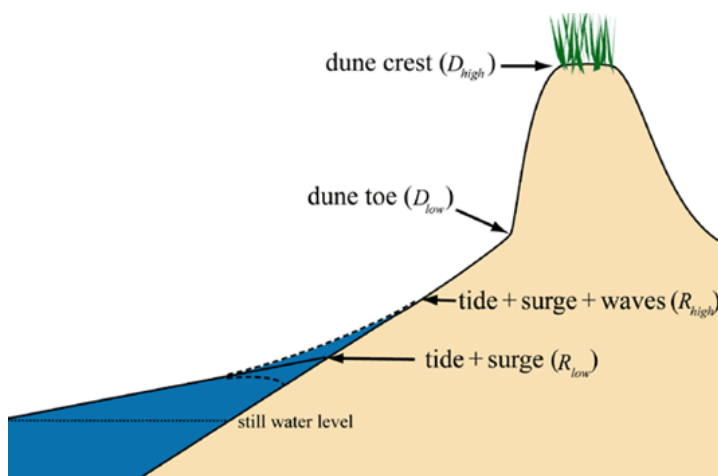


Figure 1.2: Geometric relationships between foredune geometry and wave runoff: R_{high} , R_{low} , D_{high} , and D_{low} . The dashed lines represent the swash excursion above and below wave setup (solid line). From USGS Coastal Change Hazards, 2010 (<http://coastal.er.usgs.gov/hurricanes/impact-scale/index.php>).

Study site

The 12 islands of the Virginia Coast Reserve (VCR) comprise a mixed-energy, tide-dominated barrier island system, with a tide range of 1.3 m and an average annual wave height of 0.55 m (Fenster and Dolan, 1996). The VCR barrier islands, which are south of Assateague Island on the Delmarva (DELaware MARYland VirginiA) Peninsula, are described as sediment-starved, short, discontinuous barriers predominantly influenced by tidal currents rather than alongshore drift (Oertel and Overman, 2004). The VCR barriers exhibit distinctive shoreline change patterns that have been used to divide them into three coastal compartments: the northern group (linear islands with retreat occurring parallel to shore), the middle group (drumstick-shaped islands with clockwise and counterclockwise rotational shoreline migration), and the southern group (long and short islands with varied amounts of shoreline retreat occurring non-parallel to shore; Figure 1.3) (*e.g.*, Dolan et al., 1979; Rice and Leatherman, 1983; Kochel et al., 1985; Fenster and Dolan, 1996; Hobbs et al., 2010). We focus on one representative island from each of the southern and northern coastal groups (Figure 1.3).

Smith Island, which is ~10 km long and represents the southern group, is characterized by non-parallel shoreline retreat (the northern half is migrating landward faster than the southern half) (Rice and Leatherman, 1983) and a shoreline orientation that generally trends northeast-southwest. There is a vegetative and morphologic divide between the southern third and northern two thirds of Smith Island. The northern section of Smith Island is essentially an overwash terrace ~2 m above mean high water (MHW), subject to frequent overwash/breaching and backed by a low backbarrier marsh.

Vegetation present on the overwash terrace is limited and exposed peat outcrops are visible in the swash zone (Bachmann et al., 2002). Southern Smith Island is distinctly different from the thin overwash terraces in the north in both the foreshore and backbarrier, where a taller continuous dune ridge is backed by a wide maritime forest. The most notable features in the backbarrier are the east-west trending oblique beach ridges formed by progradation of the southwest shoreline (Figure 1.4; Oertel and Overman, 2004). The topographic relief is higher than in the north and more continuous, averaging ~3 m above MHW on the foredune ridge.

In contrast to Smith Island, ~10-km-long Metompkin Island (representative of the northern group) exhibits rapid parallel shoreline retreat (Rice and Leatherman, 1983). The northern and southern halves of Metompkin Island, separated by an offset in shoreline position, differ in their shoreline change patterns and morphologic characteristics (Byrnes, 1988). For example, Southern Metompkin Island is narrow and backed by patchy shrub thickets and backbarrier marsh leading into a small lagoon. The discontinuous hummocky dunes (average elevation ~2.5 m above MHW) allow overwash fans and channels to penetrate the low areas between dunes. Northern Metompkin Island, on the other hand, is much like northern Smith Island characterized by continuous overwash terraces (~2 m above MHW) and backed by a backbarrier marsh that connects to the mainland (Figure 1.5).

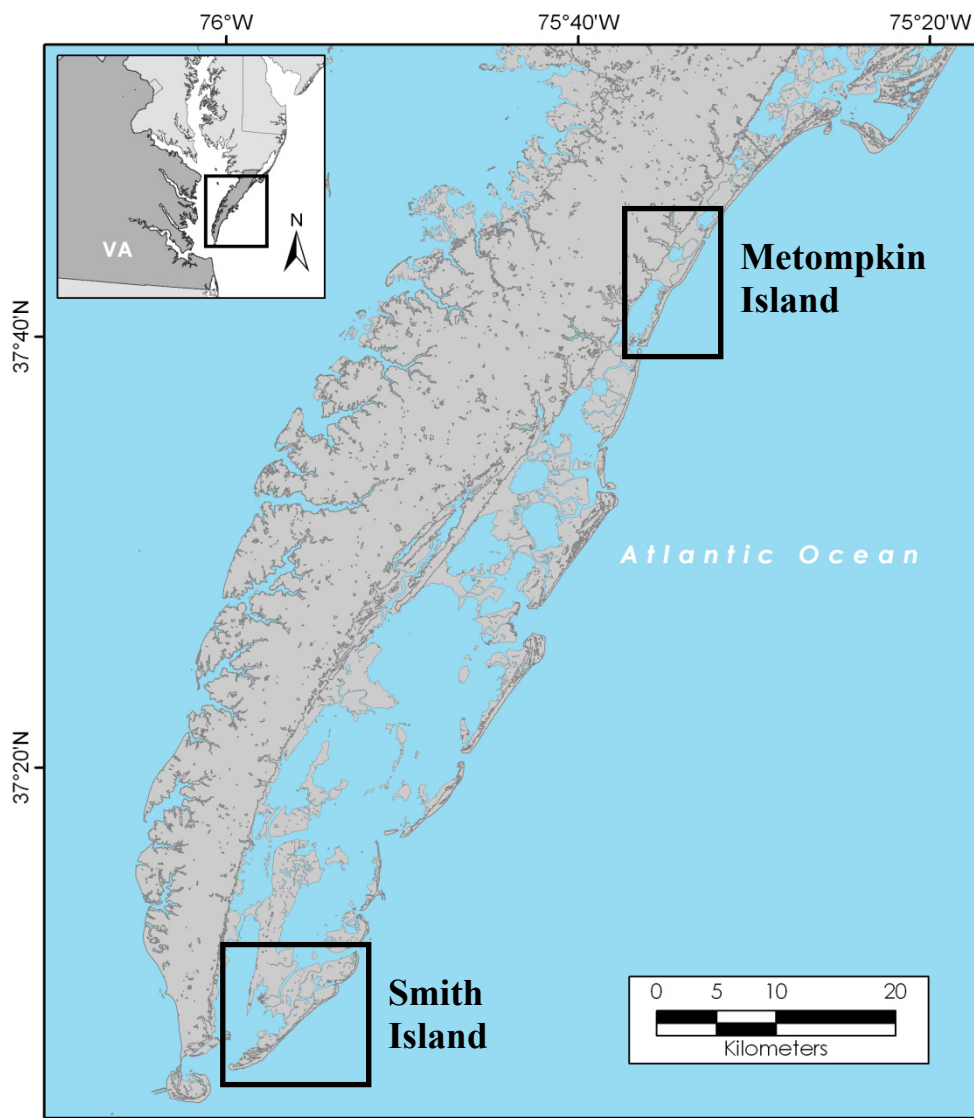


Figure 1.3: Map of the Eastern Shore of Virginia showing the location of the Virginia Coast Reserve (VCR) on the southern tip of the Delmarva Peninsula. The barrier island chain is visible along the Atlantic side of the VCR. Map courtesy of L. W. Cole, unpublished, 2010.

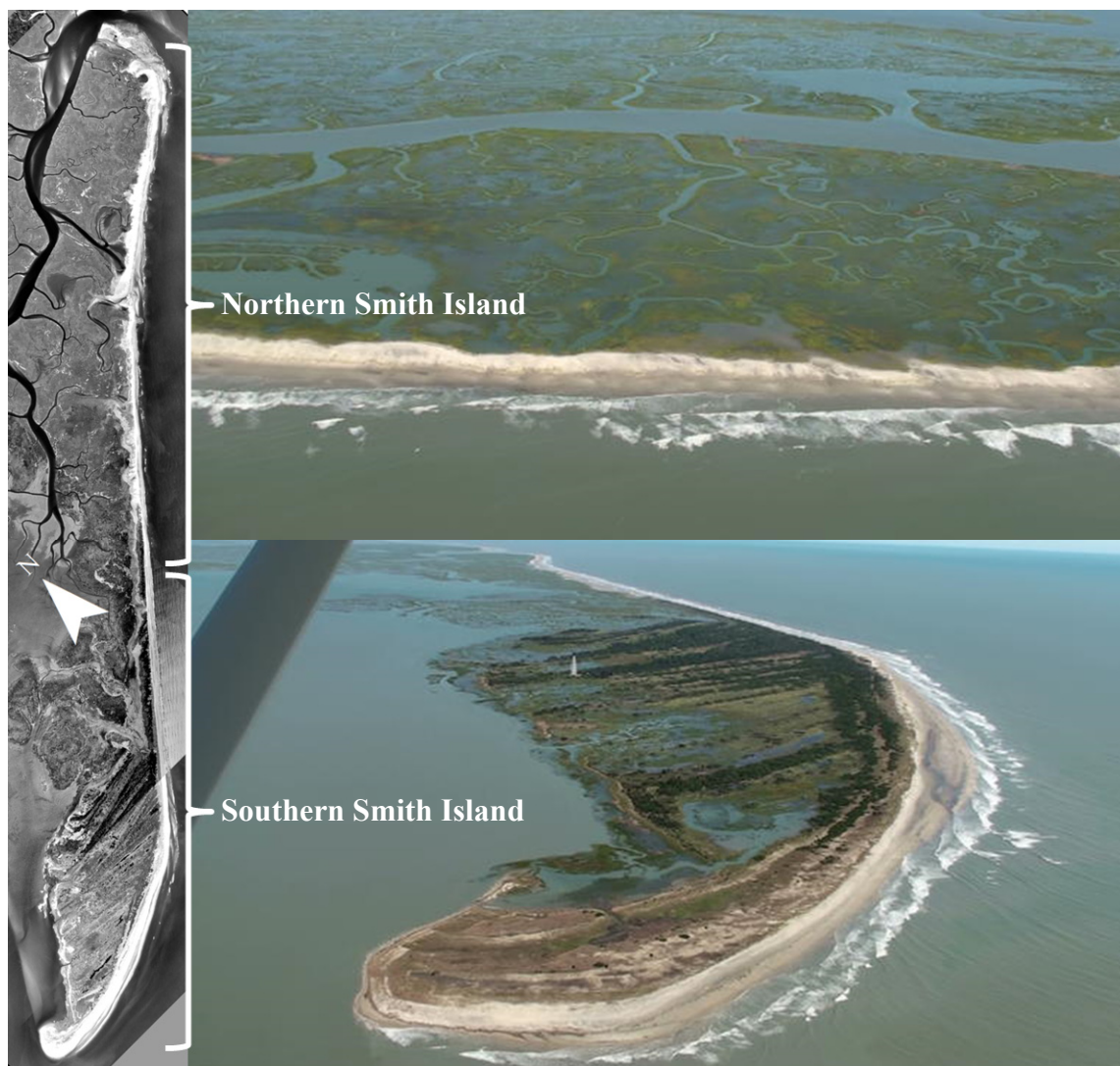


Figure 1.4: Orthorectified image of Smith Island in 2002. Inset oblique aerial images collected following Hurricane Irene in 2011 (photo credit: John Porter, 2011).



Figure 1.5: Orthorectified image of Metompkin Island in 2002. Inset oblique aerial images collected following Hurricane Irene in 2011 (photo credit: John Porter, 2011).

2. METHODS

In order to quantify alongshore barrier island recovery, alongshore morphologic features (i.e. dune height, beach width, slope) used to determine overwash probability, were extracted from airborne light detection and ranging (lidar) data. Upon extraction, the morphologic characteristics from 1998 are used as the initial conditions and the differences in overwash vulnerability to a hypothetical storm having characteristics of Hurricane Bonnie in 1998 and 2005 are used as a measure of actual recovery that occurred between 1998 and 2005. Wavelet analysis was used to evaluate alongshore variations in morphologic characteristics, storm impacts, and barrier island recovery.

Extracting morphologic characteristics

Lidar data returns spatially dense elevation data with a vertical accuracy of approximately 15 cm (Sallenger et al., 2003). We selected post-storm lidar data, collected in 1998, (immediately following Hurricane Bonnie) and calm-weather lidar data, collected in 2005, (two years following a major storm event) for the purpose of quantifying morphologic recovery following a storm event. We post-processed the scattered (x,y,z) points using methods and algorithms developed by the USGS Coastal Change Hazards group (e.g., Stockdon et al., 2007; Stockdon et al., 2009) to grid the data and extract smoothed cross-shore profiles spaced 10 m apart alongshore. From the smoothed profiles we extracted the position and elevation (referenced to the NAVD88 datum) of the most seaward dune crest (D_{high}) and toe (D_{low}), and horizontal shoreline position (MHW) (Appendix 1.1).

Through automated selection, we extracted D_{high} as the most seaward inflection point between a landward and seaward facing slope (Stockdon et al., 2009). Where dunes were present, D_{high} coincides with the top of the dune and where dunes were absent D_{high} was selected to coincide with the highest point on the berm. For the latter profiles, D_{low} does not exist. When a dune crest was present, we selected D_{low} as the maximum point of slope change seaward of D_{high} (Stockdon et al., 2009). The position of MHW was selected as 0.34 m above mean sea level, specified as the MHW datum for the state of Virginia (Weber et al., 2005). Following automated selection, the extracted features were edited in ArcGIS. The estimated vertical root mean squared (rms) accuracy based on the repeatability of these techniques is 37 cm for D_{high} and D_{low} (Elko et al., 2002; Stockdon et al., 2007). We calculated beach width as the horizontal distance between D_{high} and MHW rather than D_{low} and MHW due to the better consistency of D_{high} selection. The foreshore slope is defined as the slope between D_{low} and MHW (Figure 2.1).

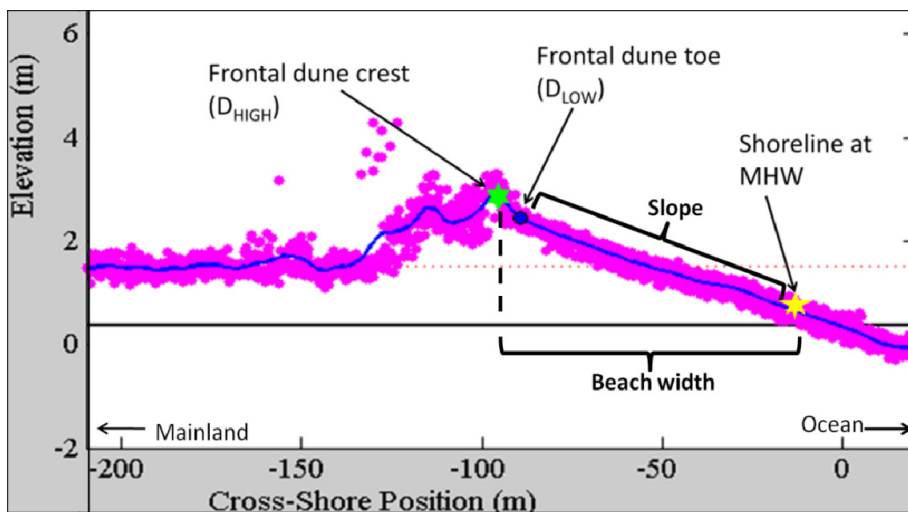


Figure 2.1: Sample cross-section showing raw lidar data (pink dots) and smoothed profile (blue line). Also shown are D_{high} (green star), D_{low} (blue dot), and the shoreline at 0.34 m (yellow star). Beach width is defined as the horizontal distance between D_{high} and shoreline position while foreshore slope is the slope between D_{low} and shoreline position. The dashed red line marks 1.5 m as the threshold for a dune/berm profile.

Quantifying recovery

Defined as the change in overwash probability from 1998 to 2005, recovery was quantified alongshore following the extraction of alongshore morphologic characteristics for Smith, and Metompkin Islands in 1998 and 2005. We explored the alongshore response and recovery of the islands to a storm (similar to Hurricane Bonnie) using overwash probability as defined by the Storm Impact Scale (Sallenger, 2000; Stockdon et al., 2007; Stockdon et al., 2009) We use the term ‘recovery’ as a measure of change in overwash probability between 1998 and 2005. Recovery (R), therefore, is represented by the following (Equation 1):

$$R = 1998 \text{ probability of overwash (\%)} - 2005 \text{ probability of overwash (\%)} \quad (1)$$

A positive value for recovery indicates a decrease in the probability of overwash in 2005 relative to 1998, and therefore represents actual barrier island recovery between the two points in time.

Vulnerability, or the probability that a given profile will experience overwash, occurs when maximum wave runup (R_{high}) levels exceed D_{high} (Sallenger, 2000). We choose to focus on vulnerability to overwash rather than vulnerability to swash, collision, or inundation regimes because: 1) of the processes represented by the four regimes, overwash processes are most important to barrier island dynamics, and 2) of the two regimes causing the most dramatic morphologic change, overwash occurs more frequently than inundation.

Following the methods of Sallenger (2000) and Stockdon et al., (2006), we quantify overwash vulnerability for each profile by defining the maximum elevation of

wave runup (R_{high}) based on storm parameters and beach slope, and then comparing R_{high} to values for D_{high} and D_{low} to determine the probability that overwash will occur. The maximum elevation of wave runup on the foreshore, R_{high} , is defined as the super-elevation of the 2% exceedence runup threshold (R_2), where only 2% of all wave runup excursions during the storm exceed the R_2 elevation, combined with the elevation of the astronomical tide and storm surge (η_{mean} , storm tide) (Equation 2) (Sallenger, 2000):

$$R_{high} = R_2 + \eta_{mean}. \quad (2)$$

Stockdon and others (2006) modified the initial 2% runup exceedence (R_2) equation from Holman (1986), to yield the following relationship (Equation 3):

$$R_2 = 1.1 \left(0.35\beta_f(H_0L_0)^{1/2} + \frac{[H_0L_0(0.563\beta_f^2+0.004)]^{1/2}}{2} \right) \quad (3)$$

Where H_0 is the deep-water significant wave height, L_0 is the deep-water wave length ($L_0=gT^2/2\pi$, where T = wave period), and β_f is the beach slope (Stockdon et al., 2006). We obtained values for H_0 (3.7 m) and T (7 s) during the peak significant wave height of Hurricane Bonnie recorded from the National Buoy Data Center, Station 44009, off the coast of Delaware Bay (28 m water depth) and a value for η_{mean} (1.1 m) from the Wachapreague tide gauge (Station Id: 8631044).

To obtain overwash probabilities at 100-m alongshore increments, we used a normal cumulative distribution function which created one overwash probability percentage for each 100 m segment based on the distribution of elevation values of D_{high} and R_{high} in each section (Appendix 1.2). We selected increments of 100 m to capture smaller spatial scale variations alongshore.

Between 1998 and 2005 a series of tropical storms and hurricanes affected the VCR, most notably, Hurricanes Dennis and Floyd in 1999, and Hurricane Isabel in September 2003. All three storms produced strong winds and beach erosion from heightened wave attack. A temporary lull in severe storm activity following Hurricane Isabel allowed for two full years of barrier island recovery before the 2005 lidar scan was collected, making the 1998 and 2005 lidar data sets an ideal pairing for assessment of barrier recovery.

Wavelet analysis

To assess alongshore variability and covariance of recovery and island morphology, we use Wavelet analysis, a statistical technique that has recently been applied to the study of spatial signals from coastal environments (e.g., Short and Trembanis, 2004; Li et al., 2005; Ruessink et al., 2006; Houser and Mathew, 2011; Lazarus et al., in press) to localize where in space variations of different spatial scales are significant. Wavelet analysis decomposes a one-dimensional signal into a two-dimensional plot of specific scales at which a signal varies spatially along the signal (also referred to as space and scale, where space signifies a localized section of the signal and scale is the spatial scale at which the signal varies). Areas of high variability are signified by high wavelet power. Wavelet power is a function of the amplitude of variability, meaning the greater the amount of change relative to the rest of the signal, the higher the power is. This method provides the ability to localize dominant modes of variability within a signal, which is not possible using a Fourier transform (Kumar and Foufoula-

Georgiou, 1997). Wavelets are ideally suited for assessing alongshore variations in spatial signals having little or no common periodicity.

Wavelet analysis can be conducted using a variety of waveforms, or shapes to localize variations within a signal. Depending on the number of oscillations and the width of the waveform, results can emphasize greater accuracy in scale versus greater space localization. We valued localization of alongshore variations above precise scale resolution leading us to use ‘Paul’ as the waveform for this study (De Moortel et al., 2004). The smooth shape of a Paul wavelet maintains precise scale resolution while the narrower width promotes accurate localization of alongshore characteristics (see De Moortel et al., 2004 and Torrence and Compo, 1998 for more discussion of wavelet parameterization and Appendix 1.3). To minimize edge effects, we employed the ‘zero padding’ technique, adding zeros to both ends of the data set to increase signal length, thereby decreasing the amplitude of variations near the edge (e.g., Meyers et al., 1993; Torrence and Compo, 1998; De Moortel et al., 2004; Grinsted et al., 2004).

To characterize the dominant scales of variance and where they occur alongshore, we used a continuous wavelet transform (CWT) to produce local wavelet power spectrums for recovery, D_{high} , beach width, and slope in 1998 and 2005. Additionally, because recovery is a function of change in vulnerability, we also assessed the alongshore variability of the following changes in morphology (2005-1998) using CWT analysis: change in D_{high} elevation (ΔD_{high}^z), change in D_{high} position (ΔD_{high}^x), change in beach width ($\Delta \text{beachwidth}$), change in slope (Δslope), and change in shoreline position ($\Delta \text{shoreline}$). All alongshore signals were input into CWT analysis as vectors where each

row (and value) represented a 100 m section of beach. Both islands are similar in length, thus, alongshore signals ranged from 10.4 to 10.6 km. We disregard high wavelet power at scales of 100-400 m because they are associated with too few data points and are of less interest with respect to alongshore recovery patterns.

We used wavelet coherence (WTC) analysis to assess how two signals covary alongshore. This method identifies where in space and scale two signals have common power (and therefore high coherence) and therefore are potentially related (e.g., Grinsted et al., 2004; Maraun and Kurths, 2004). Because there is potential for coherence to be high where only one signal has high power, Monte Carlo simulations were used to distinguish where the coherence was statistically significant (95% confidence interval) in both signals relative to red noise (random signals). We calculated the statistical significance using methods described in Torrence and Compo (1998). Values of 1 represent a linear relationship between the signals while 0 signifies no correlation. Following Torrence and Compo (1998), we examined the phase relationship between signals where coherency was significant at specific scales in space. The phase difference portrays the spatial lead or lag between the two signals (Torrence and Compo, 1998).

When two signals are coherent, the scale at which they covary may be useful in inferring the processes by which the two signals are linked. For this reason, we investigated the coherence between recovery and the individual morphologic signals extracted from 1998 and 2005, as well as the coherence between other morphologies relative to D_{high} and change in D_{high} . Additionally, we assessed coherence between

recovery and all of the changes in morphological characteristics mentioned above (i.e.,

ΔD_{high}^z , ΔD_{high}^x , $\Delta \text{beachwidth}$, Δslope and $\Delta \text{shoreline}$).

3. RESULTS AND INTERPRETATIONS

Here we present and interpret results from continuous wavelet transforms (CWT) and wavelet coherence analyses (WTC) of alongshore signals on Smith and Metompkin Island. For each island, analyses are discussed in terms of alongshore recovery patterns, morphologic characteristics, and coherence between recovery and morphology.

Metompkin Island

Because morphologic characteristics and wavelet coherence analyses exhibited different trends along the island, we consider Metompkin Island in three sections: southern (0-4,000 m), middle (4,000-7,000 m), and northern (7,000-10,400 m).

Recovery

Alongshore recovery is high as a result of high overwash probability along the majority of Metompkin Island in 1998 which decreased along the island by 2005 (where a positive recovery value reflects a decrease in overwash probability between 1998 and 2005; Figure 3.1c). The only exception occurs along the mid-island shoreline offset, where overwash vulnerability to a storm having Hurricane Bonnie characteristics remained high in 2005. The lack of recovery along the offset is reflected in the recovery signal between 6,000-7,000 m alongshore, where recovery is near zero (Figure 3.1b).

There is a lack of alongshore variability in overwash probability in 1998—particularly along the middle and northern sections—suggesting Metompkin Island was widely overwashed during Hurricane Bonnie. We interpret the lack of variability in 1998

overwash probability as wide-spread overwash because the probability was 100% along most of the middle and northern sections indicating that wave runup exceeded 1998 D_{high} elevation along most of the region

The 1998 D_{high} elevations were collected a week following Hurricane Bonnie and considering how low the dune crests were, 1998 overwash probability is likely a reflection of the actual storm impact. Overwash probability in 2005 was substantially more variable alongshore, indicating alongshore variability in recovery patterns on Metompkin Island (Figure 3.1d).

These alongshore variations in recovery are apparent in CWT analysis, where higher power (brighter red in Figure 3.1a) signifies greater variability. CWT reveals that recovery on Metompkin Island has the highest wavelet power (i.e. varies the most) along the middle and northern sections of the island (4,000-10,000 m alongshore position) at scales of ~1,600-6,400 m (although much of the high power is not within the 95% confidence interval). The high variability along the middle and northern sections of Metompkin Island is largely a function of the highly variable 2005 overwash probability, because 1998 overwash probability was relatively constant alongshore.

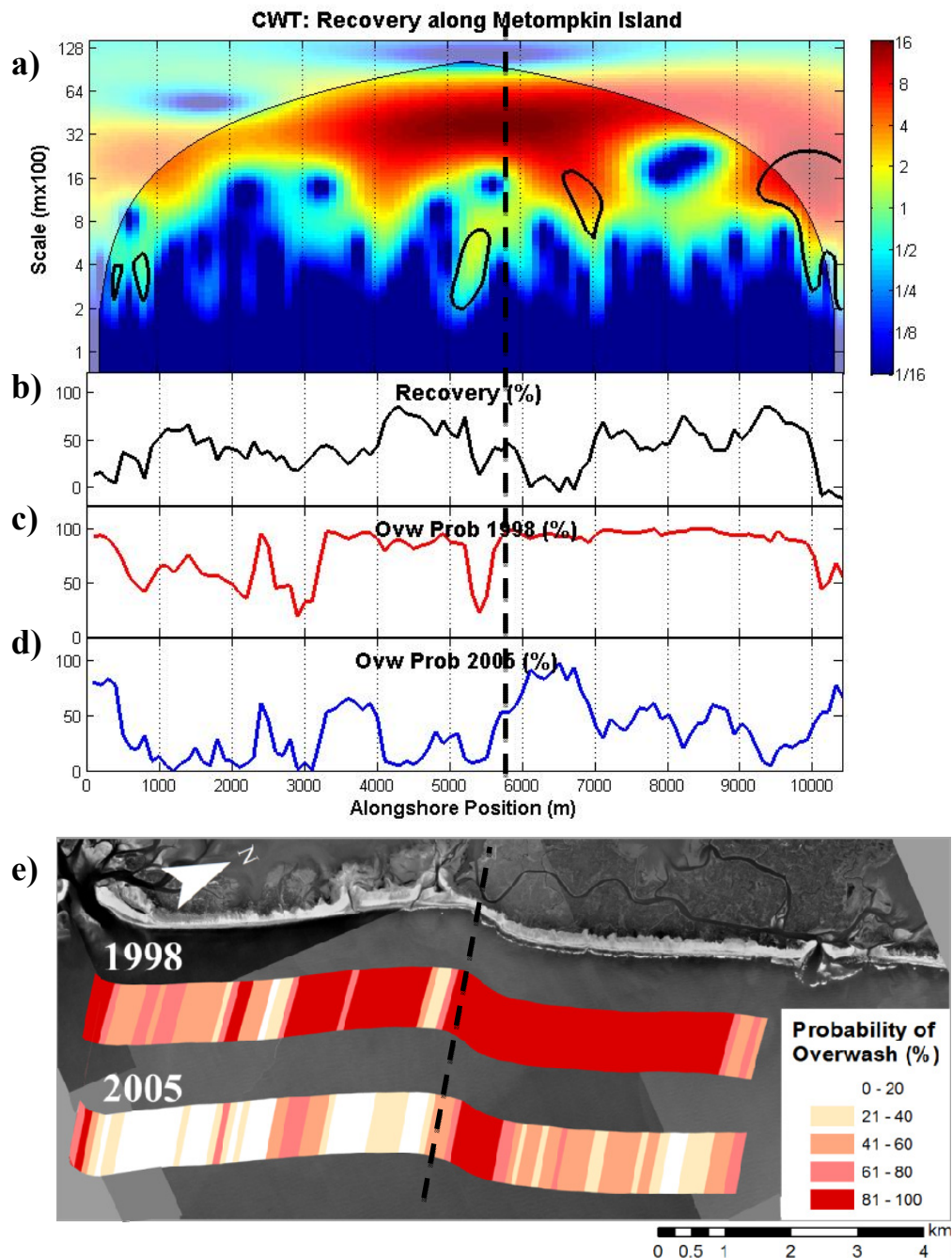


Figure 3.1: (a) Continuous wavelet transform of spatial signal of recovery showing local wavelet power spectrum as a function of alongshore position, where power is represented by the color bar and the 95% confidence interval inside the thick-black contours. The Cone of Influence (COI) is represented by the transparent regions. Alongshore signals of (b) recovery, (c) 1998 overshaw probability, and (d) 2005 overshaw probability. (e) Rotated orthorectified image of Metompkin Island in 2002 with 1998 and 2005 overshaw probability during a storm with Hurricane Bonnie characteristics superimposed. Dashed black line signifies mid-island offset.

Morphologic Characteristics

1998 D_{high} elevations (D_{high}^z) were slightly higher on average and more discontinuous along southern Metompkin Island (1.6 m average) compared to northern Metompkin Island (1.5 m average; Appendix 2.2). 2005 D_{high}^z average elevation along southern Metompkin Island increased to 2.5 m and D_{high}^z remained discontinuous alongshore, while 2005 D_{high}^z along northern Metompkin Island averaged 2.0 m (Figure 3.2a&b). The change in elevation between 1998 and 2005 D_{high}^z (ΔD_{high}^z) was positive along the entire island, meaning D_{high} elevation increased from 1998 to 2005 (Figure 3.3a). Beach width and slope were variable at smaller spatial scales in 1998 (Figure 3.2c&d) and at larger spatial scales in 2005 (Figure 3.2e&f).

Based on the Surf Similarity Index (Battles, 1974; Short and Wright 1983), the southern tip and middle sections of Metompkin Island were dissipative in 1998 and 2005 (average $\zeta = 0.14$ and $\zeta = 0.16$, respectively), while the north section of the island was primarily intermediate in both years (average $\zeta = 0.29$ and $\zeta = 0.21$, respectively; Appendix 2.2). Change in beach width ($\Delta\text{beachwidth}$), average beach width, average slope, and change in slope (Δslope) all exhibit three distinct concave peaks located in the southern, middle, and northern sections of the island (Figure 3.3c,d,e& f) consistent with locations where the change in shoreline position ($\Delta\text{shoreline}$) indicates an accretional pattern. Along the southern section, the shoreline ($\Delta\text{shoreline}$) advanced an average of ~26 m, the middle section advanced an average of ~6 m, while the north retreated an average of ~39 m between 1998 and 2005 (Figure 3.3g).

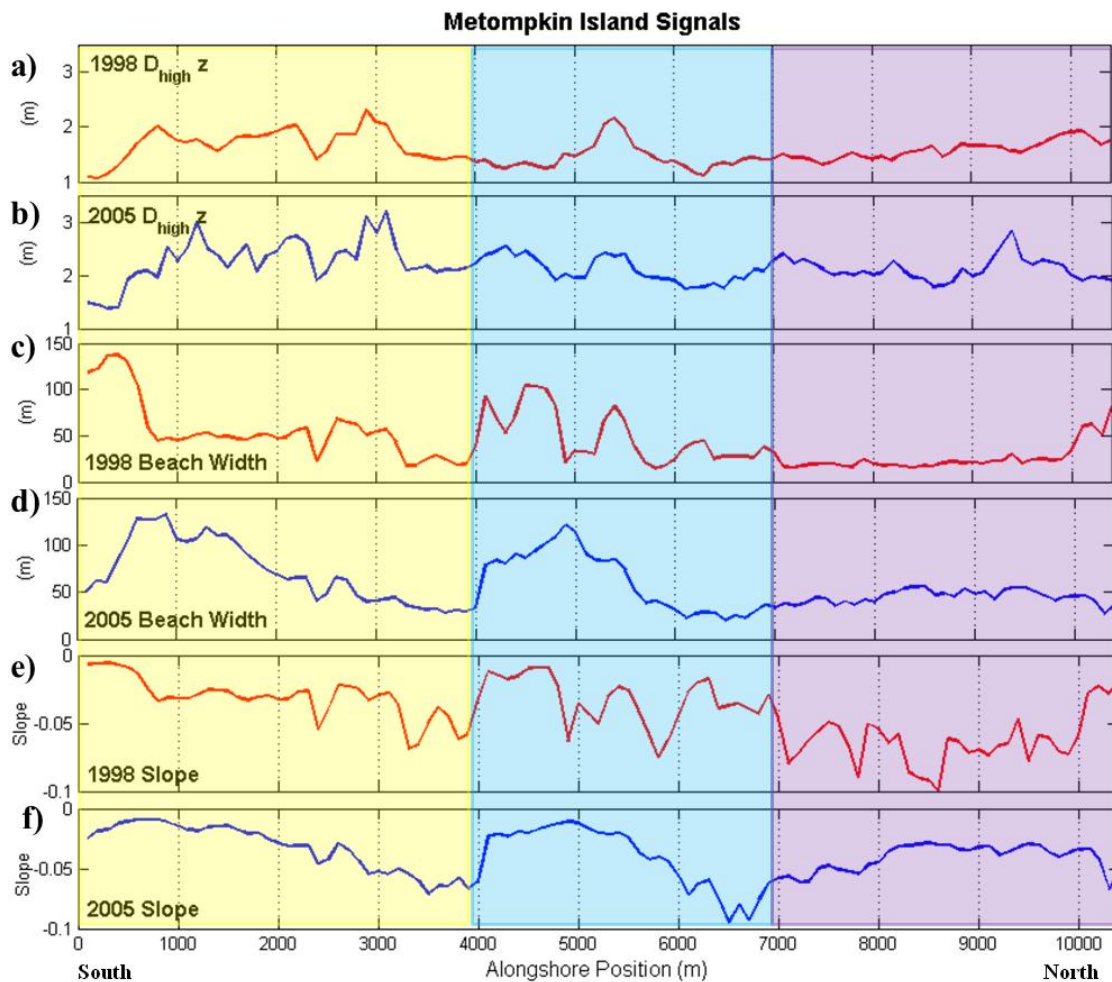


Figure 3.2: Metompkin Island spatial series of (a) 1998 D_{high}^z , (b) 2005 D_{high}^z , (c) 1998 beach width, (d) 2005 beach width, (e) 1998 slope, and (f) 2005 slope. The southern, middle and north section are represented by the yellow, blue and purple background, respectively.

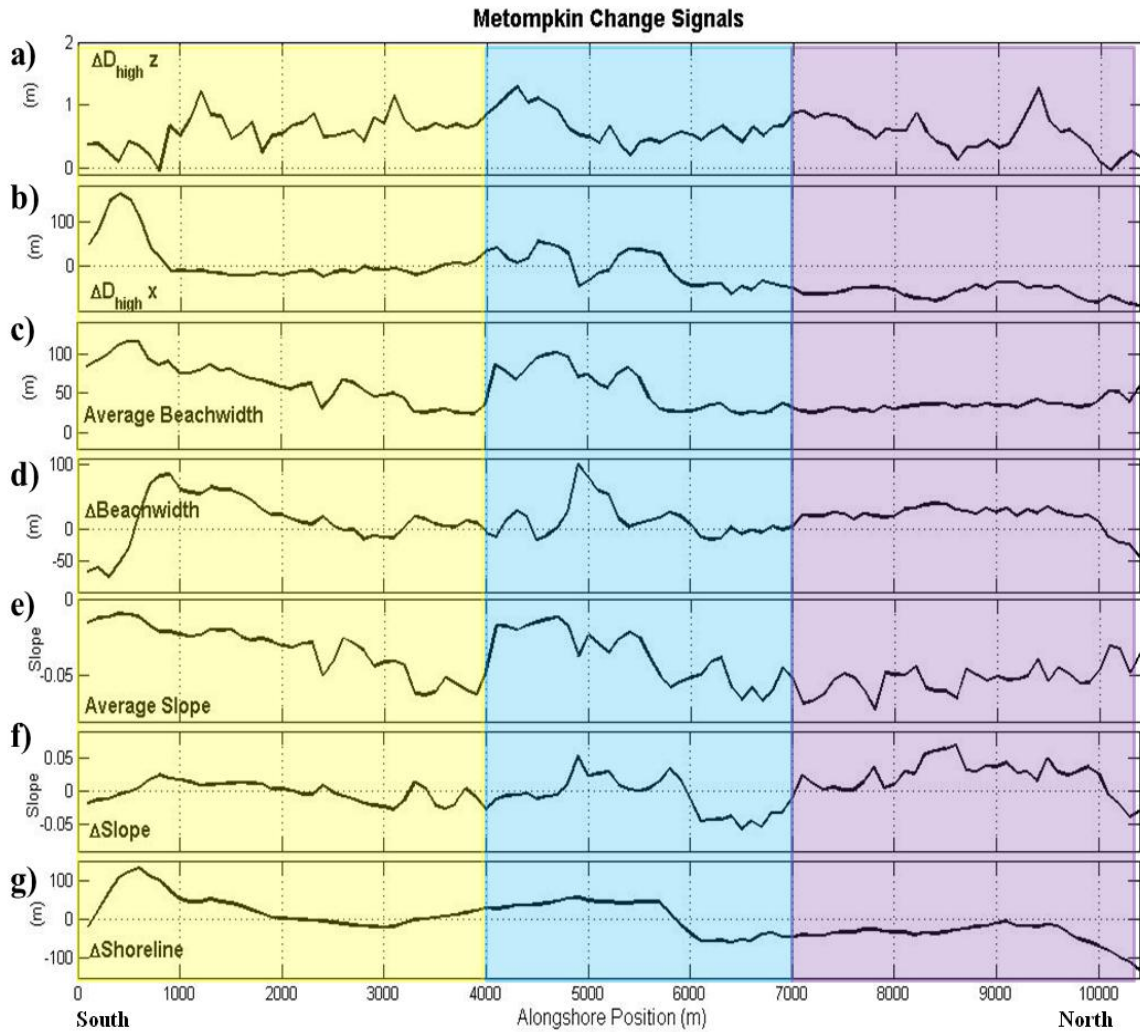


Figure 3.3: Metompkin Island spatial series of (a) change in D_{high} elevation (ΔD_{high}^z), (b) change in D_{high} position (ΔD_{high}^x), (c) average beach width, (d) change in beach width (Δ beachwidth), (e) average slope, (f) change in slope (Δ slope), and (g) change in shoreline position (Δ shoreline). The southern section is represented by the yellow transparent box, the middle by the blue transparent box, and the north by the purple transparent box.

Coherence and interpretations

Following CWT analysis of individual signals, we explore how recovery covaries with morphologic characteristics to better understand the mechanisms behind the spatial variations observed and potential interactions between signals. Overall, wavelet power is high for recovery and for each morphologic characteristic along ~80% of Metompkin Island at spatial scales of ~1600-6400 m indicating a high degree of alongshore variability at these scales (Appendix 2.2). WTC reveals that recovery is in-phase and coherent with change in D_{high} elevation (ΔD_{high}^z) along the entire island; however, these two variables are coherent at different scales along the southern, middle, and northern sections of the island (Figure 3.4a; Table 3.1). Along the southern and middle sections recovery and change in D_{high} elevation (ΔD_{high}^z) are coherent at larger spatial scales (~800-4,000 m), while along the northern region of the island they are coherent at scales of ~400-1,600 m. The phase relationship between recovery and change in D_{high} elevation (ΔD_{high}^z) indicates that areas of highest recovery correspond spatially with areas where D_{high} elevation increased most (i.e., where the dunes grew most). The high coherence values along the entire island at scales ranging between ~400-4,000 m further suggest alongshore patterns of recovery and change in D_{high} elevation (ΔD_{high}^z) may arise from a common mechanism.

To understand what may be affecting changes in D_{high} elevation (ΔD_{high}^z), and thus recovery we assessed the coherence between change in D_{high} elevation and other morphologic characteristics. 2005 D_{high}^z and change in D_{high} elevation (ΔD_{high}^z) are predominantly coherent in the southern and northern sections at smaller spatial scales

(~100-1,600 m; Figure 3.4b) while there is no notable coherence in the middle of the island. 2005 D_{high}^z and change in D_{high} elevation (ΔD_{high}^z) are in-phase, meaning the highest elevation dunes in 2005 occurred at the same locations where the dunes recovered the most elevation. Although there is little coherence between change in D_{high} elevation (ΔD_{high}^z) and 1998 D_{high}^z , there is in-phase coherence between 1998 D_{high}^z and 2005 D_{high}^z at spatial scales of ~400-1,000 m along southern Metompkin Island (similar to ΔD_{high}^z and 2005 D_{high}^z ; Figure 3.4c). This indicates that in the south, in areas where dunes were tallest in 1998 the dunes got taller, rather than increasing in height most where dunes were relatively low in 1998 (as one might intuitively expect). Ultimately, this pattern of dune growth maintains local dune peaks by building most elevation along permanent discontinuous dune crests interspersed with local overwash zones that didn't recover. Coherence between change in D_{high} elevation (ΔD_{high}^z) and 1998 and 2005 D_{high}^z characteristics explains the alongshore variability of change in D_{high} elevation and the significance of dune recovery processes to island recovery in the south and north. There is notable coherence between change in D_{high} elevation (ΔD_{high}^z) and recovery in the middle of the island (slightly out of phase) that is not coherent with variations in 1998 and 2005 D_{high}^z .

Change in D_{high} elevation (ΔD_{high}^z) is coherent and in-phase with 2005 beach width, 2005 slope, change in slope (Δslope), and average beach width at scales of ~1,600-3,200 m along the middle of Metompkin Island (where there was no coherence between change in D_{high} elevation and 1998 and 2005 D_{high}^z characteristics). Since all three foreshore characteristics are coherent with change in D_{high} elevation (ΔD_{high}^z) at the

same locations and spatial scales (as expected since beach width and slope are related), we present only the wavelet coherence analysis of average beach width and D_{high} elevation (ΔD_{high}^z) as representative of foreshore relationships with D_{high} elevation (Figure 3.4e). Average beach width and change in D_{high} elevation (ΔD_{high}^z) are coherent and 90° out of phase. The spatial lead shown by the phase relationship at scales of $\sim 1,600$ - $3,200$ m suggests the dunes along the middle of Metompkin Island gained the most elevation about 800 m south of the positive peak in average beach width (and where slope become more dissipative). This relationship between beach width and dune height may indicate that along the middle of Metompkin Island, where the beach is wide and dissipative; foreshore recovery may be important in promoting dune recovery and, potentially, recovery.

Recovery is coherent and in-phase with change in beach width ($\Delta \text{beachwidth}$) and change in slope (Δslope) on Metompkin Island in the middle and northern sections (Table 3.1; Appendix 2.2), suggesting that areas where beach width and slope recovered most correspond with areas of highest recovery. However, the coherence between recovery and change in beach width ($\Delta \text{beachwidth}$) in the north appears to be an artifact of berm selection of 1998 D_{high} (as no dunes were present), which caused D_{high} to be located farther seaward than the incipient dunes selected in 2005 (Appendix 2.2). This makes it appear that the cross-shore location of D_{high} position (D_{high}^x) moved landward faster than the shoreline and results in an apparent increase in beach width in the north.

We use average beach width (and average slope) in place of change in beach width (and change in slope) for WTC analyses because it minimizes the effect of the artificially

narrow 1998 beach by averaging rather than taking the difference between the 1998 and 2005 beaches. Recovery and average beach width are coherent and in-phase only along the middle of Metompkin Island at scales of $\sim 1,600$ - $3,200$ m (Figure 3.4d; Table 3.1). In the middle of Metompkin Island, positive peaks in recovery occur where average beach width is widest (Figure 3.4d). Average slope also shows in-phase coherence with recovery along the center of the island (Appendix 2.2), where the foreshore slopes are most dissipative and correlate with a positive peak in recovery (same phase relationship and scale as coherence between average beach width and recovery).

Changes in slope and beach width in the center of the island appear to be most influential in determining recovery and dune recovery patterns, while recovery in the northern and southern sections is heavily influenced by dune recovery. Within the middle of Metompkin Island, the area just south of the shoreline offset is exceptionally wide and dissipative, and the most dune accretion occurs south of peaks in average beach width, while the local maximum in recovery is in-phase with the widest section of Metompkin Island (on the middle of the island). Shoreline change dynamics, particularly along the offset, may be promoting the local importance of foreshore characteristics to recovery patterns, while the remainder of the island is heavily dependent on dune processes.

Alongshore variations in average slope and beach width are in-phase and coherent with change in shoreline position (Δ shoreline) at the km scale ($\sim 3,000$ - $6,000$ m) along the entire island (Figure 3.4f). Because beach width and slope are directly related to shoreline position, this is an expected result. However, it is interesting that coherence occurs only at large spatial scales between change in shoreline position with beach width and slope,

while smaller-scale variations in beach width and slope are coherent with variability in the cross shore location of D_{high} (ΔD_{high}^x) (Appendix 2.2). The relationship is in-phase because areas that accreted between 1998 and 2005 (positive peak) coincide with areas where average beach width is greatest.

	Metompkin Island
Morphologic Characteristics	Relationship with Recovery (C, phase, spatial scale)
1998 D_{high}^z	NC
2005 D_{high}^z	C, In-phase, 400-3,000
ΔD_{high}^z	C, In-phase, 400-4,000
1998 Beachwidth	NC
2005 Beachwidth	C, In-phase, 1,600-4,000
Average beachwidth	C, In-phase, 1,600-4,000
1998 Slope	NC
2005 Slope	C, In-phase, 1,000-6,000
Average slope	C, In-phase, 1,600-6,000
$\Delta \text{Shoreline}$	C, In-phase, 1,600-3,200
ΔD_{high}^x	NC

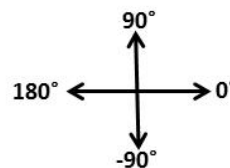


Table 3.1: Summary of coherence between recovery and morphologic characteristics along Metompkin Island. C= coherence values between 0.6-1. NC= coherence values between 0-0.59, If NC then no phase or scale. In-phase= general phase relationship between -45° — 45° . Anti-phase = general phase relationship between -135° — 135° . Phase angle is represented by diagram on the right of the table.

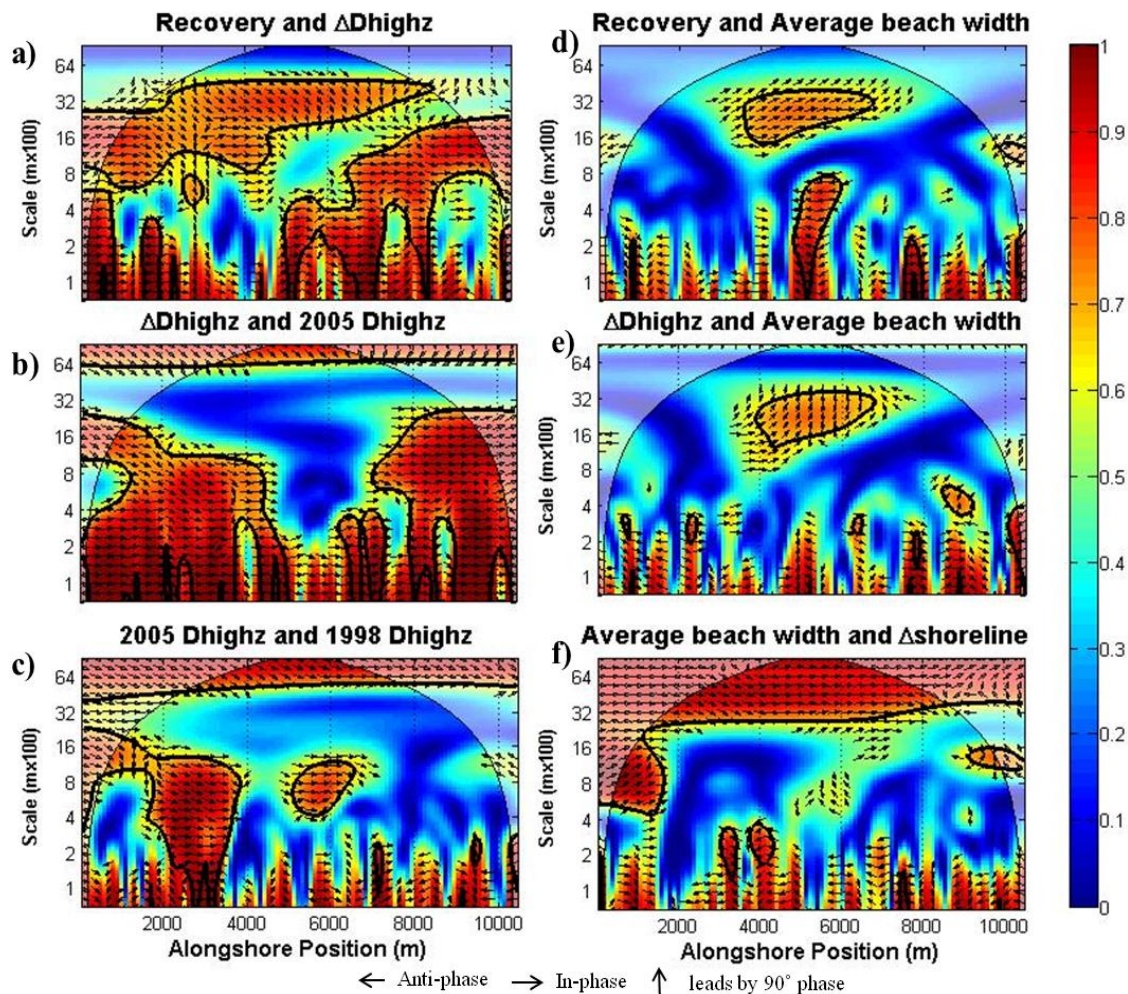


Figure 3.4: Wavelet coherence analysis and phase angle of (a) recovery and change in D_{high} elevation (ΔD_{high}^z), (b) change in D_{high} elevation (ΔD_{high}^z) and 2005 D_{high} , (c) 2005 and 1998 D_{high}^z , (d) recovery and average beach width, (e) change in D_{high} elevation (ΔD_{high}^z) and average beach width, (f) average beach width and change in shoreline position ($\Delta shoreline$). Black contours represent 95% confidence interval and transparent regions are within the COI. Color bar represents coherence where 1 (dark red) is highly coherent and linear, while 0 (dark blue) is no relationship. Spatial scale is shown on the y-axis in $m \times 10^2$ and alongshore position in the x-axis, where 0 m is the southernmost extent of the analysis and 10,400 m is the northernmost extent. The arrows depict phase relationship, where an arrow pointing right is in-phase, left is anti-phase, and up indicates a spatial lag where the signal listed first in the title is 90° out of phase and south of the second signal listed in the title.

Smith Island

Similar to Metompkin Island, Smith Island morphologic characteristics and wavelet results revealed differences in behavior that led us to consider the island in two sections: the southern section (0-5,000 m) and the northern section (5,000-10,600 m).

Recovery

Recovery varies widely along Smith Island. Overwash vulnerability in both 1998 and 2005 ranged from a low average overwash probability on the southern half (14% in 1998, 19% in 2005) to high average probability on the northern half (76% in 1998, and 71% in 2005; Figure 3.5c). As a result of highly variable overwash probabilities in 1998 and 2005, the northern section of Smith Island exhibits both dramatic recovery and increased vulnerability (represented by negative recovery values). Recovery along the southern section is high on the southern tip of Smith Island and near zero from 2,000-4,000 m alongshore. Along 2,000-2,500 m on southern Smith Island, the probability of overwash in both 1998 and 2005 was near zero and thus based on our definition, recovery is zero (Figure 3.5b). This section of Smith Island is not included in further interpretation of recovery since the quantified recovery is not representative of the degree of recovery that occurred between 1998 and 2005.

A continuous wavelet transform of recovery shows high power at larger spatial scales on most of Smith Island. Along the southern section, there is particularly high wavelet power at scales of ~800-4,000 m. The northern section has high power across a range of scales (~400-4,000 m; Figure 3.5a). The spatial scales at which recovery shows

high power on Smith Island are similar to the scales that are significant for recovery on Metompkin Island, as well as for other morphologic signals on Smith Island, further suggesting a common mechanism may be influencing spatial variability (Appendix 2.3).

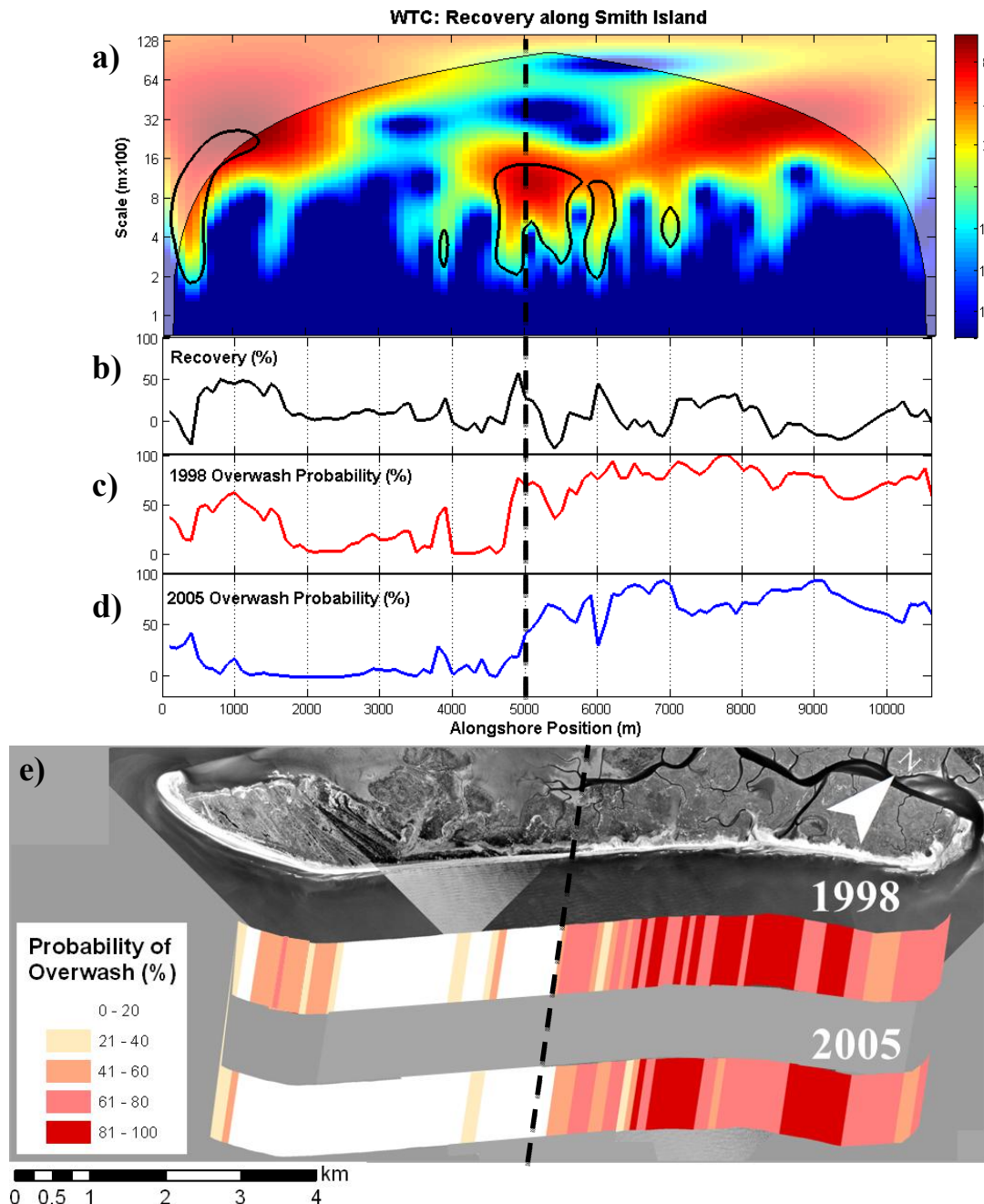


Figure 3.5: (a) Continuous wavelet transform of spatial signal of recovery showing local wavelet power spectrum as a function of alongshore position, where power is represented by the color bar and the 95% confidence interval inside the thick-black contours. The Cone of Influence (COI) is represented by the transparent regions. Alongshore signals of (b) recovery, (c) 1998 overshaw probability, and (d) 2005 overshaw probability. (e) Rotated orthorectified image of Smith Island in 2002 with 1998 and 2005 overshaw probability during a storm with Hurricane Bonnie characteristics superimposed. Dashed black line signifies southern and northern section transition.

Morphologic Characteristics

1998 and 2005 D_{high}^z was higher on average on southern Smith Island (2.5 m in 1998 and 2.8 m in 2005) than on northern Smith Island (1.6 m in 1998 and 1.8 m in 2005; Figure 3.6a&b; Appendix 2.3), while change in D_{high} elevation (ΔD_{high}^z) is highly variable along the entire island (Figure 3.7a). In 1998, beach width and slope appeared to vary along smaller spatial scales (e.g. < 1 km) and were relatively similar across the south and north of the island (Figure 3.6c&e). However, by 2005, both beach width and slope appear wider and more dissipative only on southern Smith Island (Figure 3.6d&f). According to the Surf Similarity Index most of southern and northern Smith Island was dissipative (average $\zeta = 0.17$ along the south and average $\zeta = 0.14$ along the north; Appendix 2.3) in 1998. The Surf Similarity Index classifications diverged in 2005, when the south was clearly dissipative (average $\zeta = 0.15$) and the north became mostly intermediate (average $\zeta = 0.23$; Appendix 2.3). The change in beach width and slope is positive (meaning that the beach widened and slope decreased) along the southern reach and near zero or negative along the northern reach (Figure 3.7c&d). The changes in beach width ($\Delta \text{beachwidth}$) and slope (Δslope) mimicked changes in shoreline position ($\Delta \text{shoreline}$): the southern section advanced seaward an average of ~12 m and the northern section retreated landward ~53 m (shoreline change is a variable used to calculate change in beach width and change in slope; Figure 3.7e).

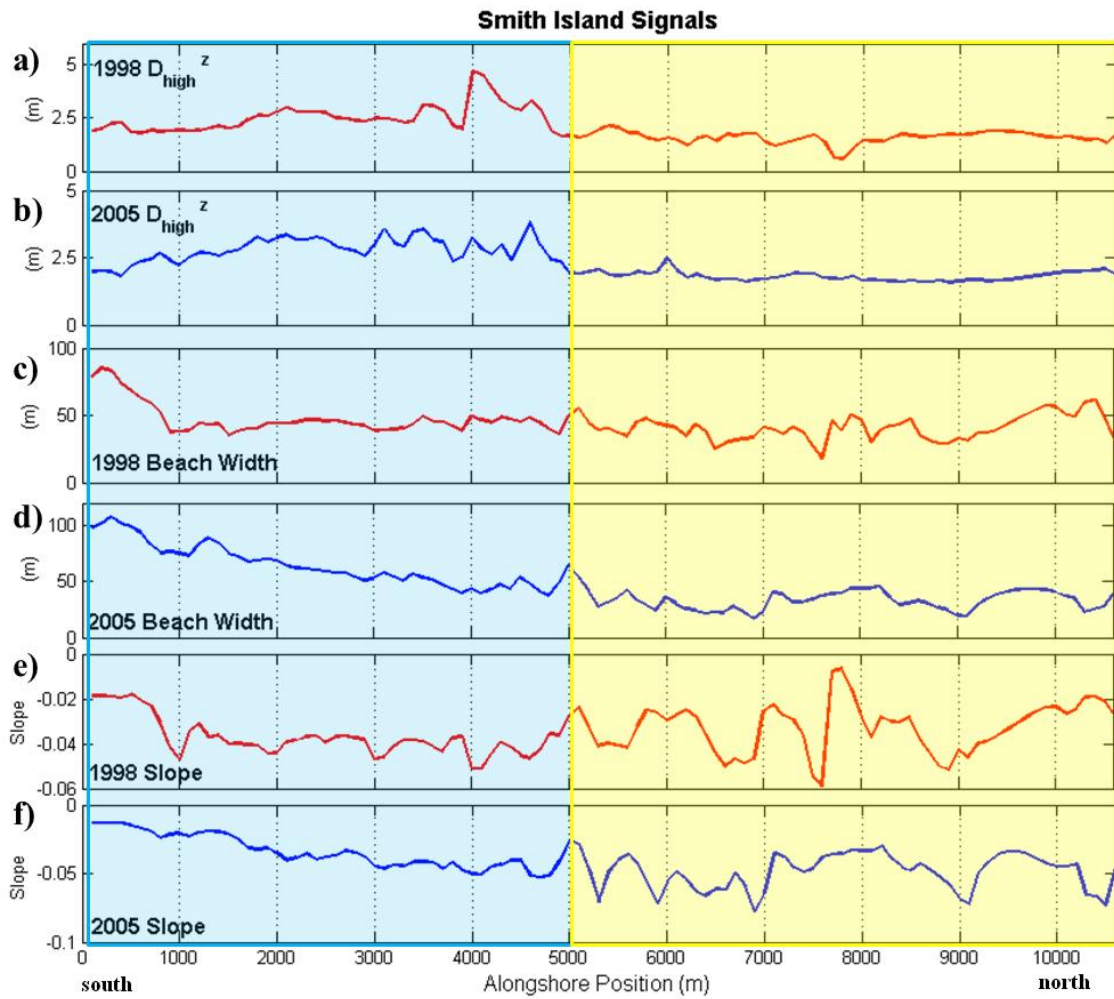


Figure 3.6: Smith Island spatial series of (a) 1998 D_{high}^z , (b) 2005 D_{high}^z , (c) 1998 beach width, (d) 2005 beach width, (e) 1998 slope, and (f) 2005 slope. The southern section is represented by the transparent blue box and the north by the transparent yellow box.

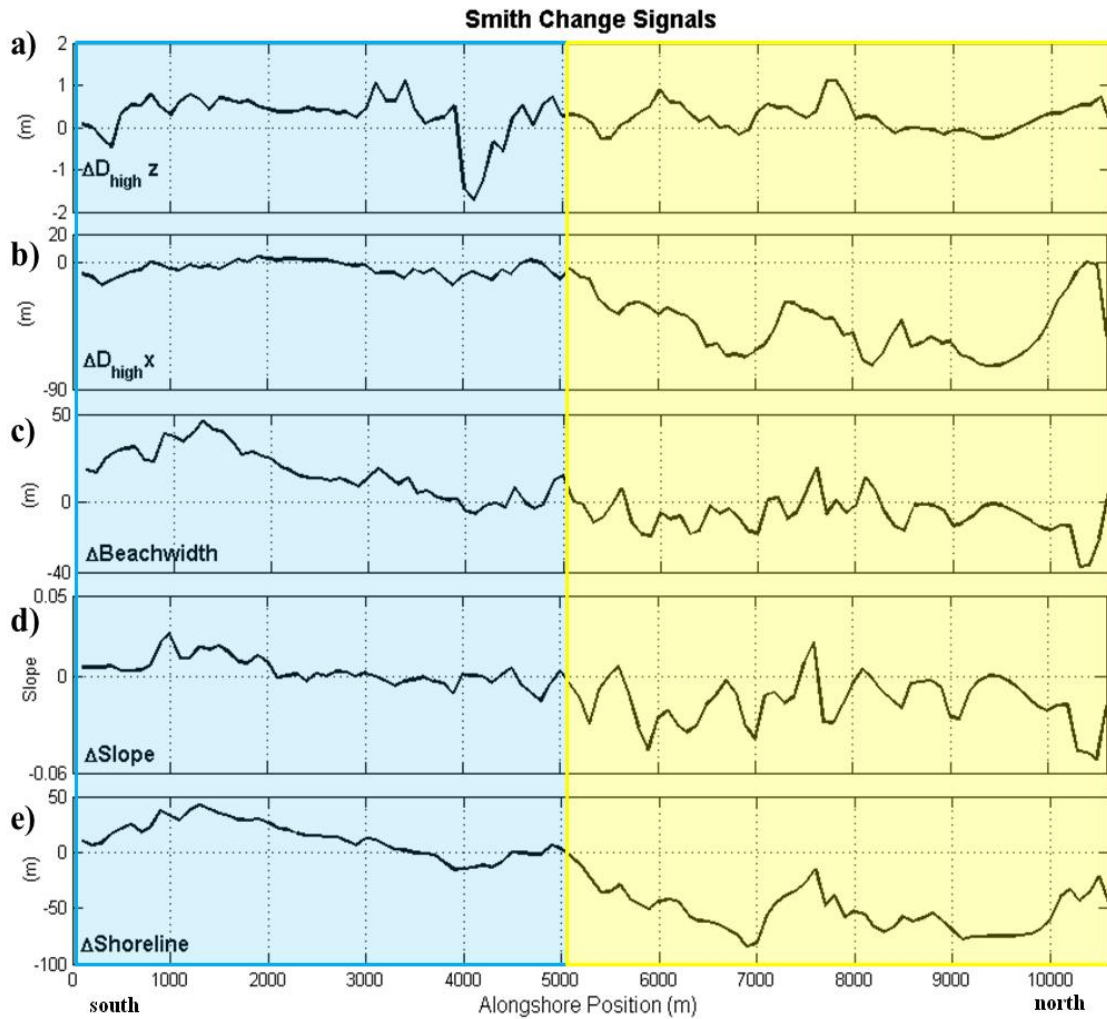


Figure 3.7: Smith Island spatial series of (a) change in D_{high} elevation (ΔD_{high}^z), (b) change in D_{high} position (ΔD_{high}^x), (c) change in beach width ($\Delta Beachwidth$), (d) change in slope ($\Delta Slope$), and (e) change in shoreline position ($\Delta Shoreline$). The southern section is represented by the transparent blue box and the north by the transparent yellow box.

Coherence and interpretations

Similar to analyses of covariance between recovery and morphologic characteristics on Metompkin Island, we explore how mechanisms affecting alongshore variation on Smith Island may be similar or different from those observed on Metompkin Island. Wavelet coherence analysis of recovery and morphologic characteristics on Smith Island reveals that different factors are important to barrier island recovery along the southern and northern sections of the island. Along northern Smith Island, recovery exhibits similar coherency with change in D_{high} elevation (ΔD_{high}^z) as observed along southern and northern Metompkin Island. Recovery and change in D_{high} elevation (ΔD_{high}^z) are in-phase and coherent on northern Smith Island at scales of ~ 800 - $3,200$ m, suggesting that this part of the island is most resilient where the dunes recovered most between 1998 and 2005; however, little to no coherence is apparent between these parameters along the southern half of the island (Figure 3.8a; Table 3.2).

To identify mechanisms that may explain the relationship between recovery and change in dune elevation along the northern half of the island, we explore how changes in dune elevation are influenced by initial dune elevation. WTC analysis of change in D_{high} elevation (ΔD_{high}^z) and initial dune elevation (1998 D_{high}^z) show a strong anti-phase coherence along most of Smith Island at scales primarily between 800 - $1,600$ m (including the area of coherence between recovery and ΔD_{high}^z observed at scales of 800 - $1,600$ m in the north; Figure 3.8b). The anti-phase relationship between change in D_{high} elevation (ΔD_{high}^z) and 1998 D_{high}^z suggests areas that likely lost most dune elevation due to Hurricane Bonnie (represented by negative peaks in 1998 D_{high}^z) recovered the most

elevation by 2005, while areas of relatively higher dune elevation in 1998 experienced little to no dune growth. Coherence between recovery on Smith Island and change in D_{high} elevation (ΔD_{high}^z) is statistically significant along the north where the dunes are lower and therefore likely to be more frequently overwashed. Although dune recovery is only related to overall recovery on northern Smith Island, D_{high} in 1998 was the morphologic characteristic most closely correlated with dune recovery between 1998 and 2005 on the entire island. The anti-phase nature of this relationship indicates that dune recovery processes resulted in increased elevation in 2005 where topographic lows existed within the dune ridge in 1998. Interestingly, although the variability in change in D_{high} elevation (ΔD_{high}^z) can be explained by the initial post-storm dune elevation (1998 D_{high}^z) along all of Smith Island, change in D_{high} elevation (ΔD_{high}^z) is only coherent with recovery along northern Smith Island (Figure 3.8a; Table 3.2) It appears, therefore, that restoration of a continuous dune ridge is an important factor in dune recovery along all of Smith Island but that this process of restoring a continuous ridge is only important to overall barrier recovery on northern Smith Island. This suggests that recovery of southern Smith Island is not related to dune characteristics, as in the north, and must be attributable to a different process. To identify the potential influence of other morphologic changes on change in D_{high} elevation (ΔD_{high}^z), we also tested the coherence between change in D_{high} elevation (ΔD_{high}^z) with change in beach width ($\Delta \text{beachwidth}$), average beach width, 1998 beach width, change in shoreline position ($\Delta \text{shoreline}$), and change in slope (Δslope); we found little to no coherence.

In contrast to the significant coherence of change in D_{high} elevation (ΔD_{high}^z) with recovery in the north, recovery is in-phase and coherent with change in beach width ($\Delta \text{beachwidth}$) at scales of $\sim 3,200$ - $6,400$ m along the entire island and at smaller spatial scales of $1,600$ - $3,200$ m just along southern Smith Island. This coherence suggests that areas of the greatest recovery along the south occur where the beach widened by 2005 (Figure 3.8c; Table 3.2). Similar relationships between recovery and change in slope (Δslope) as well as recovery and average beach width exist for the southern extent of Smith Island, although the area of coherence is smaller and not statistically significant (Appendix 2.3).

To understand what might explain the coherence between recovery and change in beach width ($\Delta \text{beachwidth}$), we explore the influence of 2005 beach width, the change in shoreline position, and the change in dune position on change in beach width ($\Delta \text{beachwidth}$). There is large-scale ($\sim 1,000$ - $6,400$ m) in-phase coherence between change in beach width ($\Delta \text{beachwidth}$) and 2005 beach width along the southern, and a portion of the northern, regions of Smith Island (Figure 3.8d). The strong influence of 2005 beach width on the change in beach width is in part due to a lack of variability in alongshore beach width in 1998. Along the southern ~ 4 km of Smith Island, the beach widened substantially between 1998 and 2005.

Although change in shoreline position ($\Delta \text{shoreline}$) is not directly correlated with recovery, it is coherent with change in beach width ($\Delta \text{beachwidth}$) (Figure 3.8e) suggesting that the co-variance of change in beach width along southern Smith Island is a function of beach widening (shoreline position accreting) rather than a function of

changes in the dune position, which remains relatively stationary on southern Smith Island (Figure 3.7b and Appendix 2.3). Change in shoreline position (Δ shoreline) and change in beach width (Δ beachwidth) are in-phase and coherent only along southern Smith Island at scales between \sim 800-6,000 m, indicating that locations where the shoreline accreted or did not move coincide with areas where the beach widened. Within the study area, southern Smith Island and the middle of Metompkin Island are the only two locations where beach width is coherent with recovery. In addition, except for the southern tip of Metompkin Island, these are the only locations where the shoreline accreted between 1998 and 2005.

	Smith Island
Morphologic Characteristics	Relationship with Recovery (C, phase, spatial scale)
1998 D_{high}^z	C, Anti-phase, 800-2,000
2005 D_{high}^z	C, In-phase, 800-2,000
ΔD_{high}^z	C, In-phase, 800-4,000
1998 Beachwidth	C, Anti-phase, 800-6,000
2005 Beachwidth	C, In-phase, 3,200-5,000
Δ Beachwidth	C, In-phase, 1,600-6,400
1998 Slope	C, Anti-phase, 800-6,400
2005 Slope	NC
Δ Slope	C, In-phase, 1,000-2,000
Δ Shoreline	C, In-phase, 1,600-3,200
ΔD_{high}^x	C, In-phase, 1,600-3,000

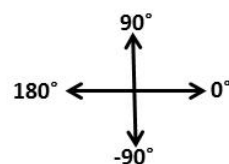


Table 3.2: Summary of coherence between recovery and morphologic characteristics along Smith Island. C= coherence values between 0.6-1. NC= coherence values between 0-0.59, If NC then no phase or scale. In-phase= general phase relationship between -45° — 45° . Anti-phase= general phase relationship between -135° — 135° . Phase angle is represented by diagram on the right of the table.

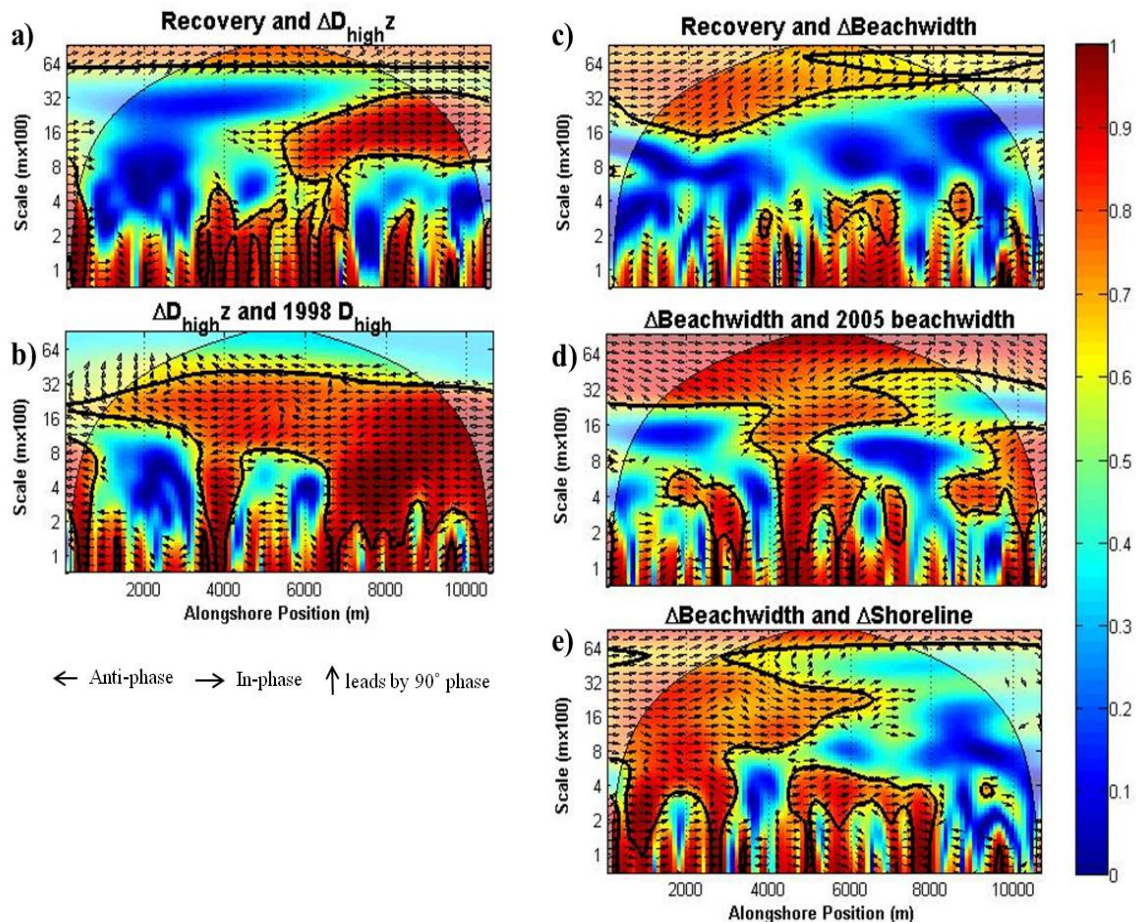


Figure 3.8: Wavelet coherence analysis and phase angle of (a) recovery and change in D_{high} elevation (ΔD_{high}^z), (b) change in D_{high} elevation (ΔD_{high}^z) and 1998 D_{high}^z , (c) recovery and change in beach width ($\Delta Beachwidth$), (d) change in beach width ($\Delta Beachwidth$) and 2005 beach width, (e) change in beach width ($\Delta Beachwidth$) and change in shoreline position ($\Delta Shoreline$). Black contours represent 95% confidence interval and transparent regions are within the COI. Color bar represents coherence where 1 (dark red) is highly coherent and linear, while 0 (dark blue) is no relationship. Spatial scale is shown along the y-axis in $m \times 10^2$ and alongshore position in the x-axis, where 0 m is the southernmost extent of the analysis and 10,600 m is the northernmost extent. The arrows depicts phase relationship, where an arrow pointing right is in-phase, left is anti-phase, and up indicates a spatial lag where the signal listed first in the title is 90° out of phase and south of the second signal listed in the title.

4. DISCUSSION

In this study, we define recovery as the change in overwash probability between two lidar data sets—one collected immediately after a storm and one collected two years following a storm. We define recovery as such with the primary intent to quantify and contrast recovery patterns alongshore and to investigate potential covariation with morphologic characteristics. However, it is important to acknowledge that our definition is limited by the fact that areas which are initially resistant to overwash (for example, portions of southern Smith Island in 1998; Figure 3.5) show no recovery if they remain resistant between 1998 and 2005. Areas where recovery was zero because they were resistant throughout 1998 to 2005 are of less interest than areas where recovery was zero because they simply didn't recover (for example, portions of middle Metompkin Island immediately north or the mid-island offset; Figure 3.1).

In general, Metompkin Island shows greater recovery alongshore, in part, because it was more vulnerable to overwash than Smith Island in 1998. On northern Metompkin Island, the overwash terraces were likely to have been uniformly overwashed during Hurricane Bonnie, limiting alongshore variability, while the southern section of the island exhibited spatially variable overwash probability in 1998. Field observations further support the spatial distinction in response to major storm events like Hurricane Bonnie on northern and southern Metompkin Island: the tall, discontinuous dune structure found along the southern half of the island promotes local overwash occurrence, while in contrast, the continuous low topography of the north reinforces widespread overwash

zones (Wolner, 2011; Wolner et al., submitted). Overwash probability in 2005 was more variable alongshore, leading to higher overall variability in the recovery signal.

Recovery along Smith Island is highly variable, and displays regions of both recovery and increased vulnerability. There is not a strong distinction between northern and southern Smith Island in terms of the amount of recovery, however, along northern Smith Island recovery is more spatially variable alongshore. The pattern of overwash probability on Smith Island is similar in 1998 and 2005—namely, the south is distinctly less vulnerable than the north. Generally, there was less recovery along the south because the barrier in this location was more resistant to overwash in both 1998 and 2005. In contrast, the north was vulnerable in 1998 and in 2005, causing the recovery signal to oscillate around zero. The vegetation of Smith Island has been noted for its distinctly different backbarrier populations on the southern and northern sections of the island: the south is host to a wide, well-developed maritime forest (which can only develop in very rarely disturbed environments), while the backbarrier in the north consists of marsh (located on the distal fringes of overwash flats; Bachmann et al., 2002). Aerial imagery shows that the sandy beach is clearly defined in the south, while the north exhibits widespread overwash zones extending onto the marsh unevenly alongshore. The differences in dune structure and backbarrier vegetation reinforce the differences in recovery patterns on Smith Island.

Dune elevation is important to recovery on Smith and Metompkin Island however, the spatial relationship between recovery and dune characteristics varies along each island. There is a notable lack of coherence between recovery and change in D_{high}

elevation on the southern section of Smith Island; while recovery and change in D_{high} elevation are coherent on northern Smith Island and all of Metompkin Island at spatial scales within 1-6 km. Southern Smith Island is the only area where 1998 overwash probability was low and where there is also no significant coherence between recovery and change in D_{high} elevation. Southern Smith Island differs morphologically from northern Smith Island and all of Metompkin Island in that it hosts tall continuous dunes fronted by a wider, more dissipative foreshore. Recovery on Smith and Metompkin Island is only coherent with change in D_{high} elevation along areas where beaches are intermediate and had high overwash probability to a storm with Hurricane Bonnie characteristics in 1998. The influence of overwash disturbance patterns is highlighted by the divergent dune recovery patterns that occurred on Smith and Metompkin Islands. Storm impact on Smith Island may have been less severe and overwash occurrence may have been more localized compared with Metompkin Island, which was likely blanketed by overwash (specifically along the middle and northern sections).

Overall recovery and dune recovery (ΔD_{high}^z) co-varied at the kilometer scale, suggesting that both parameters may be affected by common mechanisms. Changes in dune elevation were important to barrier island recovery along northern Smith Island and northern and southern Metompkin Island, however, the dune recovery processes were unique to each region. The dunes along northern Metompkin Island likely experienced widespread overwash and shows signs of dune recovery via storm berms in 1998 shifting landward to form incipient dunes by 2005. On southern Metompkin Island, the tallest dunes in 1998 maintained the tallest peaks in 2005. This pattern, unique to southern

Metompkin Island within the area studied, potentially supports the self-reinforcing landscape variations suggested by Wolner et al. (submitted), where tall, discontinuous dunes populated by dune-building grasses resist overwash even in severe storms, while intermittent overwash zones are perpetuated locally in subsequent storms as little to no recovery occurs in between the dune peaks. The opposite was observed along northern Smith Island. Where D_{high} recovers by building dune elevation most where it was lowest in 1998, essentially filling in the gaps—caused by local overwash events—and thus restoring a continuous dune ridge.

Additional coherence between recovery and change in D_{high} elevation was found along the middle of Metompkin Island that could not be explained by dune recovery processes. Theoretical models of beach and dune interactions often associate the occurrence of tall dunes with wide dissipative beaches driven by higher aeolian transport potential to the dunes (e.g. Short and Hesp, 1982; De Vries et al., 2011). Other site specific studies of the interaction between dune height and beach width have resulted in a range of observations both supporting and contrasting the conceptual models (e.g., Houser and Hamilton, 2009; De Vries et al., 2011; Houser and Mathew, 2011) and further stressing the complexity of the relationship. Houser and Mathew (2011) found local peaks in dune height occurred in between intermediate and dissipative areas on South Padre Island, TX, as a function of wave focusing south of local minimums in foreshore slope. Along the middle of Metompkin Island, local peaks in change in D_{high} elevation occur south of peaks in average beach width (and change in slope) and are coherent at the kilometer spatial scale. The spatial lead between change in D_{high} elevation

and average beach width is consistent with Houser and Mathew (2011), where the peaks in dune recovery occur about midway between the minimum and maximum peaks in average beach width and slope. The stretch of coast on Metompkin Island around the offset shoreline is the only location in this study where both dune and foreshore characteristics are coherent with recovery. The unique shoreline dynamics along the mid-island offset, where the shoreline is smoothing, may be playing a role in the observed relationship between dune and foreshore characteristics.

Southern Smith Island and the middle of Metompkin Island are the only sections where significant recovery coincided with a widening beach. Along the southern 4 km of Smith Island the width of the beach increased largely due to shoreline accretion. Aerial images show large ridge and runnel features increasing beach width, particularly along the southern bend in the shoreline. As previously mentioned, shoreline smoothing along middle of Metompkin Island (which is unique to this location) may be strengthening the importance of foreshore characteristics for both overall recovery and dune recovery, while overall recovery along the rest of the island relies heavily on dune recovery processes.

Although change in shoreline position does not appear to have a direct effect on variations in recovery in most areas, it is directly coherent with changes in beach width and slope on all of Smith and Metompkin Islands. On southern Smith Island, the shoreline accreted between 1998 and 2005, which widened the beach and flattened the foreshore slope. The observed foreshore recovery is directly coherent with overall recovery along that same area. The same is true on Metompkin Island, where two

locations along the southern and middle (mid-island offset) sections experienced shoreline accretion, becoming wider and more dissipative. Generally areas where the shoreline was accreting or remained relatively stationary between 1998 and 2005, are congruent with areas where the beach is wider and more dissipative, and ultimately less vulnerable to overwash. While areas where the shoreline has been eroding between 1998 and 2005 occur with narrower more intermediately sloping beaches and overwash is likely to occur.

There are a number of other factors and physical characteristics that potentially contribute to barrier island recovery and morphologic change. While quantifying these variables is beyond the scope of this study, it is still possible to make inferences about their potential effects. The temporal scale between data sets used in a study can influence the observed alongshore variability in recovery and morphologic characteristics. Short temporal scales (i.e. months to a few years) typically correlate with smaller spatial scale variability (meters to a kilometer). As temporal scale increases, so will the spatial scales at which morphology varies. Thus, the inferred mechanisms driving alongshore variability change with temporal and spatial scale (Lazarus et al., in press).

The spatial scale of alongshore variations is often used to infer potential mechanisms that may explain the observed spatial variability (e.g., Demarest and Leatherman, 1985; Sherman, 1995; Stockdon et al., 2007; Houser et al., 2008; Houser and Hamilton, 2009; Houser and Mathew, 2011; Lazarus et al., in press). In addition to site specific physical characteristics, the frequency of storm events may dictate which mechanisms control spatial variability. Theoretically, if recovery between events were

constrained to less than a year, the spatial variability could potentially decrease to smaller spatial scales, and may be explained by wave runup or surf zone dynamics (e.g., Lazarus et al., in press). Conversely, given substantially more time to recover between events, alongshore morphology may be affected by long-term physical drivers, such as shoreline change and alongshore sediment transport (Cowell and Thom, 1994; List et al., 2006; Lazarus et al., in press). Given sufficient time between storm events, other feedbacks have the potential to aid or inhibit recovery and dune recovery, such as vegetation presence and composition, and the occurrence of shell lag deposits (Morton et al., 1994; Bauer and Davidson-Arnott, 2002; Stallins and Parker, 2003; Psuty, 2008; Priestas and Fagherazzi, 2010; Houser and Mathew, 2011; Wolner et al., submitted).

Island width has been found to promote dune recovery because of the larger sediment supply inherently associated with wider islands (Houser et al., 2008; Houser and Hamilton, 2009; Priestas and Fagherazzi, 2010). Though lidar coverage did not extend across the entire width of the islands, aerial photos from 2002 clearly show that southern Smith is wider than northern Smith and all of Metompkin Island during high tide conditions (estimated average widths of 1.0 km, 0.3 km and 0.4 km, respectively). Interestingly, the widest stretch of southern Smith (extending from 1,000-4,000 m alongshore) was also the most resistant to overwash in both 1998 and 2005.

5. CONCLUSIONS

Morphologic characteristics on the barrier islands of the Virginia Coast Reserve (VCR) are highly variable; as a result, storm response and recovery varied significantly on Smith and Metompkin Islands between 1998 and 2005. The most resilient areas typically have high initial overwash probabilities in 1998; a function of how recovery is defined in this study.

Not surprisingly, along all of Metompkin Island and northern Smith Island there is a strong association between recovery and change in D_{high} , or dune recovery processes. Although dune recovery is the best predictor of recovery on most of Metompkin Island and northern Smith Island, site-specific variations in dune processes were evident on the various sections. Initial foredune structure (i.e. continuous, discontinuous, or overwash terraces) and overwash disturbance patterns potentially dictate dune recovery processes and patterns. However, beach width, slope, and shoreline change are not associated with alongshore D_{high} variations (with the exception being along the shoreline offset on Metompkin Island). Other physical conditions may likely influence dune structure that could not be quantified in this study, but it is clear that dune recovery is a key predictor of overall recovery on narrow and intermediate beaches impacted by overwash.

Recovery on southern Smith Island and the middle of Metompkin Island is strongly associated with the recovery of foreshore characteristics on wide dissipative beaches. Smith Island and the middle of Metompkin Island are the only locations where the shoreline accreted between surveys—these are also the only sections where overall recovery is correlated with wide dissipative beaches and foreshore recovery.

Although dune recovery processes are highly site specific, beach characteristics in concert with storm impact regimes can be used to generally predict alongshore barrier recovery. In locations where the beach is narrower (and intermediate) and the shoreline has been eroding, following overwash occurrence (widespread or local occurrence), dune recovery patterns will predict the spatial variability in barrier island recovery. Where the dune gains the most elevation, recovery will be greatest, and less vulnerable to overwash in subsequent storms. Areas where the beach is wide (and dissipative) and the shoreline is stationary or accreting are typically more resistant to overwash, and in these locations alongshore recovery will more likely be linked to increases in beach width (Figure 4.1).

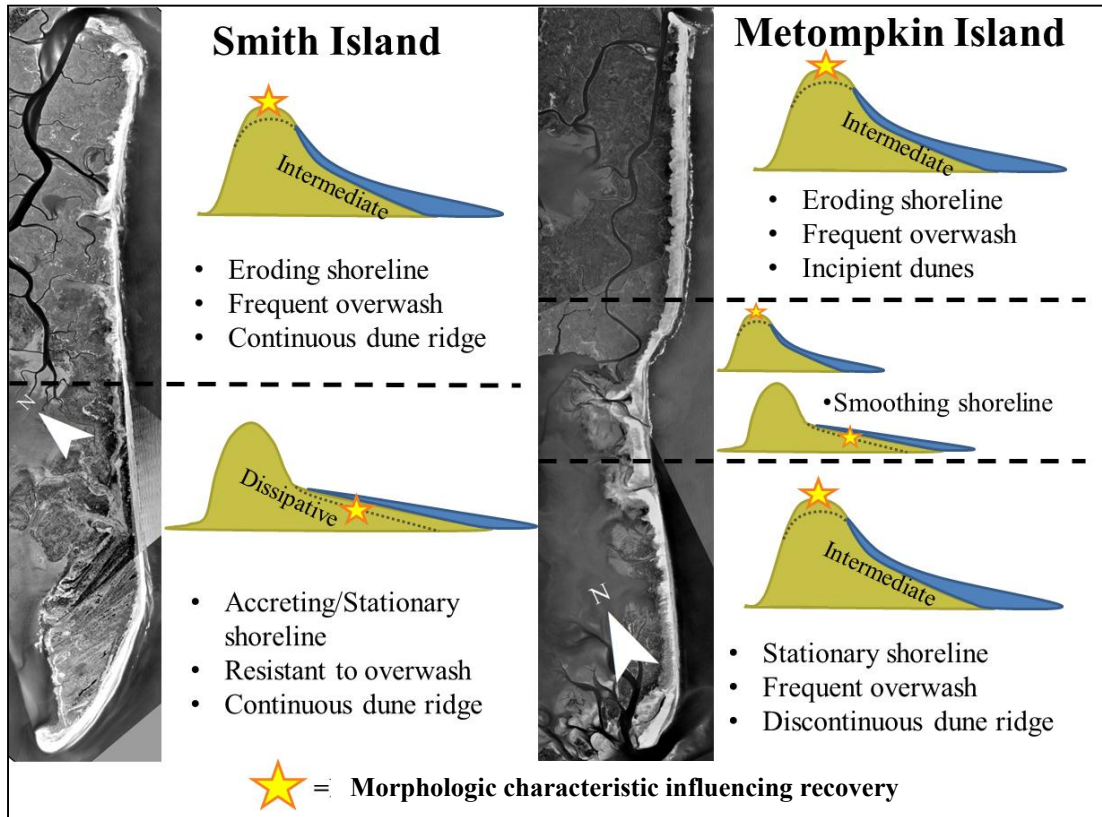


Figure 5.1: Orthorectified images from 2002 of Smith (left) and Metompkin (right) Islands. Dashed black line represents division of observed island morphologic characteristics and recovery patterns. Beach profile diagrams are general representations of dune and foreshore characteristics associated with specific sections on Smith and Metompkin Island. Dashed brown line on the beach profiles represents general post-storm condition, where the majority of storm impact affected the beach during a storm similar to Hurricane Bonnie in 1998. Tan profile represents general morphologic recovery observed following a storm. Yellow star signifies morphology critical to alongshore barrier island recovery (i.e. foreshore recovery like beach width and slope, or dune ridge recovery via increased D_{high} elevation).

REFERENCES

- Bachmann, C. M., Donato, T. F., Lamela, G. M., Rhea, W. J., Bettenhausen, M. H., Fusina, R. A., et al. 2002. Automatic classification of land cover on Smith Island, VA, using HyMAP imagery. *Geoscience and Remote Sensing, on IEEE Transactions*, 40 (10): 2313-2330.
- Battjes, J. A. 1974. Surf similarity *Proc. 14th Coastal Engineering Conference*: 466-80.
- Bauer, B. O., and R. G. D. Davidson-Arnott. 2002. A general framework for modeling sediment supply to coastal dunes including wind angle, beach geometry, and fetch effects. *Geomorphology* 49: 89-108.
- Byrnes, M. R. 1988. Holocene geology and migration of a low-profile barrier island system, Metompkin Island, Virginia. Doctoral dissertation, Old Dominion University.
- Church, J. A., and N. J. White. 2006. A 20th century acceleration in global sea-level rise. *Geophysical Research Letters* 33 (L01602).
- Cowell, P.J. and B.G. Thom, 1994. Morphodynamics of coastal evolution. In *Coastal Evolution: Late Quaternary shoreline morphodynamics* CD. eds Carter, R.W.G. and Woodroffe. Cambridge, UK: Cambridge University Press.
- De Moortel, I., S. A. Munday, and A. W. Hood. 2004. Wavelet analysis: The effects of varying basic wavelet parameters. *Solar Physics* 222: 203-28.
- De Vries, S., B. Arens, M. Stive, and R. Ranasinghe. 2011. Dune growth trends and the effect of beach width on annual timescales. *Coastal Sediments*.
- Demarest, J. M., and Leatherman, S. P. 1985. Mainland influence on coastal transgression: Delmarva Peninsula. *Barrier Islands: Marine Geology*, 63 (1-4): 19-33.
- Dolan, R., B. P. Hayden, and C. Jones. 1979. Barrier island configuration. *Science* 204 (4391): 401-3.
- Donnelly, C., T. V. Wamsley, N. C. Kraus, M. Larson, and H. Hanson. 2006. Morphologic classification of coastal overwash. *Coastal Engineering*, San Diego, California, USA.
- Elko, N. A., A. H. Sallenger, K. Guy, H. F. Stockton, and K. L. M. Morgan. 2002. Barrier island elevations relevant to potential storm impacts: 1. techniques. *USGS Open File Report* 02-287.

- Emanuel, K. A. 2005. Increasing destructiveness of tropical cyclones over the past 30 years. *Nature* 436: 686-8.
- Fenster, M. S., and R. Dolan. 1996. Assessing the impact of tidal inlets on adjacent barrier island shorelines. *Journal of Coastal Research* 12 (1): 294-310.
- FitzGerald, D. M., M. S. Fenster, B. A. Argow, and I. V. Buynevich. 2008. Coastal impacts due to sea-level rise. *Annual Review of Earth and Planetary Sciences* 36: 601-47.
- Grinsted, A., J. C. Moore, and S. Jevrejeva. 2004. Application of the cross wavelet transform and wavelet coherence to geophysical time series. *Nonlinear Processes in Geophysics* 11: 561-6.
- Hayden, B. P., R. Dolan, and P. Ross. 1980. Barrier island migration. In *Thresholds in geomorphology.*, eds. Coates D.R., Vitek J.D. London, United Kingdom (GBR): George Allen & Unwin.
- Hobbs, C. H. III, D. E. Krantz, and G. L. Wikel. 2010. Coastal processes and offshore geology. In *The geology of Virginia*, eds. C. Bailey.
- Holman, R. A. 1986. Extreme value statistics for wave run-up on a natural beach. *Coastal Engineering*, 9: 527-544.
- Houser, C., and S. Hamilton. 2009. Sensitivity of post-hurricane beach and dune recovery to event frequency. *Earth Surface Processes and Landforms* 34: 613-28.
- Houser, C., C. Hapke, and S. Hamilton. 2008. Controls on coastal dune morphology, shoreline erosion and barrier island response to extreme storms. *Geomorphology* 100: 223-40.
- Houser, C., and S. Mathew. 2011. Alongshore variation in foredune height in response to transport potential and sediment supply: South Padre Island, Texas. *Geomorphology* 125: 62-72.
- Intergovernmental Panel on Climate Change (IPCC). *Intergovernmental panel on climate change 4th assessment report (AR4): Synthesis report (SYR)*. Cambridge, UK: Cambridge University Press.
- Judge, E. K., M. F. Overton, and J. S. Fisher. 2003. Vulnerability indicators for coastal dunes. *Journal of Waterway, Port, Coastal and Ocean Engineering*: 270-8.

- Knutson, T. R., J. L. McBride, J. Chan, K. Emanuel, G. Holland, C. Lansea, I. Held, J. P. Kossin, A. K. Srivastava, and M. Sugi. 2010. Tropical cyclones and climate change. *Nature Geosciences* 3: 157-163.
- Kochel, R. C., J. H. Kahn, R. Dolan, B. P. Hayden, and P. F. May. 1985. U.S. mid-Atlantic barrier island geomorphology. *Journal of Coastal Research* 1 (1): 1-9.
- Kumar, P., and E. Foufoula-Georgiou. 1997. Wavelet analysis for geophysical applications. *Reviews of Geophysics* 35 (4): 385-412.
- Lazarus, E. D., A. Ashton, A. B. Murray, S. Tebbens, and S. Burroughs. In press. Cumulative versus transient shoreline change: Dependencies on temporal and spatial scale. *Geophysical Research Letters*.
- Leatherman, S. P., A. T. Williams, and J. S. Fisher. 1977. Overwash sedimentation associated with a large-scale northeaster. *Marine Geology* 24 (2): 109-21.
- Leatherman, S. P., and R. E. Zaremba. 1987. Overwash and aeolian processes on a U.S. northeast coast barrier. *Sedimentary Geology* 52: 183-206.
- Li, Y., L. Murray, and D. Reeve. 2005. Multi-scale variability of beach profiles at Duck: A wavelet analysis. *Coastal Engineering* 52: 1133-53.
- List, J. H., A. S. Farris, and C. Sullivan. 2006. Reversing storm hotspots on sandy beaches: Spatial and temporal characteristics. *Marine Geology* 226 (3): 261-79.
- Maraun, D., and J. Kurths. 2004. Cross wavelet analysis: Significance testing and pitfalls. *Nonlinear Processes in Geophysics* 11: 505-14.
- Meyers, S., B. Kelly, and J. O'Brien. 1993. An introduction to wavelet analysis in oceanography and meteorology: With application to the dispersion of yanai waves. *Monthly Weather Review* 121 (10): 2858-66.
- Moore, L. J., J. H. List, S. J. Williams, and D. Stolper. 2010. Complexities in barrier island response to sea level rise: Insights for numerical model experiments, North Carolina outer banks. *Journal of Geophysical Research* 115: 27.
- Morton, R. A., J. G. Paine, and J. C. Gibeaut. 1994. Stages and durations of post-storm beach recovery, southeastern Texas coast, U.S.A. *Journal of Coastal Research* 10 (4): 884-908.
- Morton, R. A., and A. H. Sallenger. 2003. Morphological impacts of extreme storms on sandy beaches and barriers. *Journal of Coastal Research* 19 (3): 560-73.

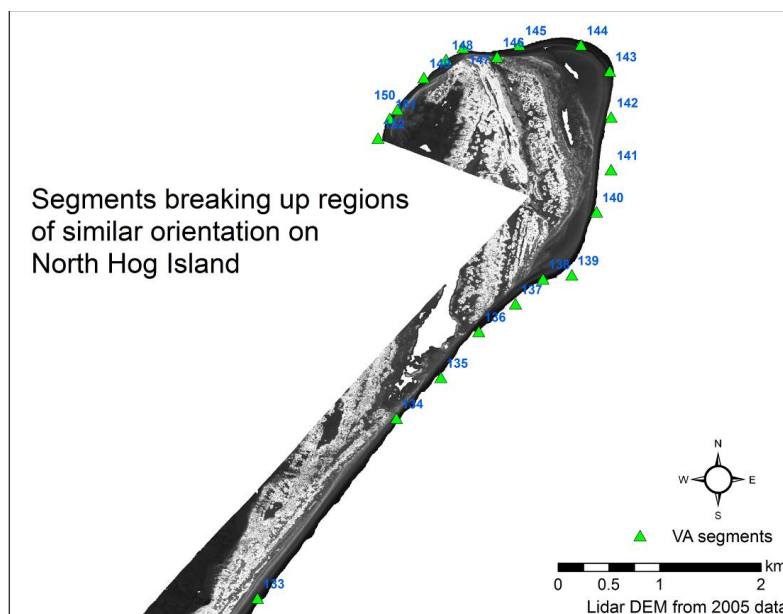
- Oertel, G. F., and K. Overman. 2004. Sequence morphodynamics at an emergent barrier island, middle Atlantic coast of North America. *Geomorphology* 58 (1-4): 67-83.
- Priestas, A. M., and S. Fagherazzi. 2010. Morphological barrier island changes and recovery of dunes after Hurricane Dennis, St. George Island, Florida. *Geomorphology* 114: 614-26.
- Psuty, N. 2008. The coastal foredune: A morphological basis for regional coastal dune development. *Coastal Dunes* 171 (1): 11-27.
- Rice, T. E., and S. P. Leatherman. 1983. Barrier island dynamics: The eastern shore of Virginia. *Southeastern Geology* 24: 125-37.
- Ruessink, B. G., G. Coco, R. Ranasinghe, and I. L. Turner. July, 2006. A cross-wavelet study of alongshore nonuniform nearshore sandbar behavior. *Proc. of the 2006 International Joint Conference on Neural Networks, Vancouver, Canada*: 8743-50.
- Sallenger, A. H. 2000. Storm impact scale for barrier islands. *Journal of Coastal Research* 16 (3): 890-5.
- Sallenger, A. H., W. Krabill, R. Swift, J. Brock, J. List, M. Hansen, R. Holman, et al. 2003. Evaluation of airborne scanning lidar for coastal change applications. *Journal of Coastal Research* 19 (1): 125-33.
- Sherman, D. J. 1995. Problems of scale in the modeling and interpretation of coastal dunes. *Marine Geology* 124: 339-49.
- Short, A. D., and P. A. Hesp. 1982. Wave, beach and dune interactions in southeastern Australia. *Marine Geology* 48: 259-84.
- Short, A. D., and A. C. Trembanis. 2004. Decadal scale patterns in beach oscillation and rotation Narrabeen Beach, Australia---time series, PCA and wavelet analysis. *Journal of Coastal Research* 20 (2): 523-32.
- Short, A. D., and L. D. Wright. 1983. Physical variability of sandy beaches. In *Sandy beaches as ecosystems*, eds. A. McLachlan, T. Erasmus, 133-144. The Netherlands: Junk: The Hague.
- Stallins, J. A., and A. J. Parker. 2003. The influence of complex systems interactions on barrier island dune vegetation pattern and process. *Annals of the Association of American Geographers* 93 (1): 13-29.

- Stockdon, H. F., K. S. Doran, and A. H. Sallenger. 2009. Extraction of lidar-based dune-crest elevations for use in examining the vulnerability of beaches to inundation during hurricanes. *Journal of Coastal Research* SI (53): 59-65.
- Stockdon, H. F., R. A. Holman, P. A. Howd, and A. H. Sallenger. 2006. Empirical parameterization of setup, swash, and runup. *Coastal Engineering* 53: 573-88.
- Stockdon, H. F., A. H. Sallenger, R. A. Holman, and P. A. Howd. 2007. A simple model for the spatially-variable coastal response to hurricanes. *Marine Geology* 238: 1-20.
- Torrence, C., and G. P. Compo. 1998. A practical guide to wavelet analysis. *Bulletin of the American Meteorological Society* 79 (1): 61-78.
- Weber, K. M., J. H. List, and K. L. M. Morgan. 2005. An operational mean high water datum for determination of shoreline position from topographic lidar data. *U.S. Geological Survey Open File Report 2005-1027*.
- Webster, P. J., G. J. Holland, J. A. Curry, and H. R. Chang. 2005. Changes in tropical cyclone number, duration, and intensity in a warming environment. *Science* 309: 1844-6.
- Wolner, C. W. V. W. 2011. Ecomorphodynamic feedbacks and barrier island evolution, Virginia Coast Reserve, USA. Masters of Science, University of Virginia.
- Wolner, C. W. V. W., L. J. Moore, D. R. Young, S. T. Brantley, S. N. Bissett, and R. A. McBride. In review. Ecomorphodynamic feedbacks and barrier island response to disturbance: Insights from the Virginia barrier islands, mid-Atlantic bight, USA. Submitted to: *Geomorphology*.
- Zhang, K., B. Douglas, and S. P. Leatherman. 2002. Do storms cause long-term beach erosion along the U.S. east barrier coast? *The Journal of Geology* 110: 493-502.

APPENDIX 1: METHODS

1.1 Feature extraction procedures

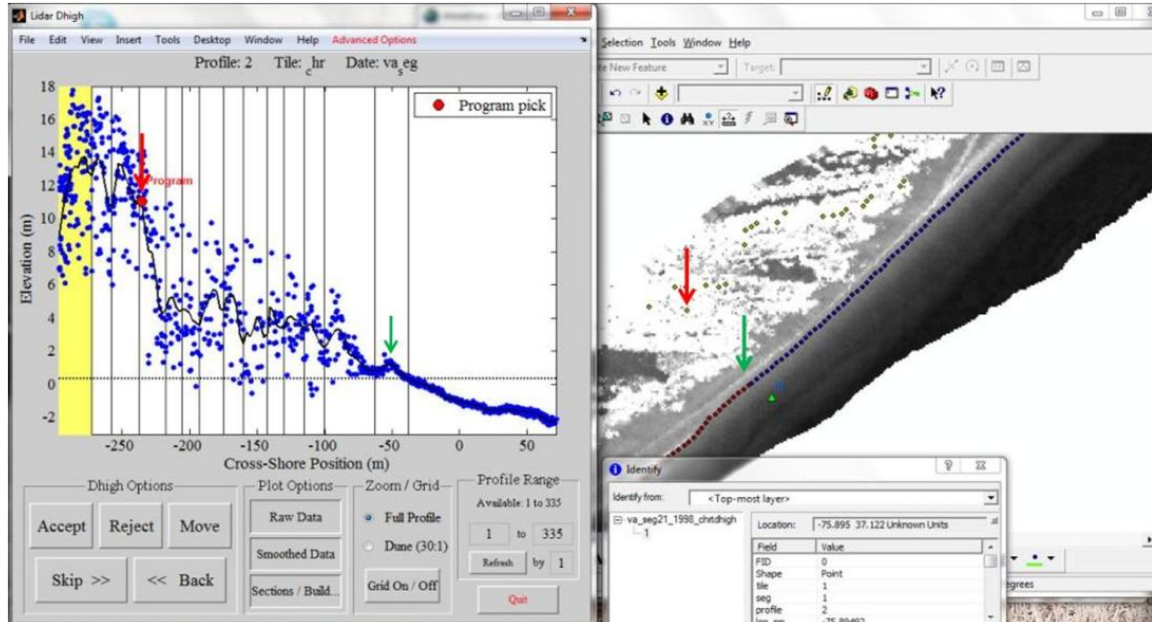
1. Grid lidar and extract profiles using Matlab algorithms provided by USGS Coastal Change Hazards Group.
 - a. To grid lidar, we generated an ArcGIS point file to break up the coast into segments of similar orientation. The same point feature was used for both 1998 and 2005 to keep the location of cross-shore profiles consistent even though shoreline orientation varied between years.
 - b. Once aligned north south, each segment was gridded and cross-shore profiles were extracted east-west every 10 m alongshore.
 - c. One cross-shore profile represents a 5 m wide area in the alongshore direction. The raw data points within one smoothed profile correspond to a 2.5 m area to the north and 2.5 m to the south of a transect.
 - d. Before smoothing the profiles, we filtered the raw data based on their normalized mean square error (NEi), which provides a means for removing transects over inlets or in areas of poor coverage.
 - e. We extracted profiles along the entire VCR in 1998 and 2005 and generated about 10,000 transects for each year.



North Hog Island and the segments (green triangles) used to separate the coast into regions of similar orientation. Image source: lidar DEM from the 2005 data.

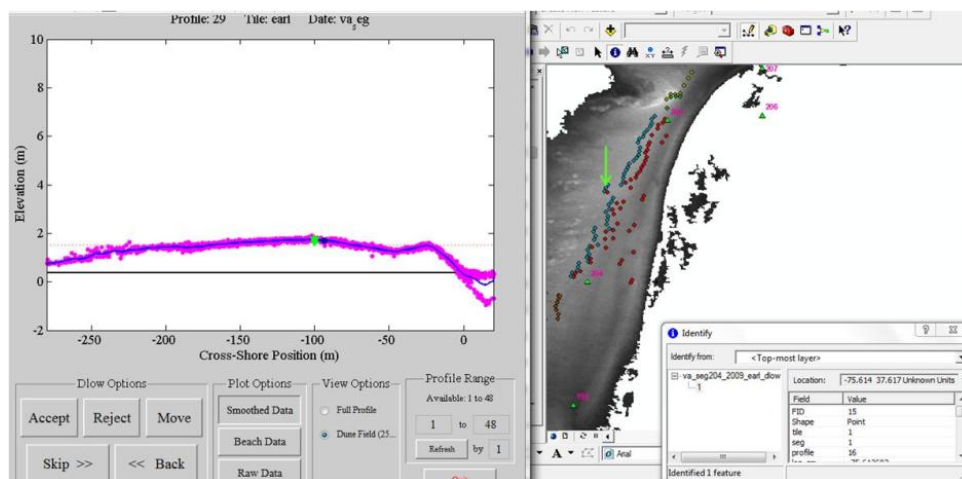
2. From smoothed profiles, the shoreline position was defined as the mean high water (MHW) elevation as defined for the state of Virginia, 0.34 m (Weber et al., 2005).
 - a. The lateral position of this intersection is determined by the seaward-most eastern facing point at 0.34 m elevation. The purpose of using MHW is to avoid water interference with the lidar signal.
 - b. After automated selection generates ArcGIS feature points, manual editing is required to delete incorrect points in ArcMap, then converted back to .mat files.

3. We used a Matlab graphical user interface (GUI) to automatically select dhight for each profile. The code selects dhight by segmenting the smoothed profiles at troughs and defines peaks as inflection points between a seaward and landward facing slope (*i.e.* dune crests, relic dunes, or vegetation) ideally picking the highest seaward-most peak to represent the foredune. The automated program has a tendency to incorrectly identify points in areas of low dunes or significant vegetation coverage, so a significant amount of manual editing is required to verify dhight points. The following are the processes involved in manually editing dhight selections.
 - a. Once the automated GUI selects dhight, the user can go back and adjust the GUI settings to manually edit each transect within the GUI and adjust the selected dhight peak.
 - b. We accompanied the cross-shore profile view in the GUI with ArcMap displaying the dhight points alongshore.
 - c. We verified or corrected the dhight points based on the following:
 - i. If the dune appeared to be the most seaward dune.
 - ii. If the dune was ideally present through multiple lidar scans.
 - iii. If the dune appeared to be located at a point consistent with the other nearby selections alongshore.
 - iv. If there was no dune present we selected the berm or the peak of the overwash terrace.



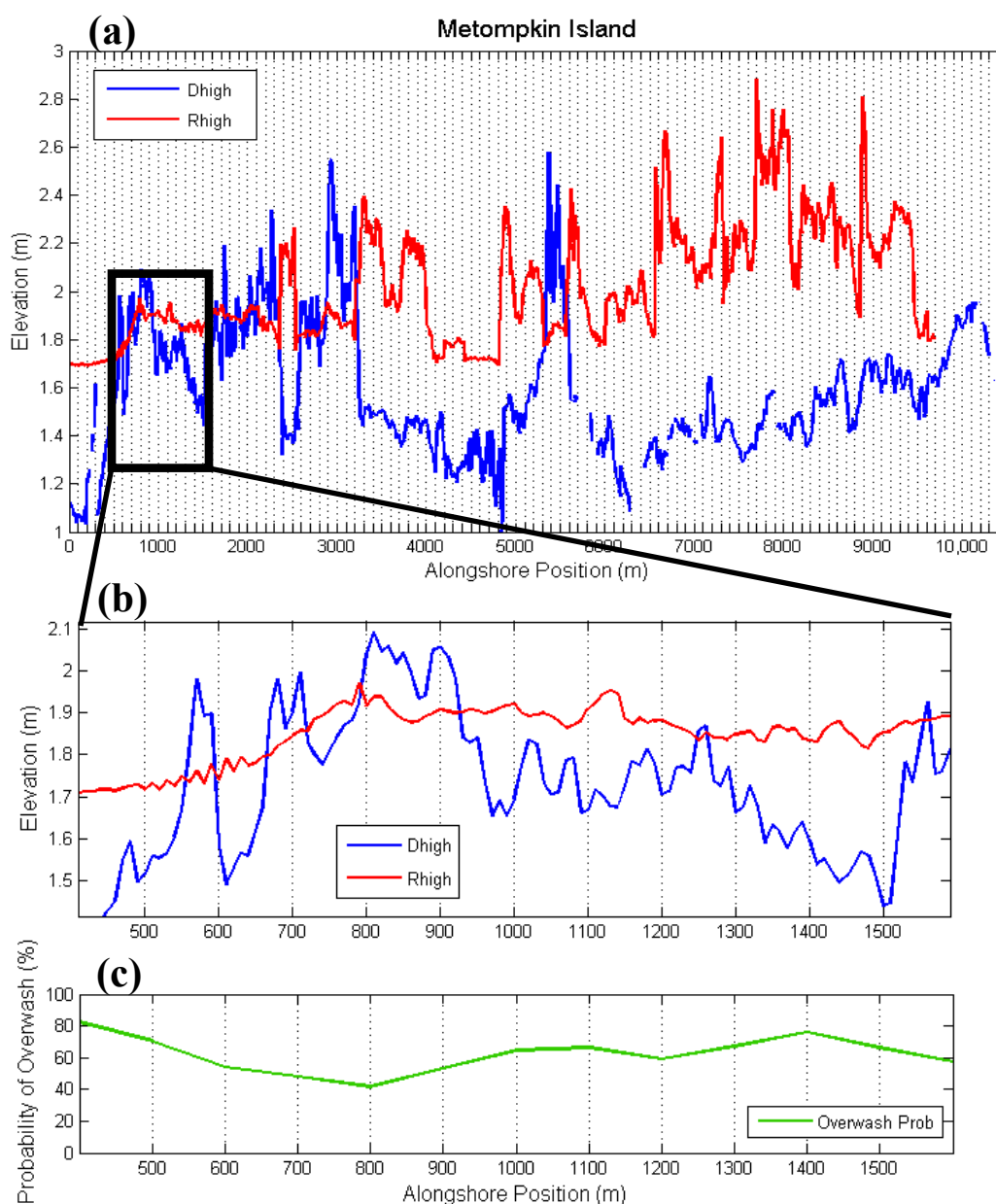
Screen capture of the editing process for dhigh. Profile (left) showing raw lidar data (blue dots), smoothed profile (black line), segments breaking up smoothed profile by slope and troughs (vertical black lines), automatically selected dhigh (red dot and arrow), and where the user will move the correct dhigh point to (green arrow). The 1998 lidar shown in ArcMap (right) also has shoreline (dark blue) and dhigh (light green/yellow) points plotted. The red arrow corresponds to the dhigh point being edited and the green arrow marks where the manually corrected dhigh point will move to. An additional note about this example is that this is the 1998 data prior to elevation correction and the smoothed profiles were raised 0.99m.

4. Extraction of dlow is similar to extraction of dhigh, where dlow is defined as the point of transition, seaward of dhigh, between a steep slope facing east and a flatter slope to indicate the transition from the foredune to the foreshore. Or, the point of greatest slope change. Therefore, the selection of dlow in Matlab automatically selects a point that is confined between the shoreline and dhigh on each transect.
 - a. We set constraints in the ‘Advanced Options’ to limit the elevation range a dlow may be selected. A berm threshold defines an elevation point at which anything above is considered dune and anything below is a berm.
 - b. After processing and editing dhigh points we used an elevation threshold of 1.5 m for the VCR to define whether a profile was a berm or dune profile.
 - c. In the case of a dhigh peak below 1.5 m it is flagged as a berm profile and no dlow was selected. These methods are defined by the Sallenger Storm Impact Scale where the berm acts as the dhigh and dlow (Sallenger, 2000; Elko et al., 2002). We noticed the dlow selection using the Matlab code was less consistent at picking the dune toe than the dune crest in the VCR. In many instances there was not a distinguishable toe but a gradual transition into the foreshore. In this case the automatically selected d lows were left for consistency, however, when it clearly picked an incorrect point, we manually moved the dlow in the GUI similar to the one used to edit dhigh.
 - d. Due to the greater difficulty with editing the dlow, we chose to use the dhigh location with the shoreline position as the measure of beach width.



Screen capture of dlow editing process. Left image shows raw lidar (pink dots), smoothed profile (blue line), dhigh (green star), and dlow (blue dot) in a profile that is near the threshold for a berm profile but just enough above 1.5 m that it qualifies as a dune. The image on the right shows the points in the left image with the green arrow. This is an overwash dominated region on the southern end of Cedar Island where the beach is between an overwashed dune or incipient dune or spit.

1.2 Overwash probabilities



(a) Alongshore data series of d_{high} and R_{high} spaced 10 m apart in 1998 on Metompkin Island. Each 100 m section is shown in between the vertical dashed lines along the x-axis. (b) Zoomed in spatial series of d_{high} and R_{high} from top panel showing alongshore data and 100 m sections that will be smoothed to create one overwash probability for each 100 m shown between the vertical dashed lines. (c) Overwash probability referring to panel (b) where one probability value represents 100 m alongshore and is determined by R_{high} values plotted with mean d_{high} on a normal cumulative distribution function.

1.3 Wavelet analysis parameters

The continuous wavelet transform (CWT) and wavelet coherence (WTC) analyses were conducted using Matlab functions Copyright (C) 2002-2004, Aslak Grinsted and available at <http://www.pol.ac.uk/home/research/>. The software includes the capability to do significance testing against red noise, correct for autocorrelation, and pad the time series with zeros. The following are the settings used in CWT and WTC analysis where all default options are in black and parameters specifically chosen for this study are in red italics and definition of parameters are written following % symbol.

CWT:

```
'Pad',1,...
%pad the time series with zeroes (1='yes',0='no')
'Dj',1/12, ...
%this will do 12 sub-octaves per octave=octaves per scale
'S0',0.5*dt,...
%minimum scale: 0.5*dt starts at a scale of 50 m
'Mother','Paul', ...
%mother waveform
'MaxScale',[100],...
%maximum scale, 100 means max scale of 10,000 m
'AR1','auto');
%autocorrelation coefficient: 'auto'=naïve ar1 estimator
```

WTC:

```
'Pad',1,...
%pad the time series with zeroes (1='yes',0='no')
'Dj',1/12, ...
%this will do 12 sub-octaves per octave=octaves per scale
'S0',0.5*dt,...
%minimum scale: 0.5*dt starts at a scale of 50 m
'Mother','Paul', ...
%mother waveform
'MaxScale',[100],...
%maximum scale, 100 means max scale of 10,000 m
'MonteCarloCount',300,...
%number of surrogate data sets in significance calculation
'AR1','auto',...
%autocorrelation coefficient: 'auto'=naïve ar1 estimator
```

1.4 Surf similarity index

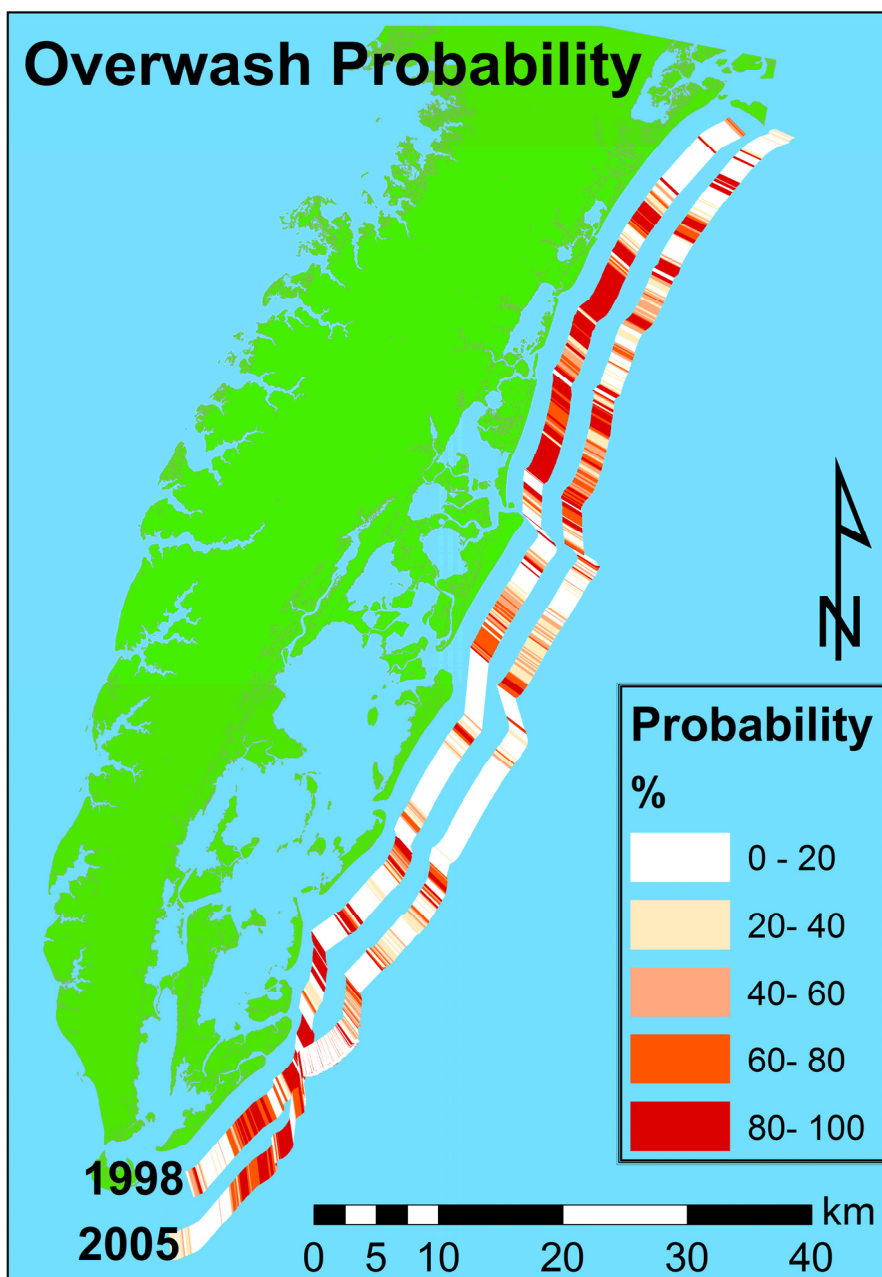
To distinguish between beach states we used the Surf Similarity Index (ζ) (SSI) defined by Battjes (1974). Where slope (β_f), significant wave height (H_o), and deep-water wavelength ($L_o = gT^2/2\pi$, where T = wave period) are used to determine the SSI with the equation below (Stockdon et al., 2006).

$$\zeta = \tan \frac{\beta_f}{(H_o/L_o)^{0.5}}$$

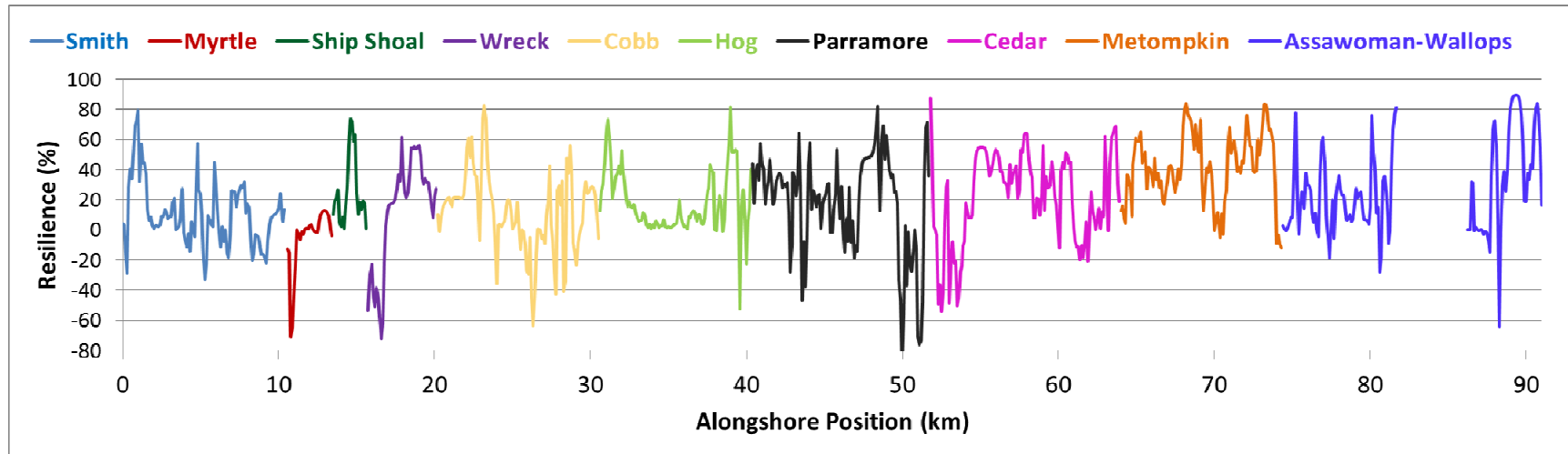
The SSI characterizes beaches into one of three states dissipative ($\zeta < 0.23$), intermediate ($\zeta = 0.23-1$), or reflective ($\zeta > 1$).

APPENDIX 2: SUPPLEMENTARY DATA

2.1 VCR resilience



Overwash probability of entire VCR in 1998 and 2005 using maximum Hurricane Bonnie conditions.



Resilience calculated alongshore of all islands in the VCR. No values were found in the middle of Assawoman and Wallops due to a lack of coverage in the 1998 lidar data.

2.2 Metompkin Island

Morphologic Summary Tables:

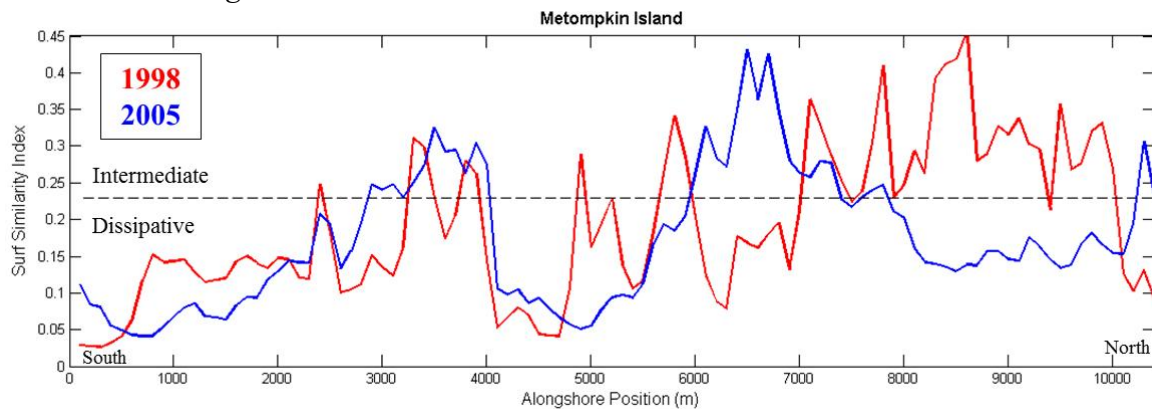
Metompkin Island (entire island 0-10,400 m)	$D_{high}^z \pm SD$ (m)	$D_{low}^z \pm SD$ (m)	Beach width \pm SD (m)	Slope \pm SD	Overwash probability \pm SD (%)	Shoreline change \pm SD (m)	Change in $D_{high}^x \pm SD$ (m)
1998	1.58 \pm 0.25	1.08 \pm 0.66	43.96 \pm 29.38	-0.042 \pm 0.02	79.05 \pm 21.07		
2005	2.17 \pm 0.32	1.71 \pm 0.36	59.59 \pm 29.18	-0.038 \pm 0.02	38.10 \pm 25.82	-0.73 \pm 47.29	-16.35 \pm 47.81
North Metompkin Island (7,000-10,400 m)	$D_{high}^z \pm SD$ (m)	$D_{low}^z \pm SD$ (m)	Beach width \pm SD (m)	Slope \pm SD	Overwash probability \pm SD (%)	Shoreline change \pm SD (m)	Change in $D_{high}^x \pm SD$ (m)
1998	1.58 \pm 0.16	1.10 \pm 0.61	25.84 \pm 14.84	-0.063 \pm 0.02	89.60 \pm 14.08		
2005	2.12 \pm 0.22	1.64 \pm 0.12	44.77 \pm 7.18	-0.041 \pm 0.01	40.96 \pm 16.32	-38.91 \pm 27.57	-57.85 \pm 14.14
Middle Metompkin Island (4,000-7,000 m)	$D_{high}^z \pm SD$ (m)	$D_{low}^z \pm SD$ (m)	Beach width \pm SD (m)	Slope \pm SD	Overwash probability \pm SD (%)	Shoreline change \pm SD (m)	Change in $D_{high}^x \pm SD$ (m)
1998	1.44 \pm 0.24	0.74 \pm 0.73	48.53 \pm 27.95	-0.033 \pm 0.02	83.85 \pm 17.91		
2005	2.10 \pm 0.24	1.75 \pm 0.14	61.46 \pm 32.65	-0.0412 \pm 0.03	43.99 \pm 32.15	8.91 \pm 43.47	-4.01 \pm 37.65
South Metompkin Island (0-4,000 m)	$D_{high}^z \pm SD$ (m)	$D_{low}^z \pm SD$ (m)	Beach width \pm SD (m)	Slope \pm SD	Overwash probability \pm SD (%)	Shoreline change \pm SD(m)	Change in $D_{high}^x \pm SD$ (m)
1998	1.68 \pm 0.28	1.33 \pm 0.54	56.72 \pm 32.56	-0.031 \pm 0.02	65.89 \pm 21.97		
2005	2.27 \pm 0.43	1.74 \pm 0.56	71.44 \pm 33.16	-0.033 \pm 0.02	30.99 \pm 26.35	26.13 \pm 42.23	11.41 \pm 49.36

Averages and standard deviations of beach characteristics extracted from lidar data in 1998 and 2005. Averages reflect whole island values as well as sections along Metompkin Island (i.e., northern, middle, and southern Metompkin Island). For definitions of variables please refer to the table below and Figure 2.1.

Variables	Definitions
D_{high}^z	Elevation of the most seaward dune crest
ΔD_{high}^z	Change in elevation of dune crest (2005-1998)
ΔD_{high}^x	Change in cross-shore position of most seaward dune crest (2005-1998)
D_{low}^z	Elevation of the most seaward dune toe
Slope	Foreshore slope between D_{low}^z and shoreline (MHW)
Δ slope	Change in slope between D_{low}^z and shoreline (MHW) (2005-1998)
Beach width	Horizontal width between D_{high}^x and shoreline position (MHW)
Δ beachwidth	Change in horizontal width between D_{high}^x and shoreline position (2005-1998)
Δ shoreline	Change in cross-shore position of shoreline (MHW) (2005-1998)

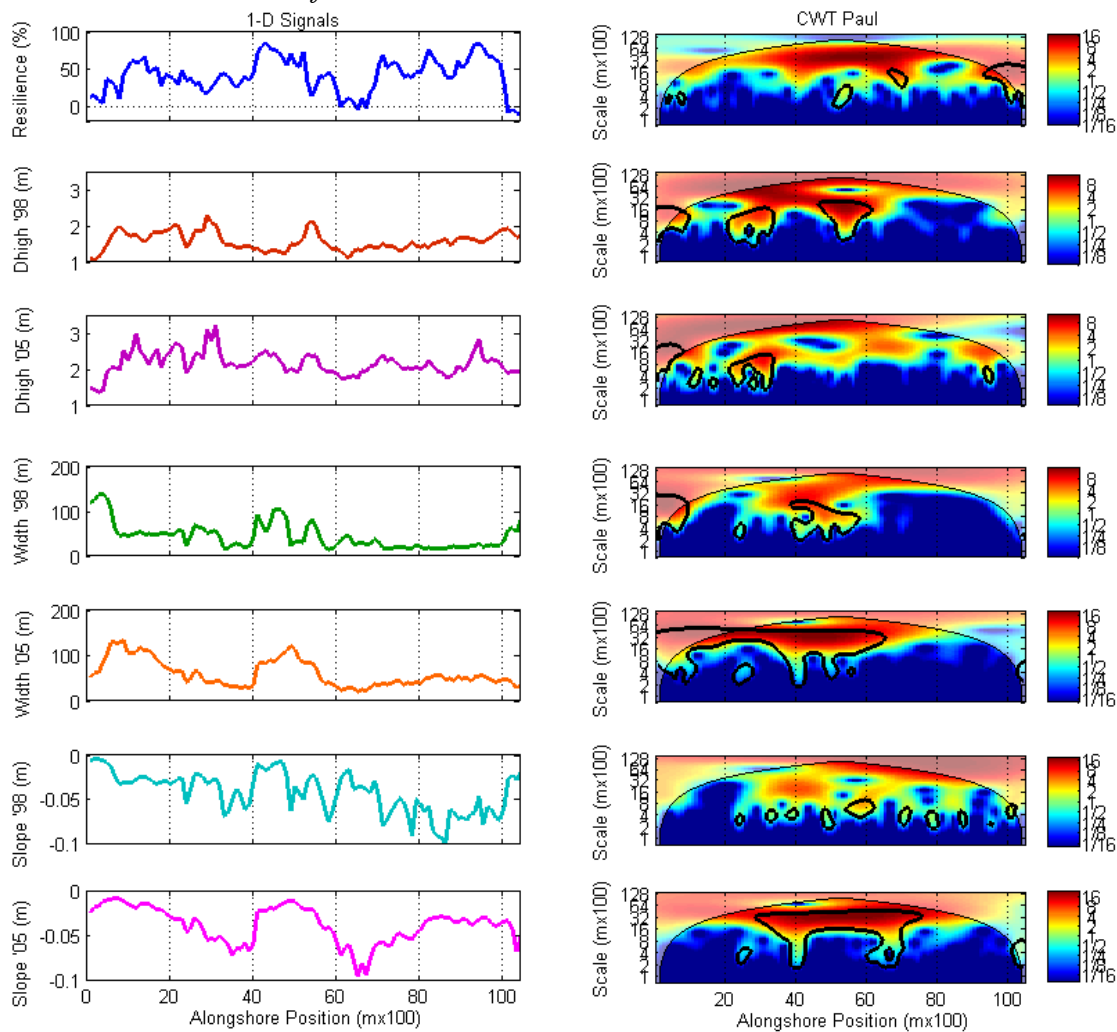
Definitions of morphologic variables extracted from lidar data and used in analyses.

Additional 1-D signals:

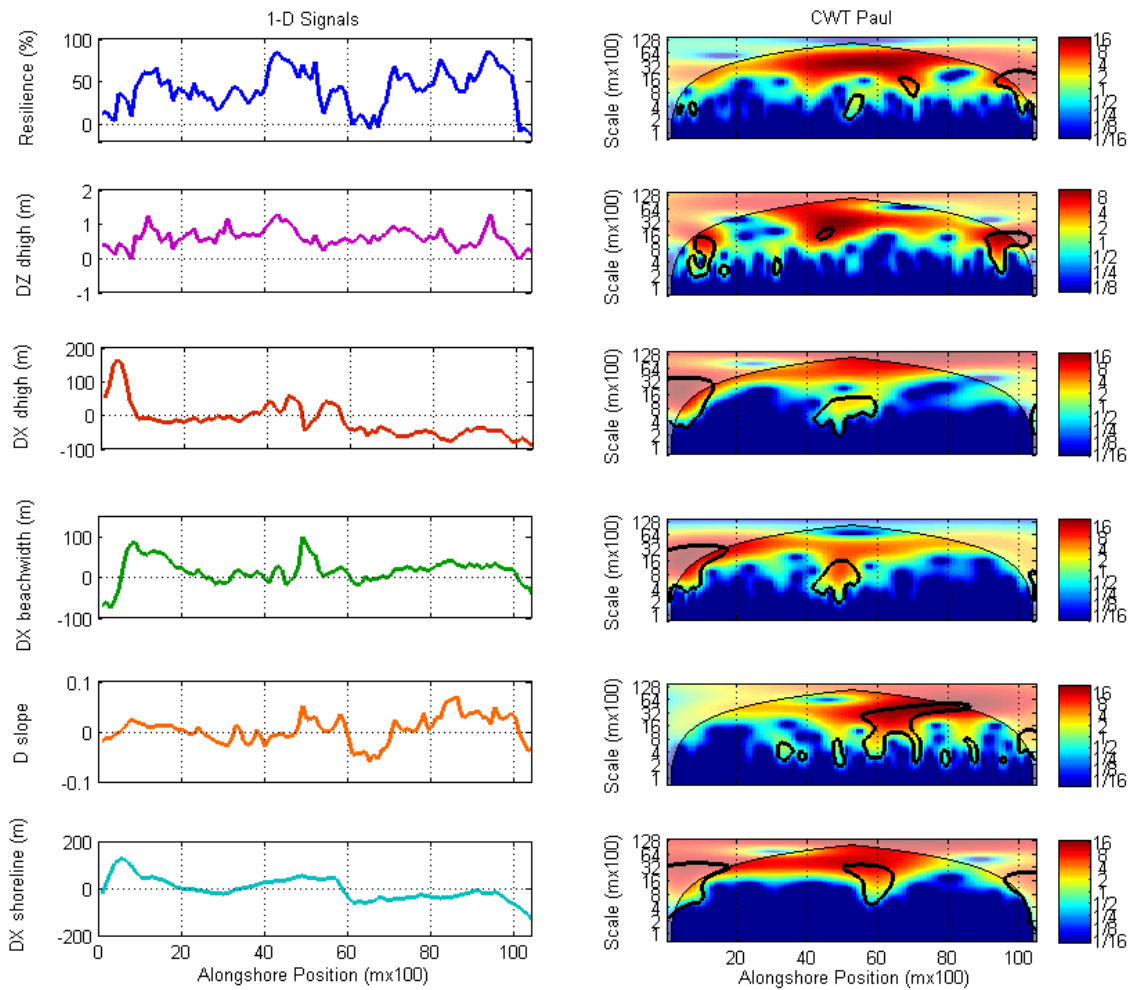


Surf Similarity Index (ζ) values calculated for Metompkin Island in 1998 (red) and 2005 (blue). Beaches are classified as dissipative when $\zeta < 0.23$ and as intermediate when $0.23 < \zeta < 1$, values greater than 1 are considered reflective.

Continuous wavelet transforms:

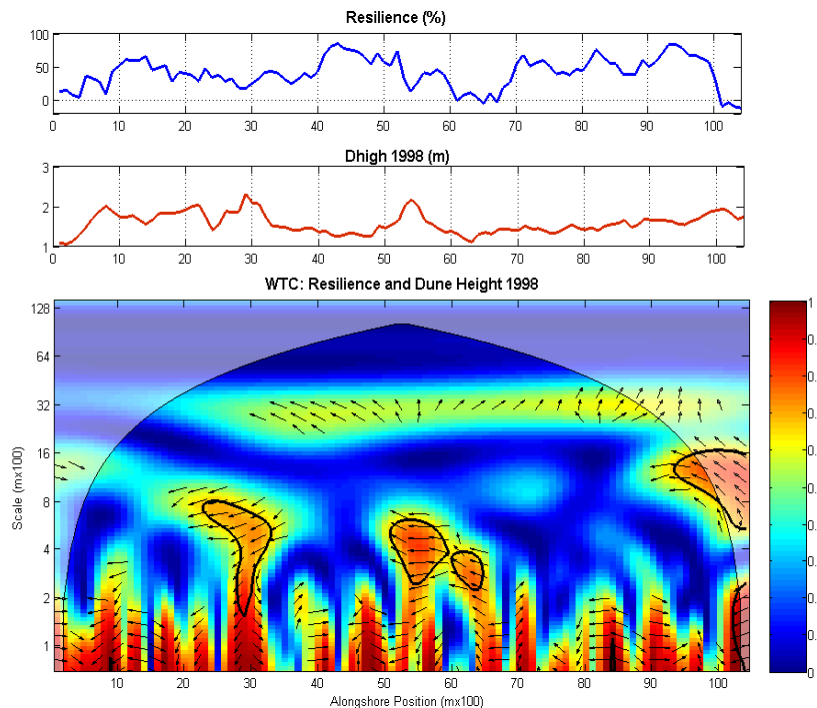


Left panels of 1-D morphologic signals in 1998 and 2005 along Metompkin Island. Right panels are corresponding CWT analyses using a Paul waveform. Scale bar depicts wavelet power where high power (in red) signifies the most variability along local space and scales.

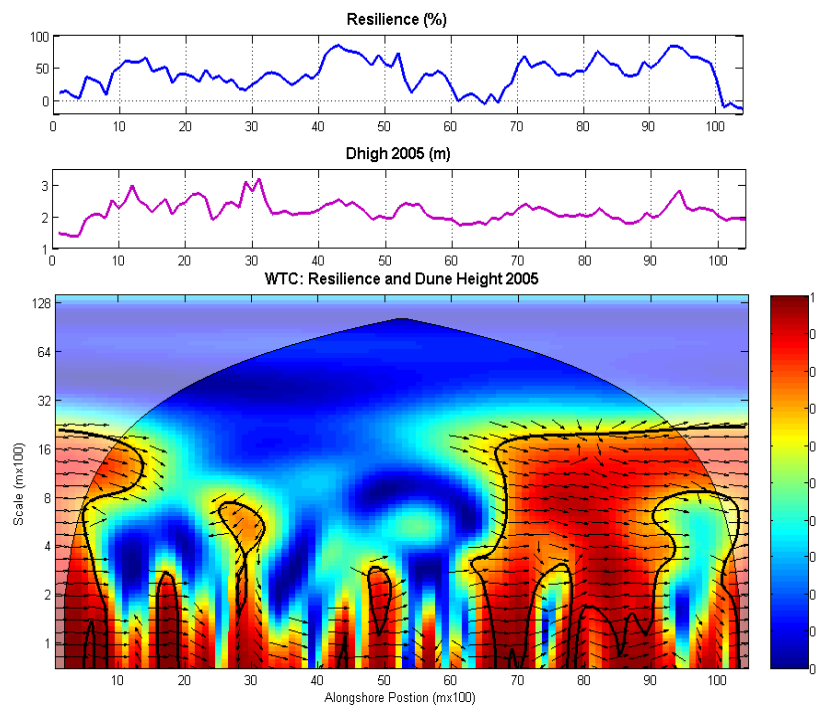


Left panel includes 1-D signals of morphologic *change* between 1998 and 2005 while right panels are corresponding CWT analyses of signals.

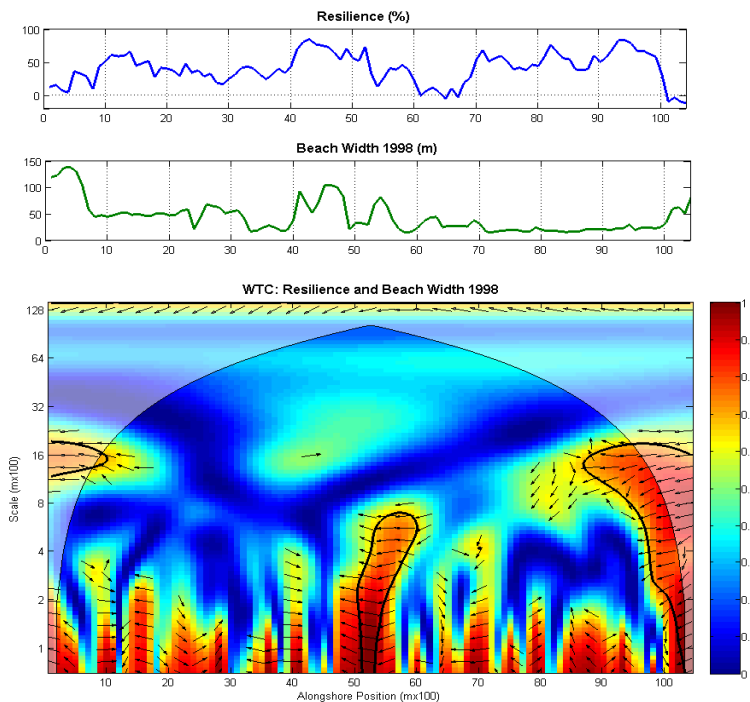
Wavelet coherence analyses:



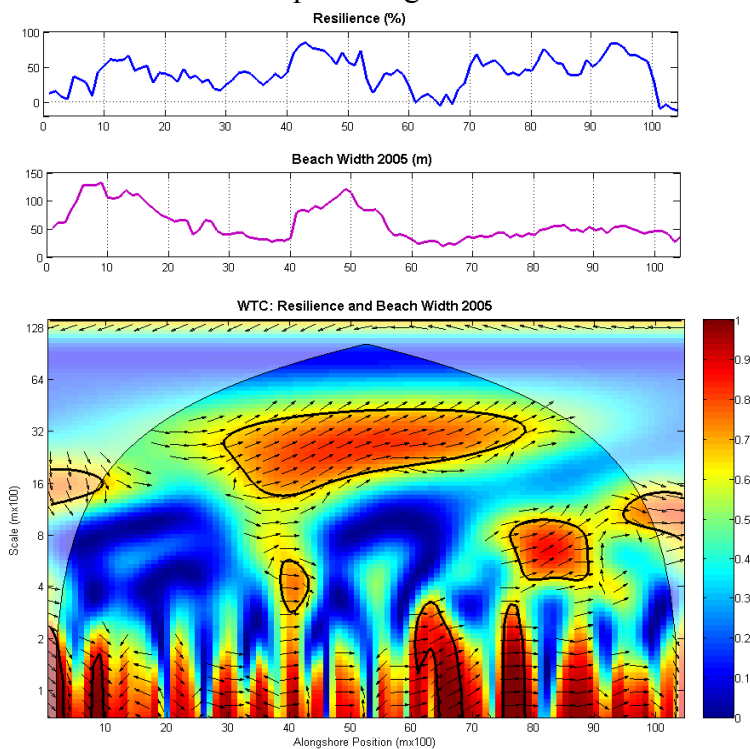
Wavelet coherence and phase angle of resilience and dhigh in 1998.



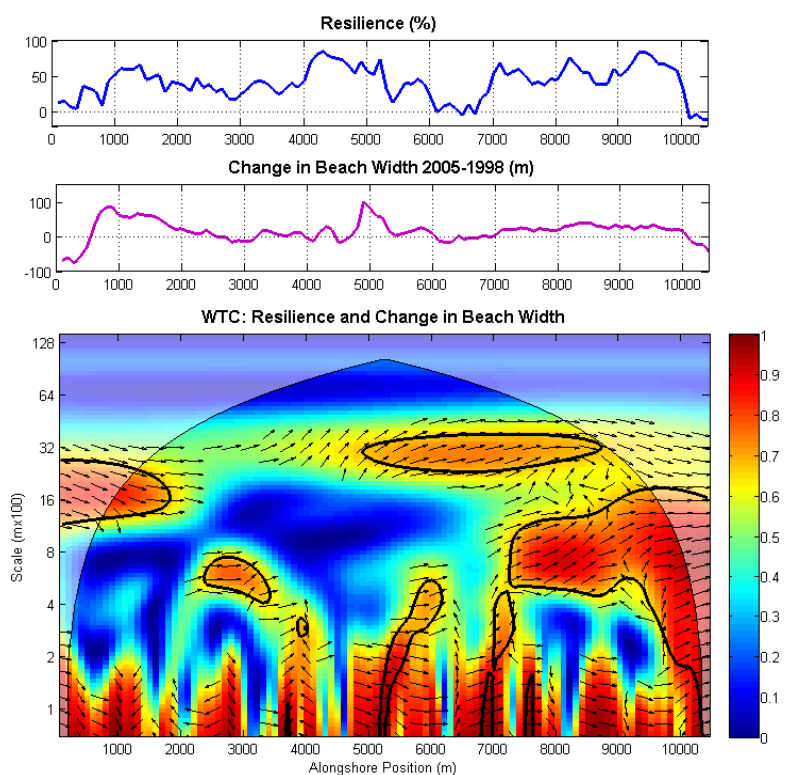
Wavelet coherence and phase angle of resilience and dhigh in 2005. Thick black contours represent 95% confidence interval and transparent regions are within the COI. Arrows pointing right are in-phase while arrows pointing left are anti-phase. Arrows pointing up are 90° out of phase where the top panel is south of the middle panel.



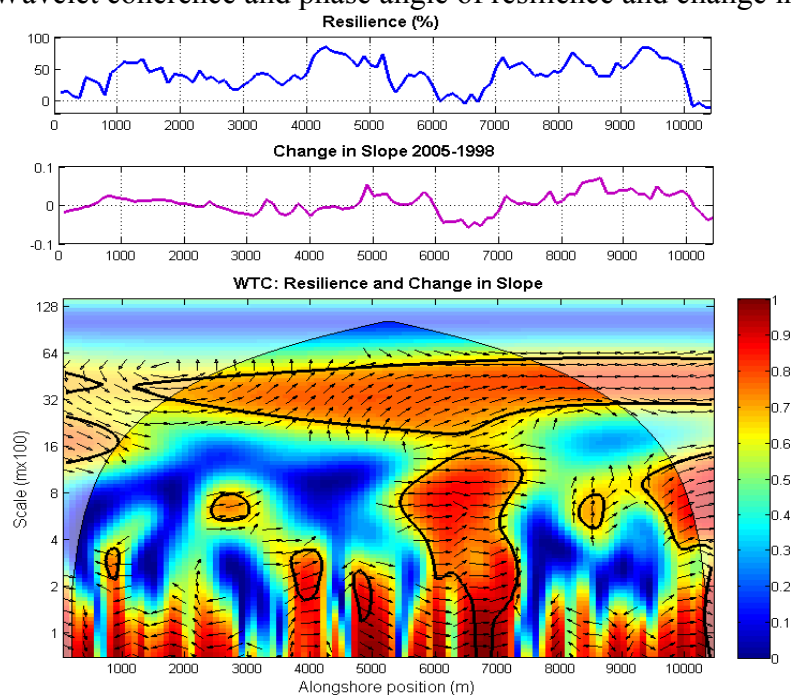
Wavelet coherence and phase angle of resilience and beach width in 1998.



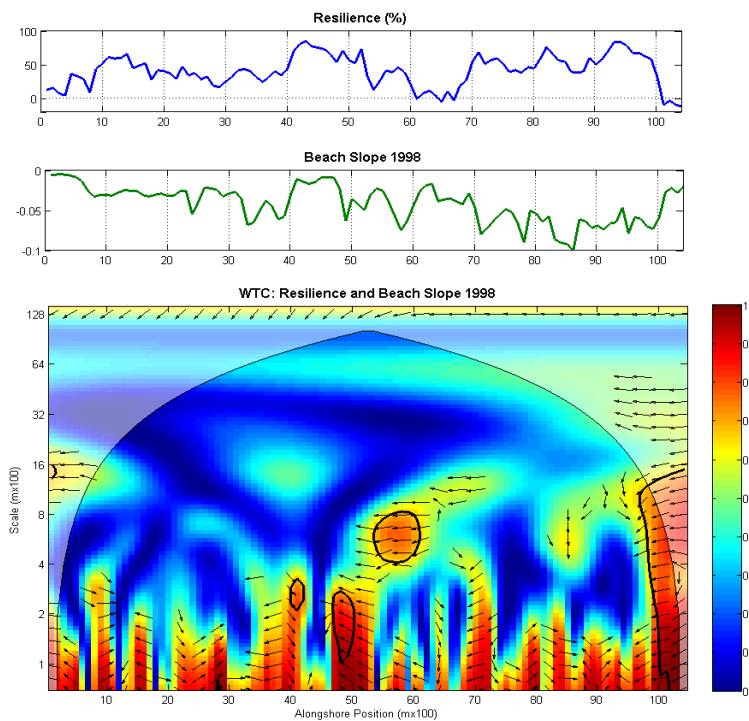
Wavelet coherence and phase angle of resilience and beach width in 2005. Thick black contours represent 95% confidence interval and transparent regions are within the COI. Arrows pointing right are in-phase while arrows pointing left are anti-phase. Arrows pointing up are 90° out of phase where the top panel is south of the middle panel.



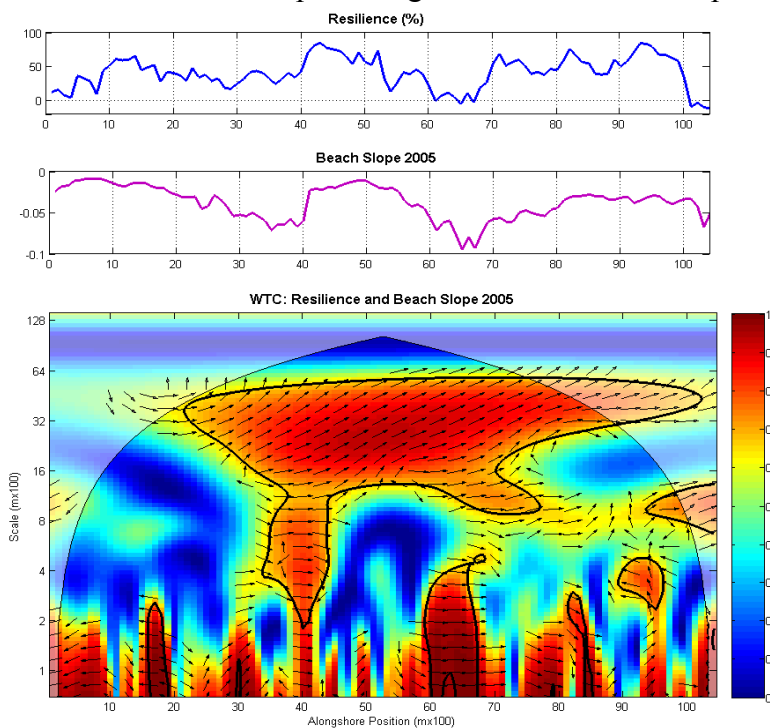
Wavelet coherence and phase angle of resilience and change in beach width.



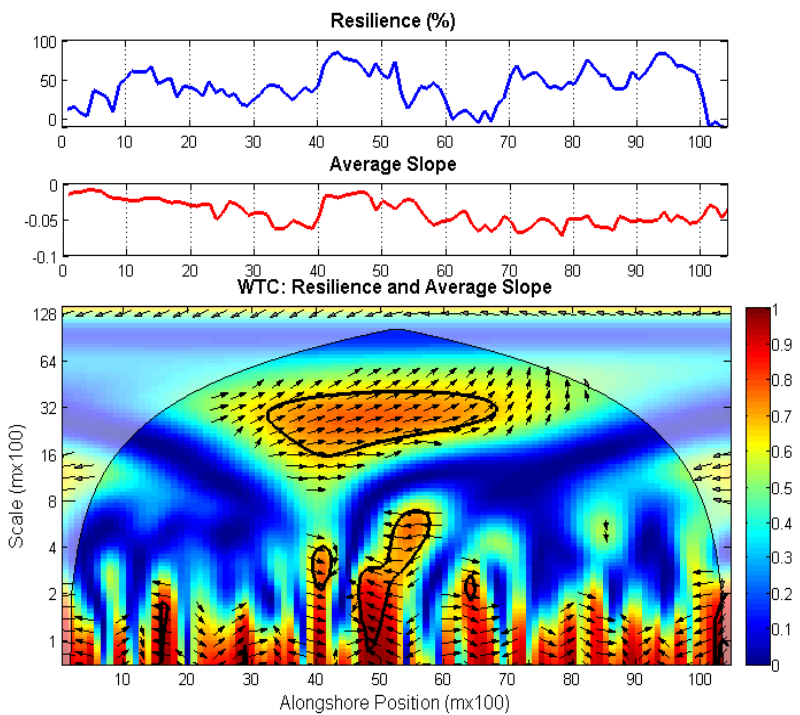
Wavelet coherence and phase angle of resilience and change in slope. Thick black contours represent 95% confidence interval and transparent regions are within the COI. Arrows pointing right are in-phase while arrows pointing left are anti-phase. Arrows pointing up are 90° out of phase where the top panel is south of the middle panel.



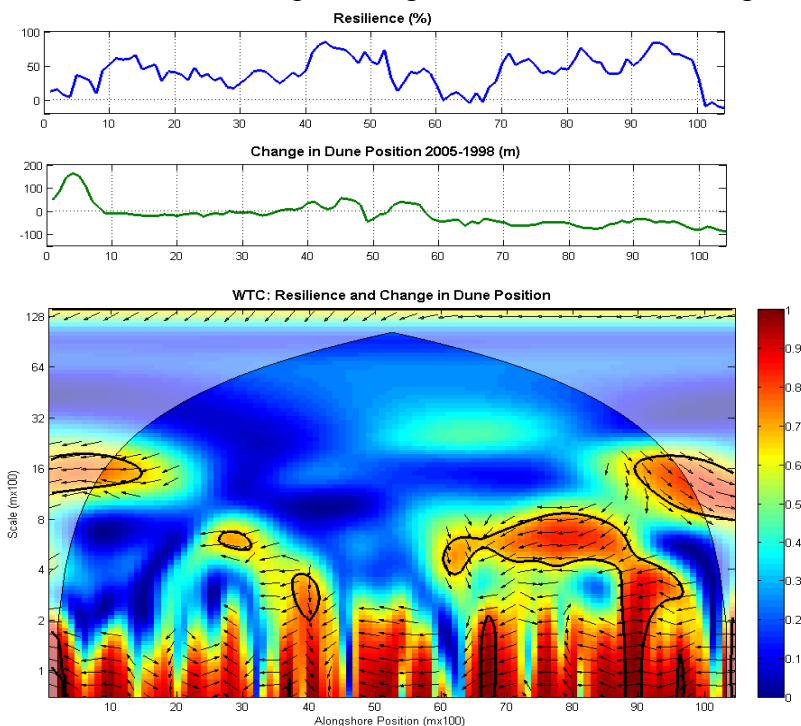
Wavelet coherence and phase angle of resilience and slope in 1998.



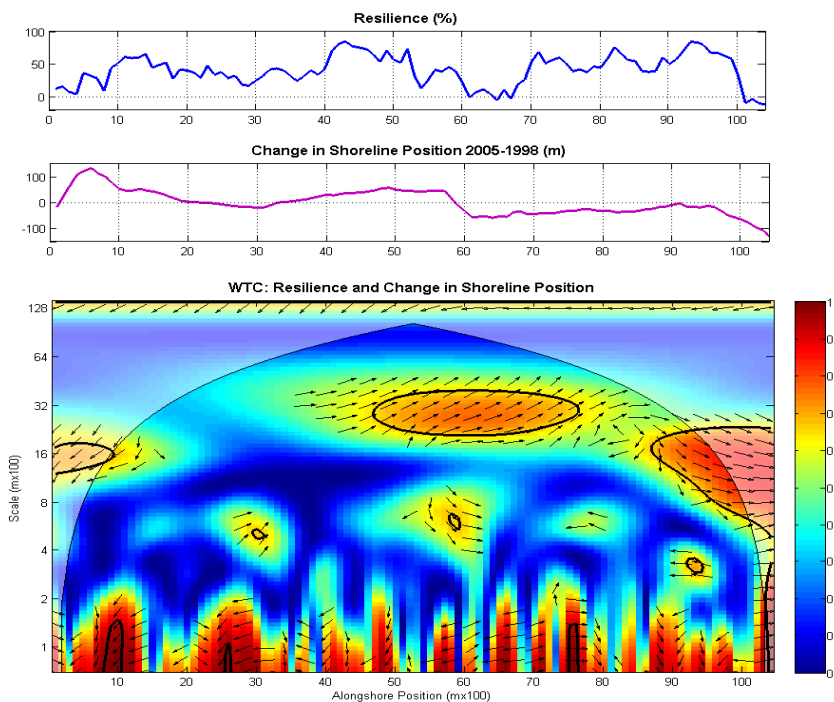
Wavelet coherence and phase angle of resilience and slope in 2005. Thick black contours represent 95% confidence interval and transparent regions are within the COI. Arrows pointing right are in-phase while arrows pointing left are anti-phase. Arrows pointing up are 90° out of phase where the top panel is south of the middle panel.



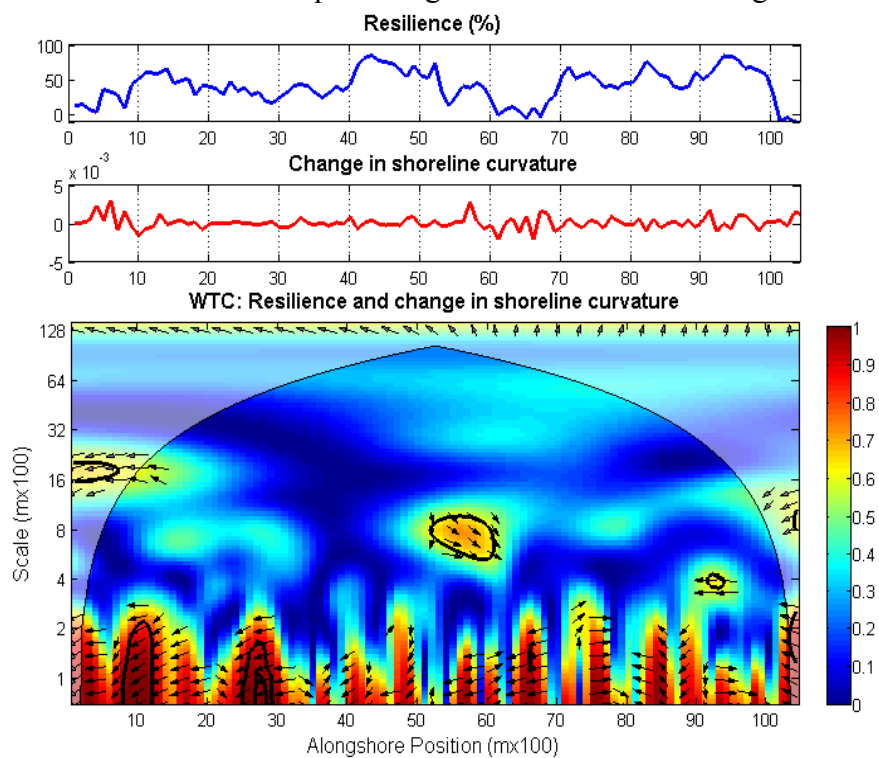
Wavelet coherence and phase angle of resilience and average slope.



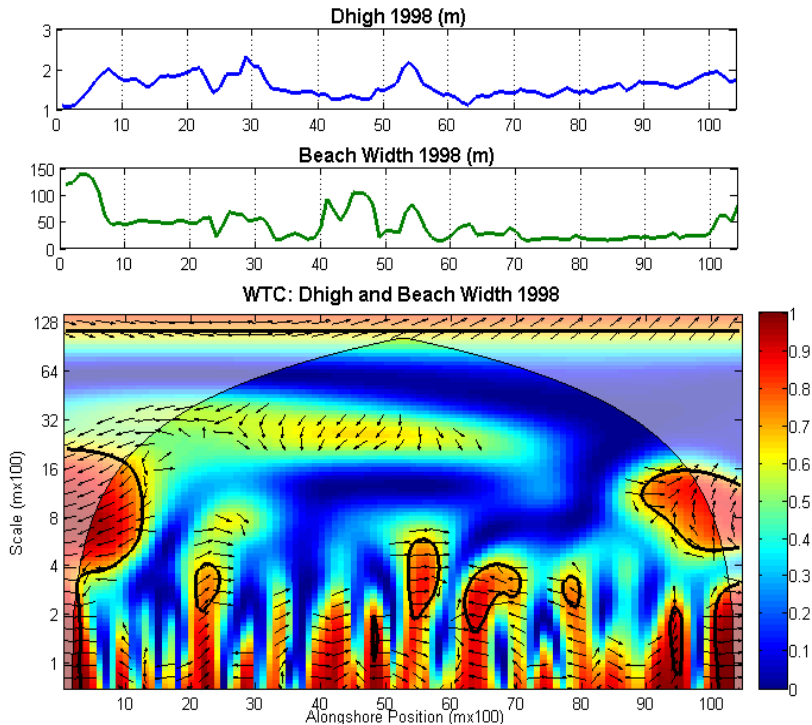
Wavelet coherence and phase angle of resilience and change in dune position. Thick black contours represent 95% confidence interval and transparent regions are within the COI. Arrows pointing right are in-phase while arrows pointing left are anti-phase. Arrows pointing up are 90° out of phase where the top panel is south of the middle panel.



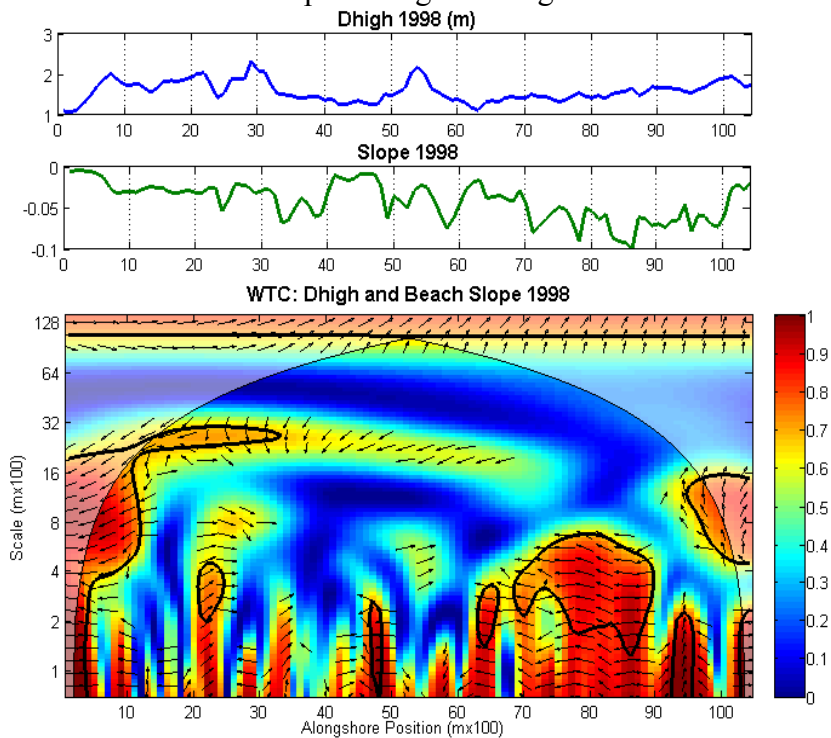
Wavelet coherence and phase angle of resilience and change in shoreline position.



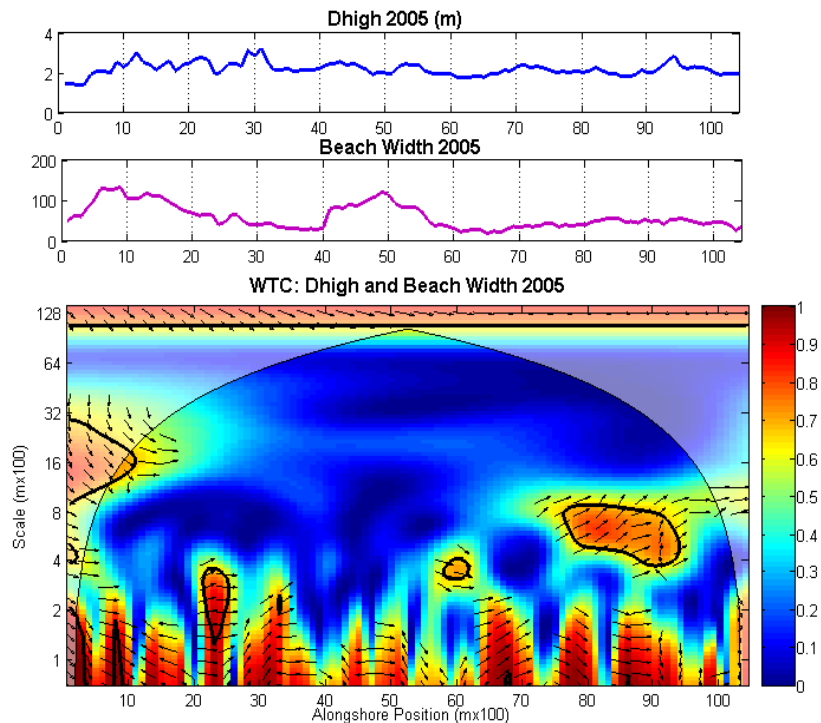
Coherence and phase angle of resilience and change in shoreline curvature. Thick black contours represent 95% confidence interval and transparent regions are within the COI. Arrows pointing right are in-phase while arrows pointing left are anti-phase. Arrows pointing up are 90° out of phase where the top panel is leading the middle panel.



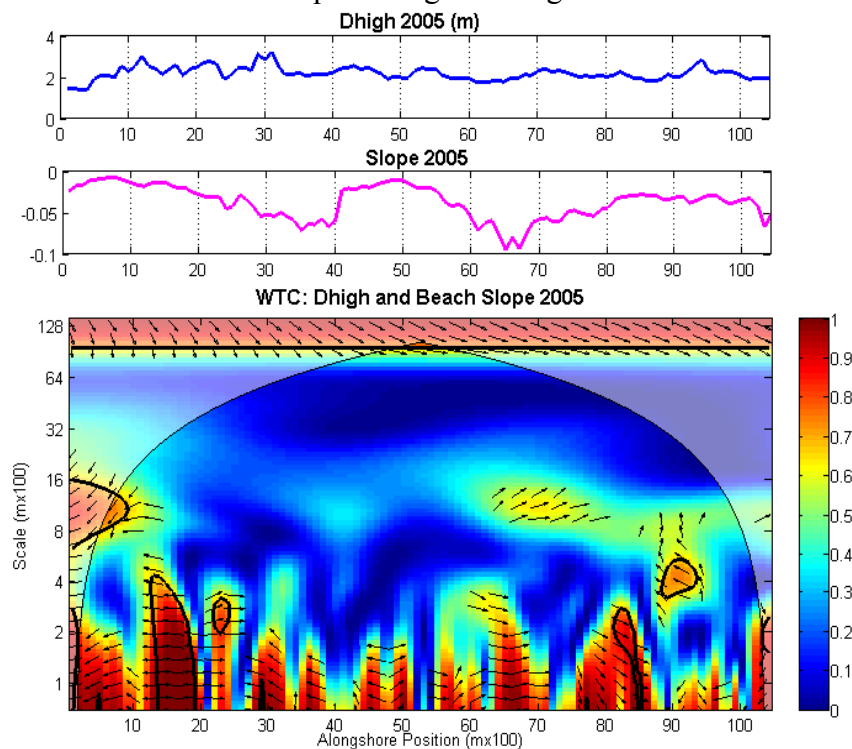
Wavelet coherence and phase angle of dhigh in 1998 and beach width in 1998.



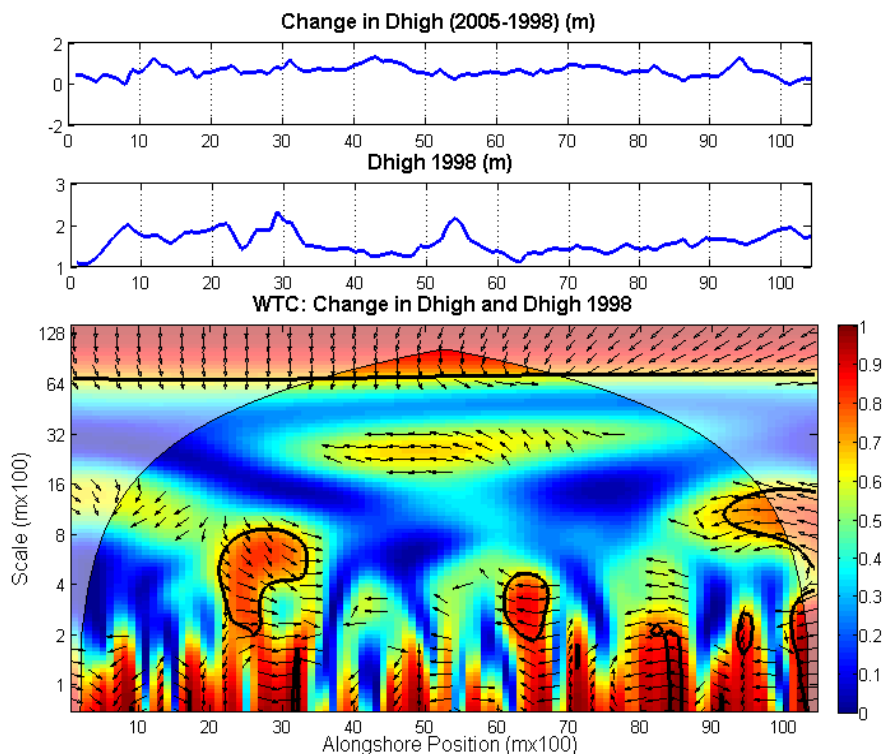
Wavelet coherence and phase angle of dhigh in 1998 and slope in 1998. Thick black contours represent 95% confidence interval and transparent regions are within the COI. Arrows pointing right are in-phase while arrows pointing left are anti-phase. Arrows pointing up are 90° out of phase where the top panel is south of the middle panel.



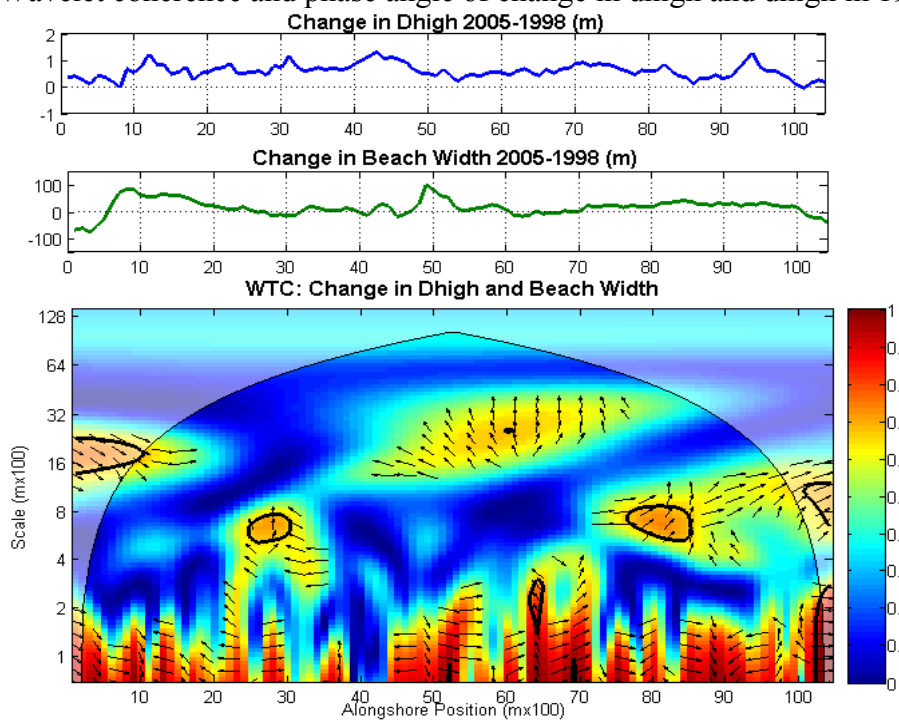
Wavelet coherence and phase angle of dhigh in 2005 and beach width in 2005.



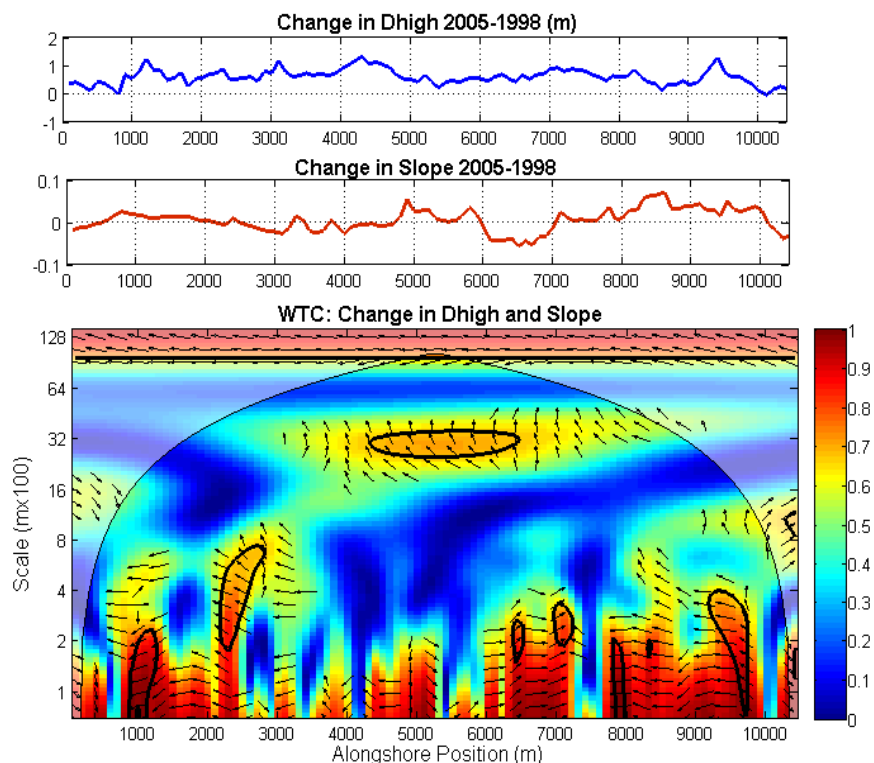
Wavelet coherence and phase angle of dhigh in 2005 and slope in 2005. Thick black contours represent 95% confidence interval and transparent regions are within the COI. Arrows pointing right are in-phase while arrows pointing left are anti-phase. Arrows pointing up are 90° out of phase where the top panel is south of the middle panel.



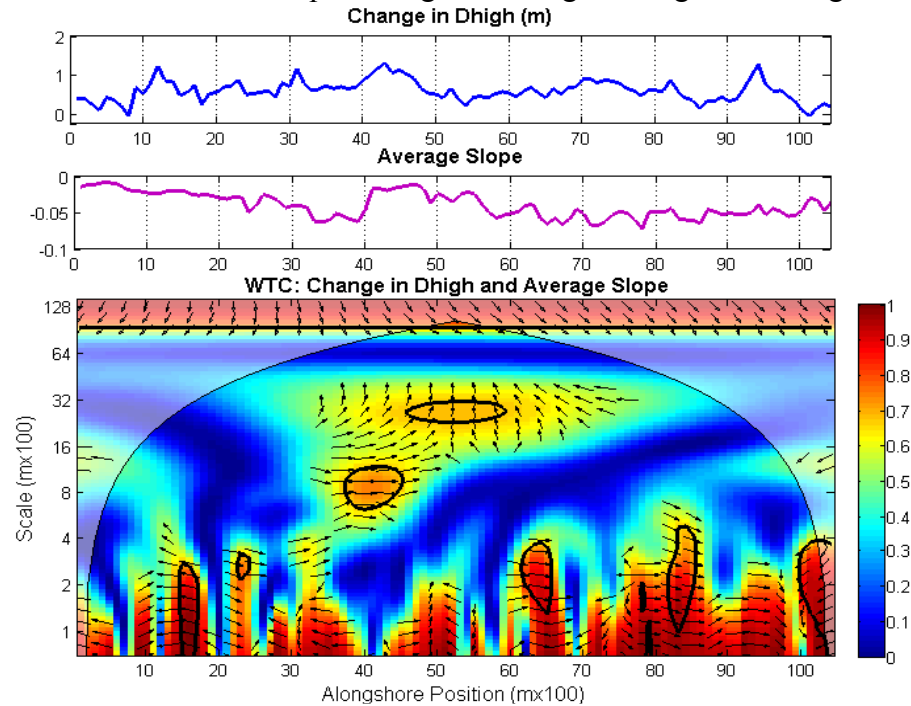
Wavelet coherence and phase angle of change in dhigh and dhigh in 1998.



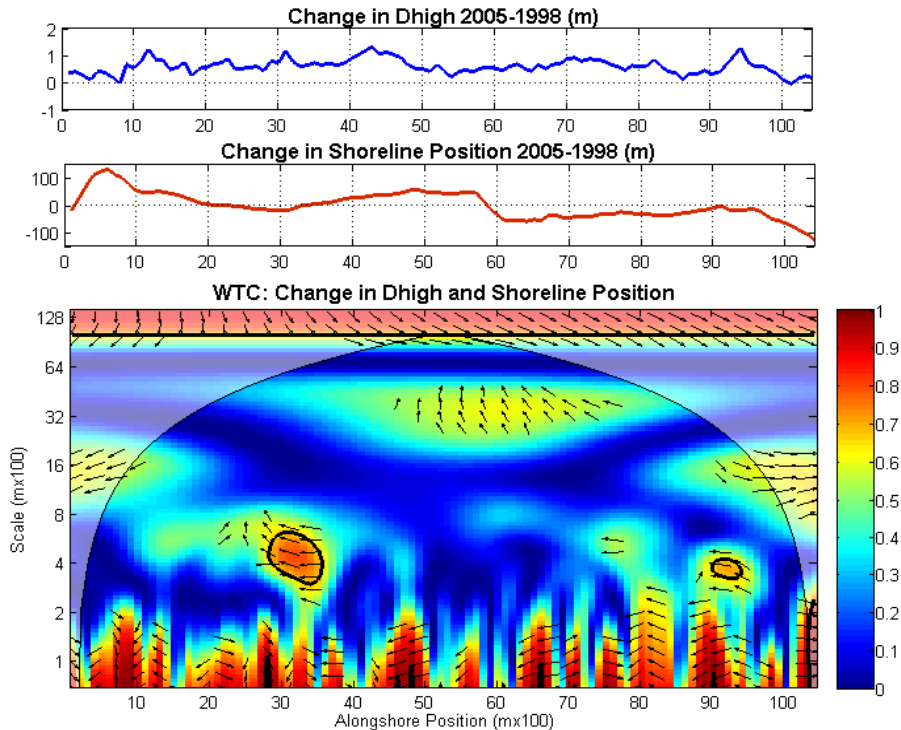
Wavelet coherence and phase angle of change in dhigh and change in beach width. Thick black contours represent 95% confidence interval and transparent regions are within the COI. Arrows pointing right are in-phase while arrows pointing left are anti-phase. Arrows pointing up are 90° out of phase where the top panel is south of the middle panel.



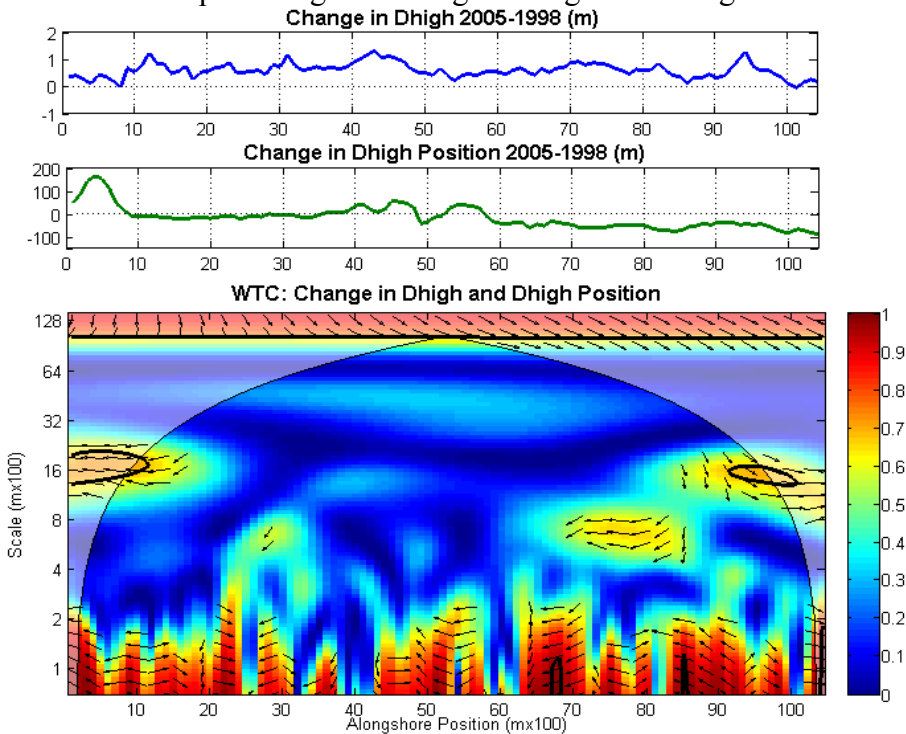
Wavelet coherence and phase angle of change in dhhigh and change in slope.



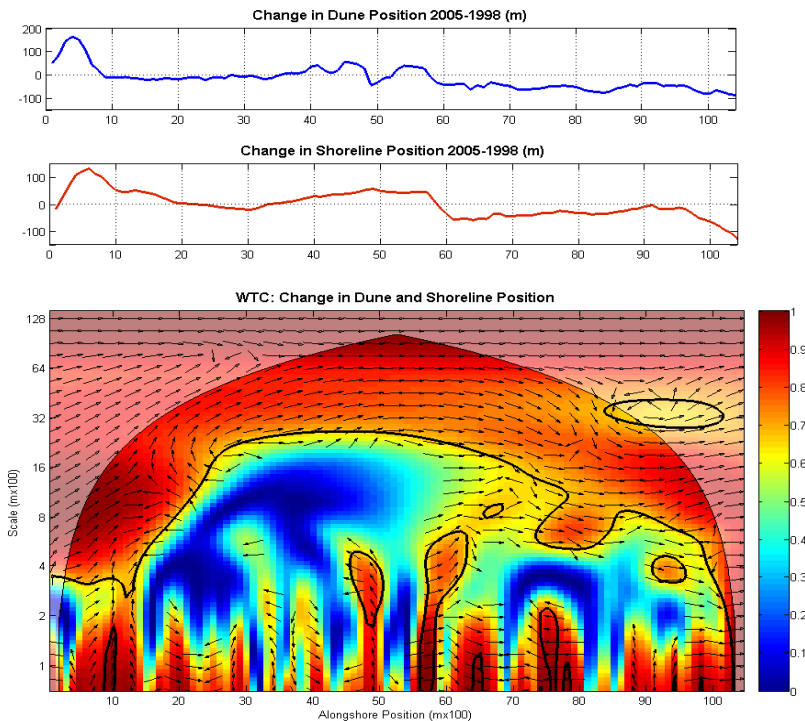
Wavelet coherence and phase angle of change in dhhigh and average slope. Thick black contours represent 95% confidence interval and transparent regions are within the COI. Arrows pointing right are in-phase while arrows pointing left are anti-phase. Arrows pointing up are 90° out of phase where the top panel is south of the middle panel.



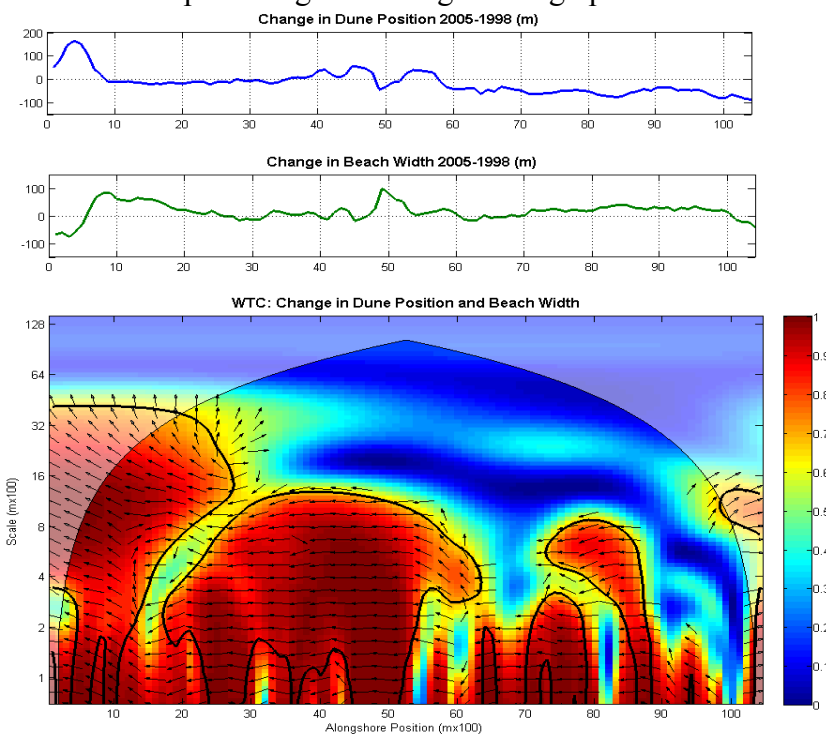
Coherence and phase angle of change in dhigh and change in shoreline position



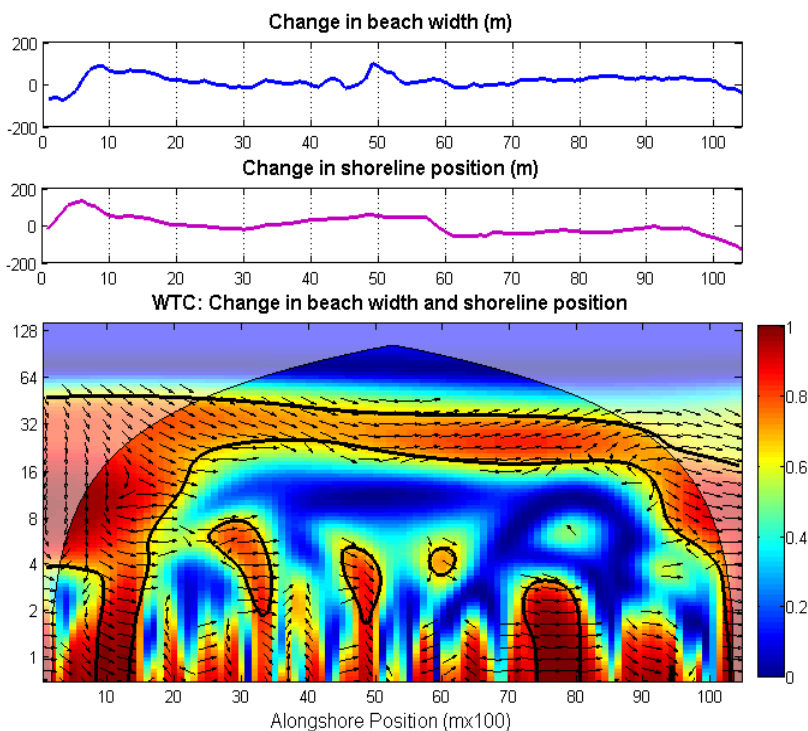
Coherence and phase angle of change in dhigh and change in dhigh position. Thick black contours represent 95% confidence interval and transparent regions are within the COI. Arrows pointing right are in-phase while arrows pointing left are anti-phase. Arrows pointing up are 90° out of phase where the top panel is south of the middle panel.



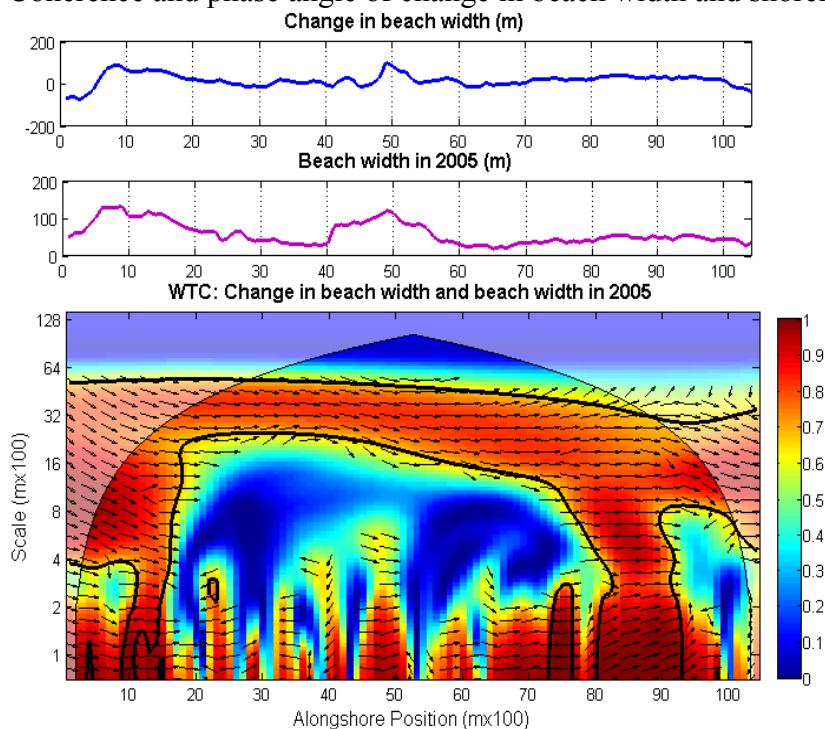
Coherence and phase angle of change in dune position and shoreline position.



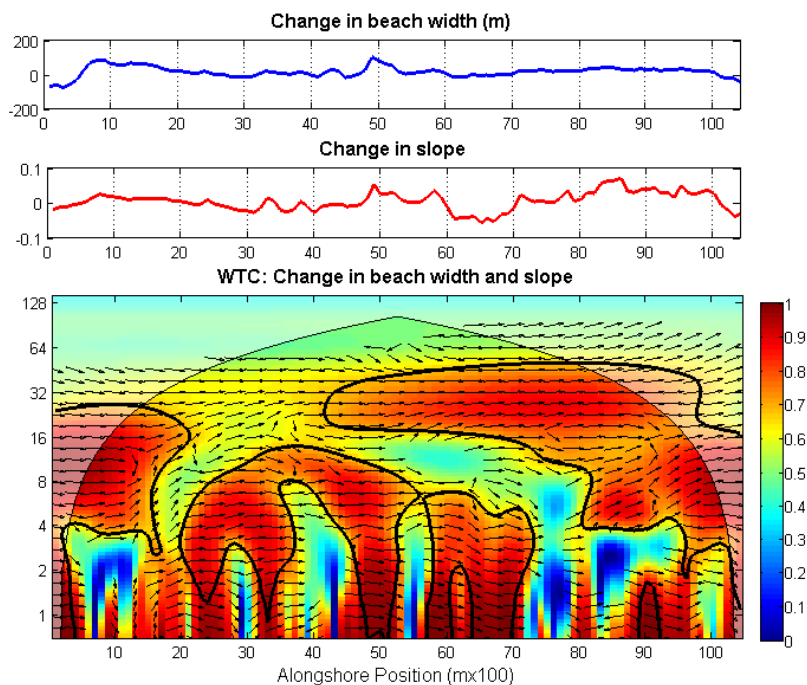
Coherence and phase angle of change in dune position and change in beach width. Thick black contours represent 95% confidence interval and transparent regions are within the COI. Arrows pointing right are in-phase while arrows pointing left are anti-phase. Arrows pointing up are 90° out of phase where the top panel is south of the middle panel.



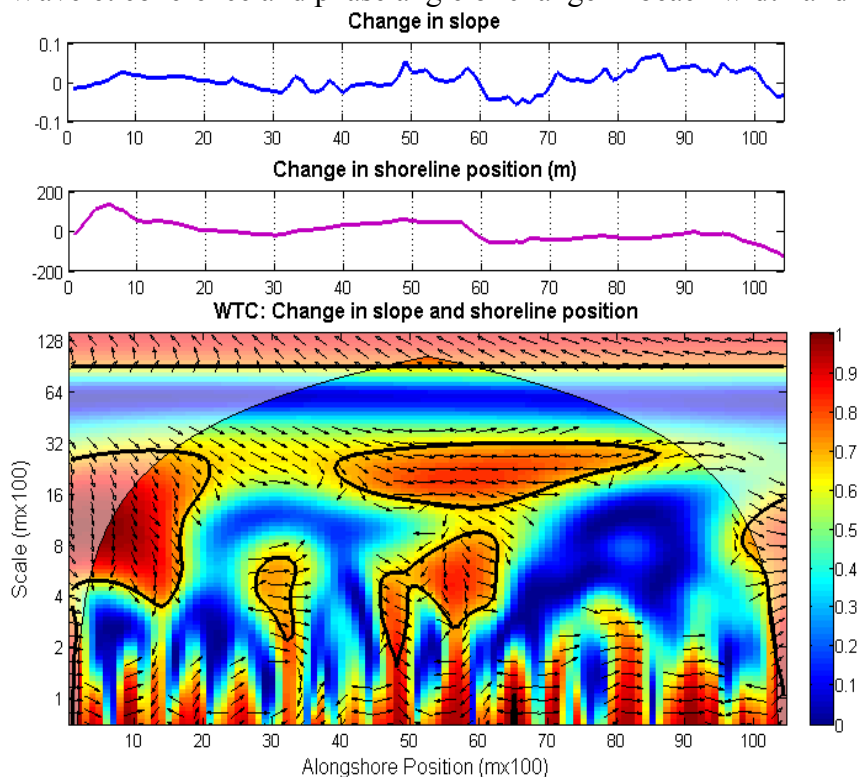
Coherence and phase angle of change in beach width and shoreline position.



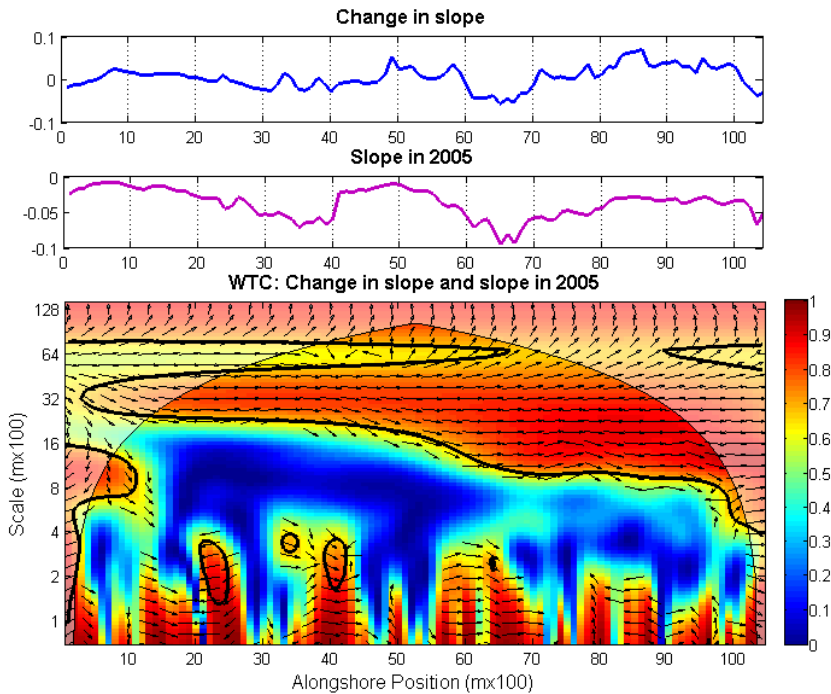
Coherence and phase angle of change in beach width and beach width in 2005. Thick black contours represent 95% confidence interval and transparent regions are within the COI. Arrows pointing right are in-phase while arrows pointing left are anti-phase. Arrows pointing up are 90° out of phase where the top panel is south of the middle panel.



Wavelet coherence and phase angle of change in beach width and slope.



Wavelet coherence and phase angle of change in slope and shoreline position. Thick black contours represent 95% confidence interval and transparent regions are within the COI. Arrows pointing right are in-phase while arrows pointing left are anti-phase. Arrows pointing up are 90° out of phase where the top panel is south of the middle panel.



Wavelet coherence and phase angle of change in slope and slope in 2005. Thick black contours represent 95% confidence interval and transparent regions are within the COI. Arrows pointing right are in-phase while arrows pointing left are anti-phase. Arrows pointing up are 90° out of phase where the top panel is south of the middle panel.

2.3 Smith Island

Morphologic Summary Tables:

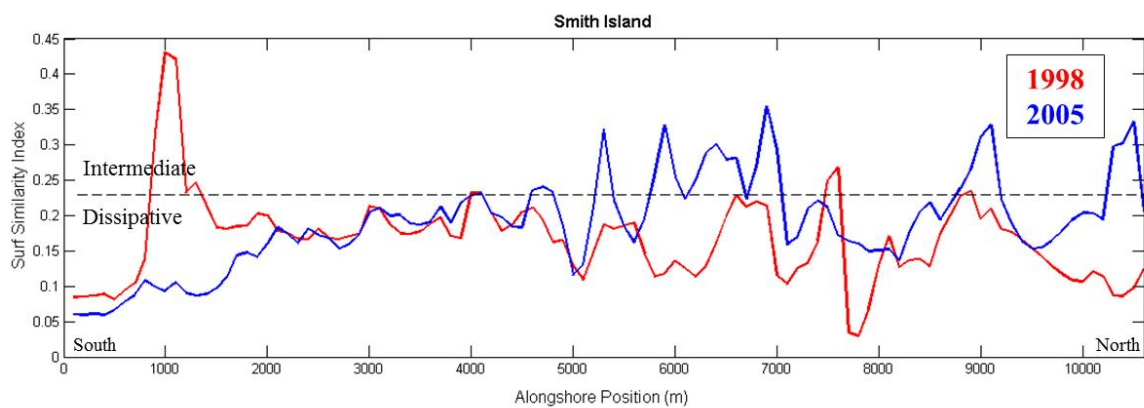
Smith Island (entire island 0- 10,400 m)	$D_{high}^z \pm SD$ (m)	$D_{low}^z \pm SD$ (m)	Beach width \pm SD (m)	Slope \pm SD	Overwash probability \pm SD (%)	Shoreline change \pm SD (m)	Change in $D_{high}^x \pm SD$ (m)
1998	2.02 \pm 0.67	1.64 \pm 0.16	42.94 \pm 11.80	-0.037 \pm 0.01	50.72 \pm 31.85		
2005	2.26 \pm 0.60	1.78 \pm 0.32	47.86 \pm 20.86	-0.042 \pm 0.01	42.17 \pm 33.76	-22.09 \pm 36.92	-26.07 \pm 25.36
North Smith Island (5,000- 10,600 m)	$D_{high}^z \pm SD$ (m)	$D_{low}^z \pm SD$ (m)	Beach width \pm SD (m)	Slope \pm SD	Overwash probability \pm SD (%)	Shoreline change \pm SD (m)	Change in $D_{high}^x \pm SD$ (m)
1998	1.59 \pm 0.28	1.53 \pm 0.06	40.76 \pm 9.11	-0.033 \pm 0.01	74.87 \pm 13.44		
2005	1.81 \pm 0.17	1.56 \pm 0.11	33.72 \pm 9.21	-0.048 \pm 0.01	71.22 \pm 13.85	-51.73 \pm 20.16	-44.69 \pm 20.50
South Smith Island (0-5,000 m)	$D_{high}^z \pm SD$ (m)	$D_{low}^z \pm SD$ (m)	Beach width \pm SD (m)	Slope \pm SD	Overwash probability \pm SD (%)	Shoreline change \pm SD (m)	Change in $D_{high}^x \pm SD$ (m)
1998	2.52 \pm 0.65	1.76 \pm 0.17	47.50 \pm 11.69	-0.037 \pm 0.01	22.62 \pm 20.97		
2005	2.80 \pm 0.45	2.03 \pm 0.29	64.29 \pm 18.77	-0.034 \pm 0.01	8.39 \pm 10.09	12.38 \pm 15.86	-4.42 \pm 5.17

Averages and standard deviations of beach characteristics extracted from lidar data in 1998 and 2005. Averages reflect whole island values as well as sections along Smith Island (i.e., northern, and southern Smith Island). For definitions of variables please refer to the table below and Figure 2.1.

Variables	Definitions
D_{high}^z	Elevation of the most seaward dune crest
ΔD_{high}^z	Change in elevation of dune crest (2005-1998)
ΔD_{high}^x	Change in cross-shore position of most seaward dune crest (2005-1998)
D_{low}^z	Elevation of the most seaward dune toe
Slope	Foreshore slope between D_{low}^z and shoreline (MHW)
Δ slope	Change in slope between D_{low}^z and shoreline (MHW) (2005-1998)
Beach width	Horizontal width between D_{high}^x and shoreline position (MHW)
Δ beachwidth	Change in horizontal width between D_{high}^x and shoreline position (2005-1998)
Δ shoreline	Change in cross-shore position of shoreline (MHW) (2005-1998)

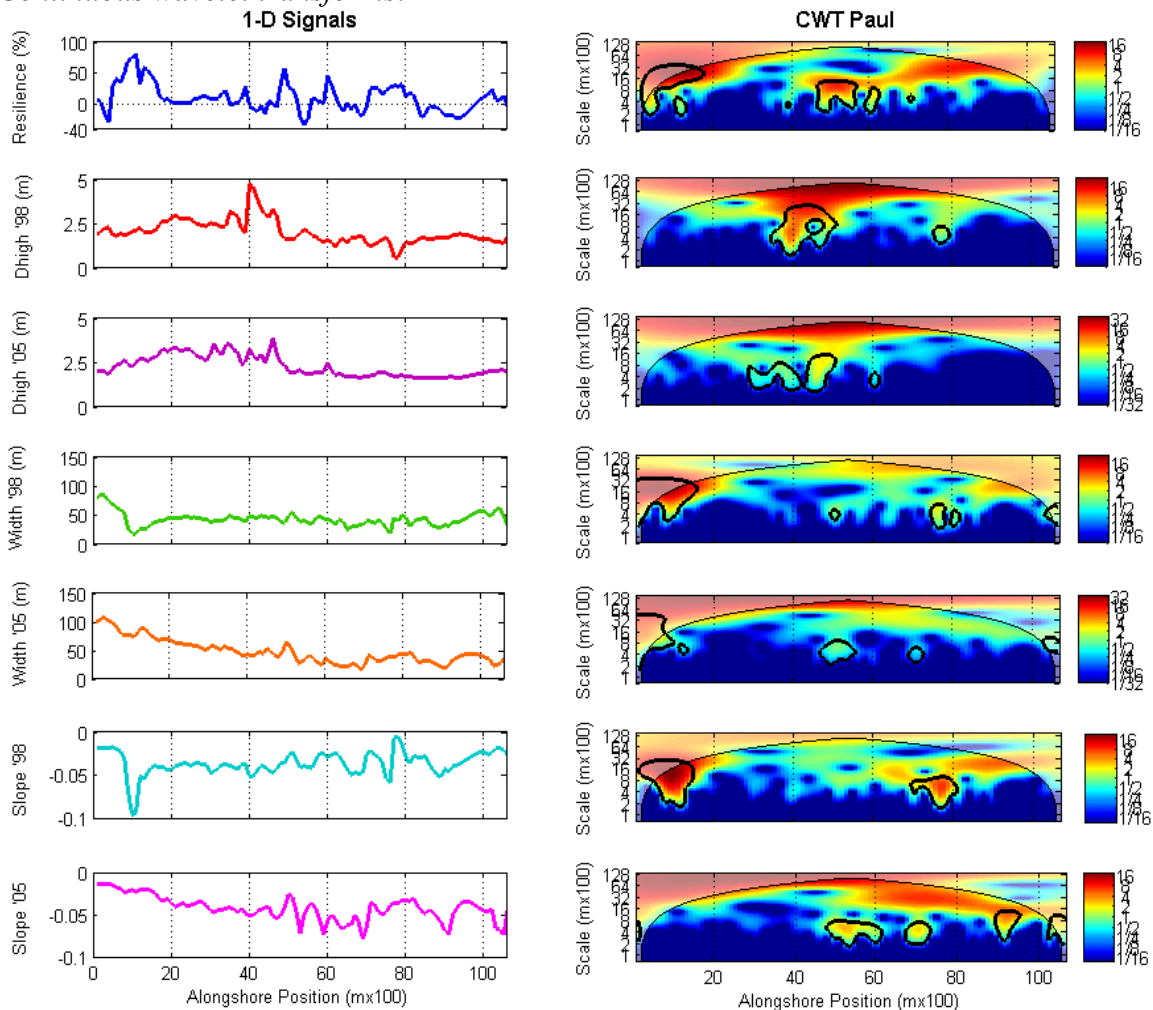
Definitions of morphologic variables extracted from lidar data and used in analyses.

Additional 1-D Signals:

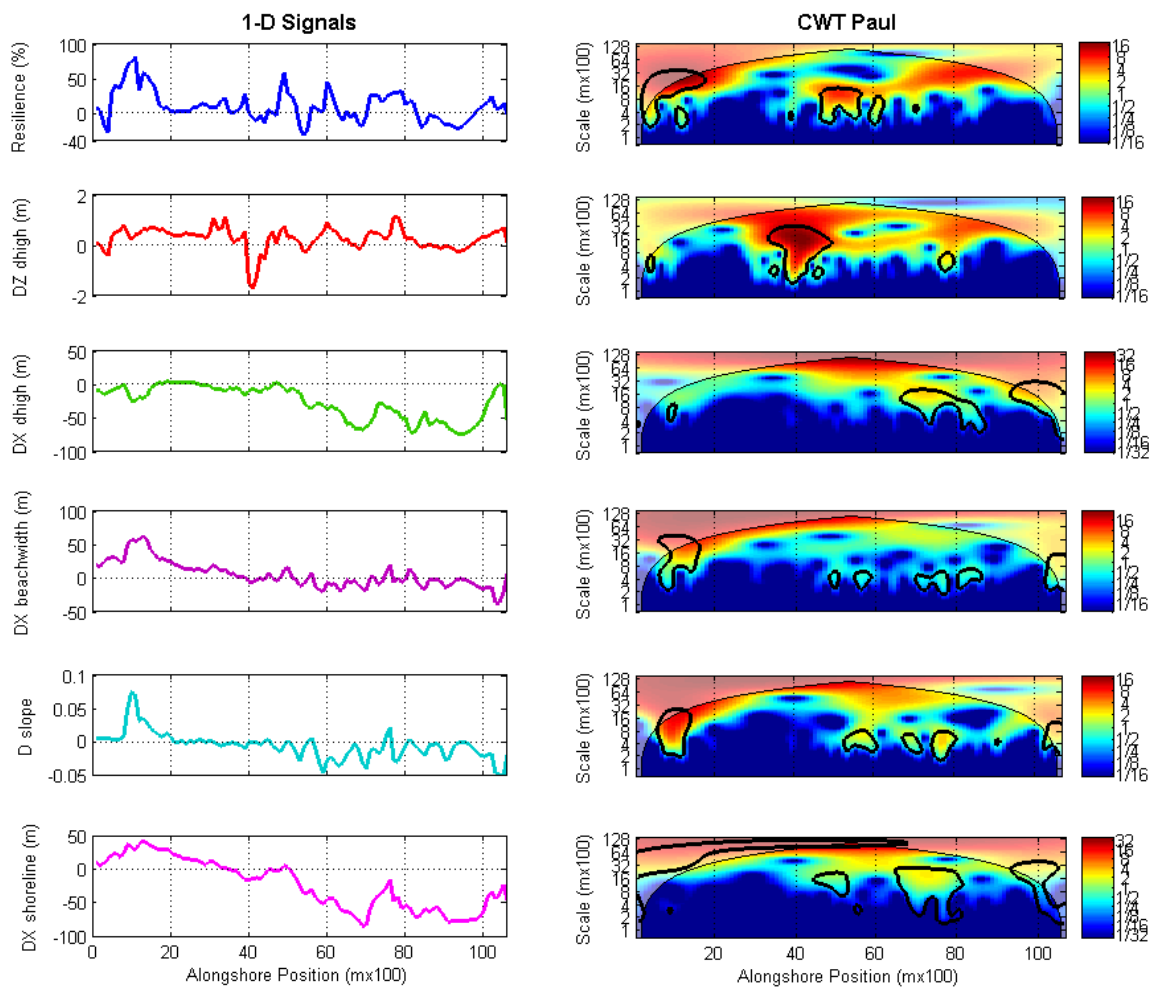


Surf Similarity Index (ζ) values calculated for Smith Island in 1998 (red) and 2005 (blue). Beaches are classified as dissipative when $\zeta < 0.23$ and as intermediate when $0.23 < \zeta < 1$, values greater than 1 are considered reflective.

Continuous wavelet transforms:

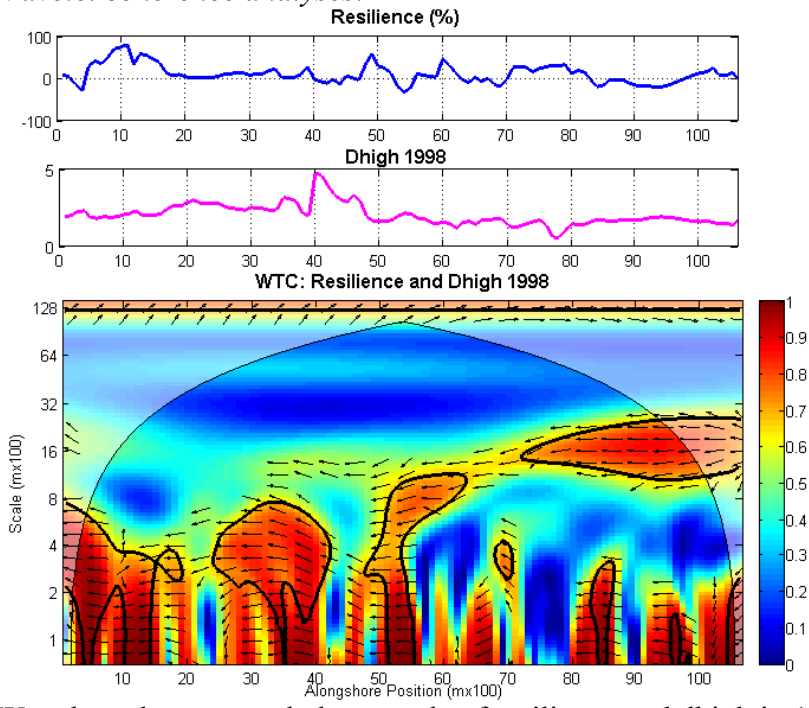


Left panels of 1-D morphologic signals in 1998 and 2005 along Smith Island. Right panels are corresponding CWT analyses using a Paul waveform. Scale bar depicts wavelet power where high power (in red) signifies the most variability along local space and scales.

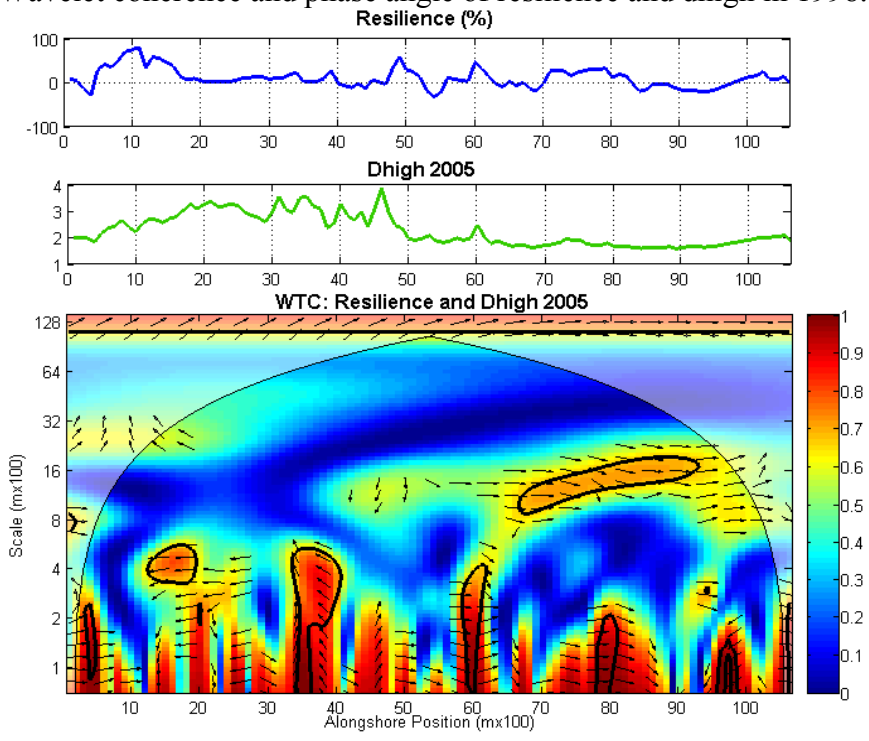


Left panel includes 1-D signals of morphologic *change* between 1998 and 2005 while right panels are corresponding CWT analyses of signals.

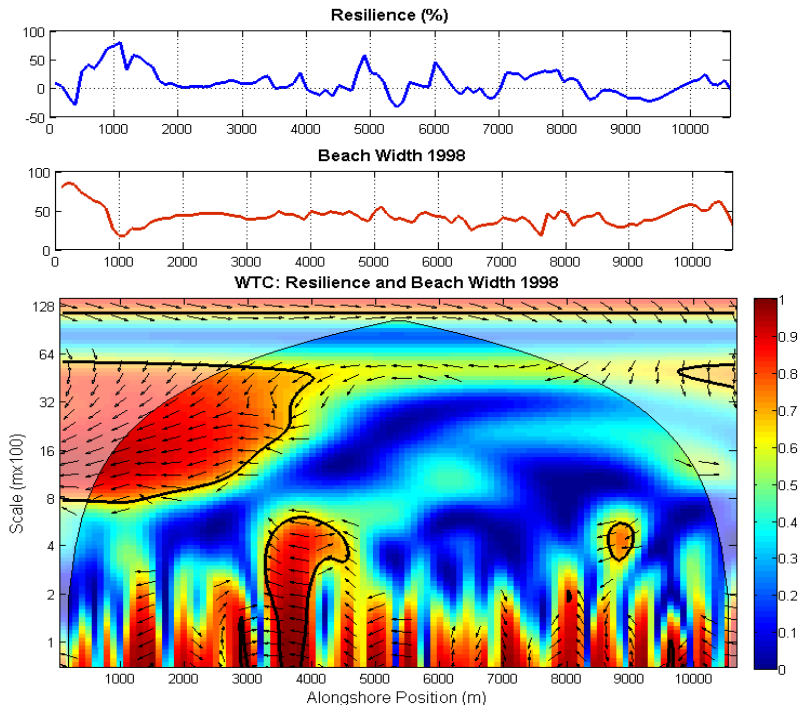
Wavelet coherence analyses:



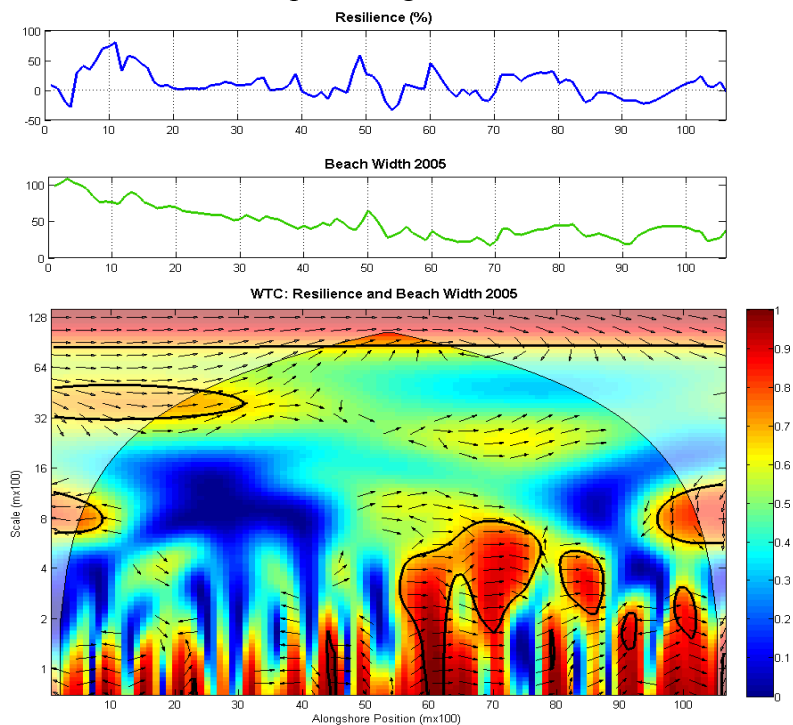
Wavelet coherence and phase angle of resilience and dhigh in 1998.



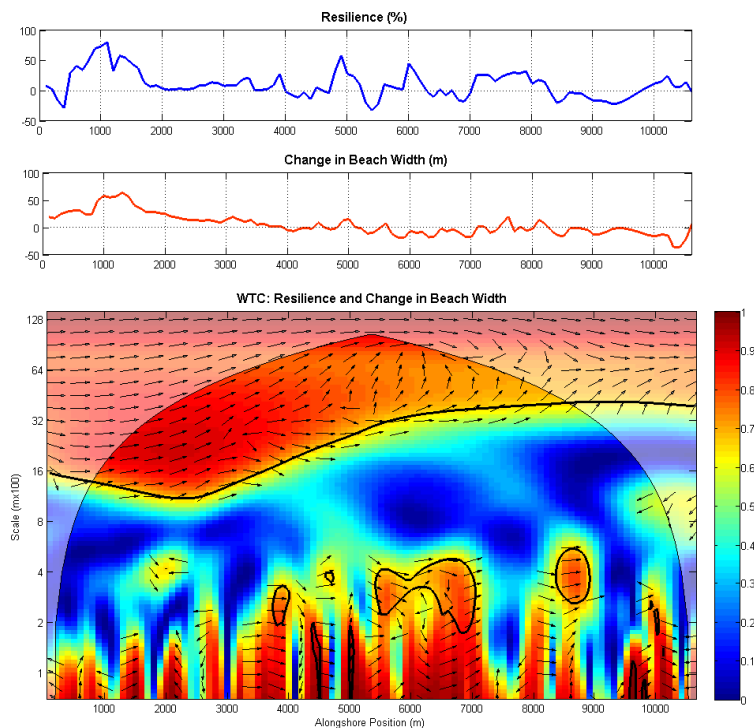
Wavelet coherence and phase angle of resilience and dhigh in 2005. Thick black contours represent 95% confidence interval and transparent regions are within the COI. Arrows pointing right are in-phase while arrows pointing left are anti-phase. Arrows pointing up are 90° out of phase where the top panel is south of the middle panel.



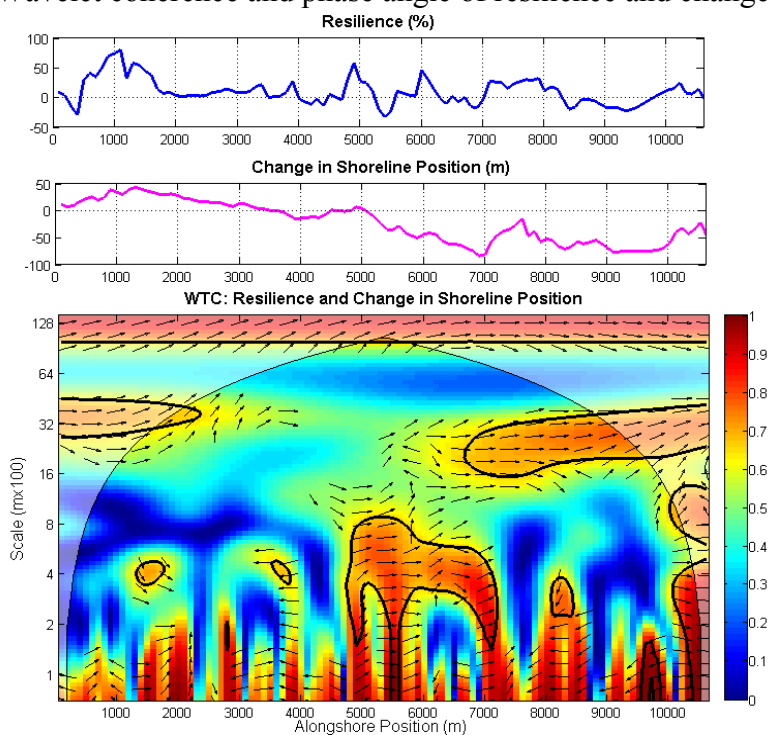
Wavelet coherence and phase angle of resilience and beach width in 1998.



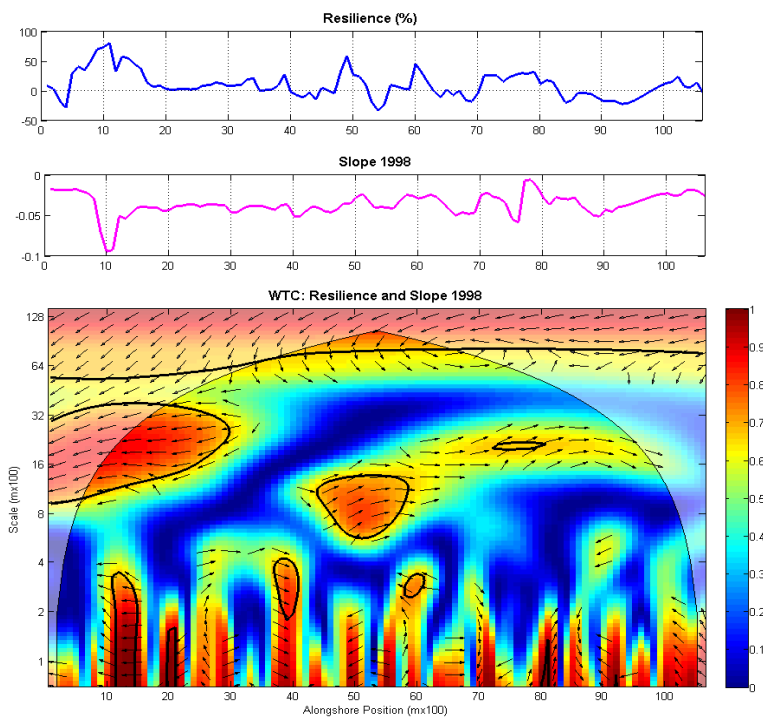
Wavelet coherence and phase angle of resilience and beach width in 2005. Thick black contours represent 95% confidence interval and transparent regions are within the COI. Arrows pointing right are in-phase while arrows pointing left are anti-phase. Arrows pointing up are 90° out of phase where the top panel is south of the middle panel.



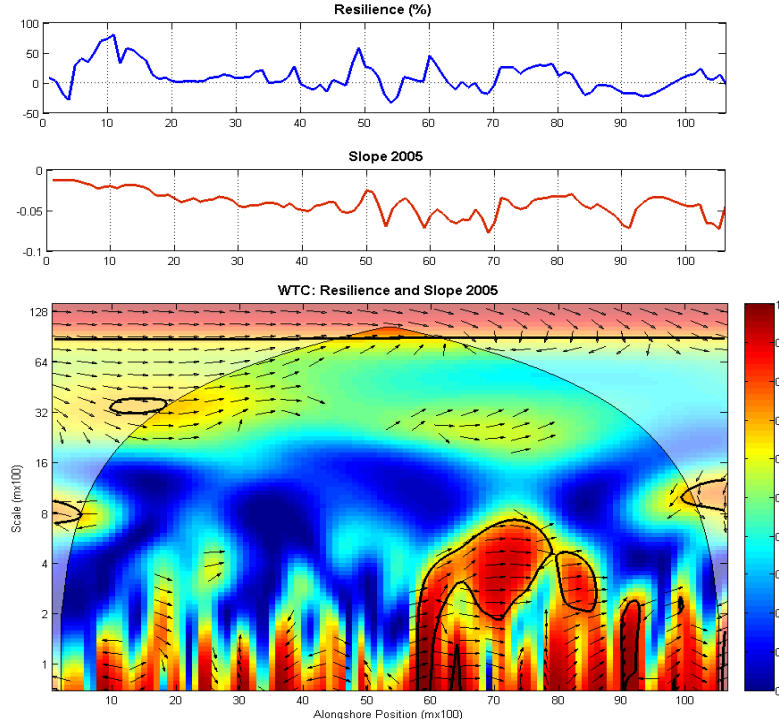
Wavelet coherence and phase angle of resilience and change in beach width.



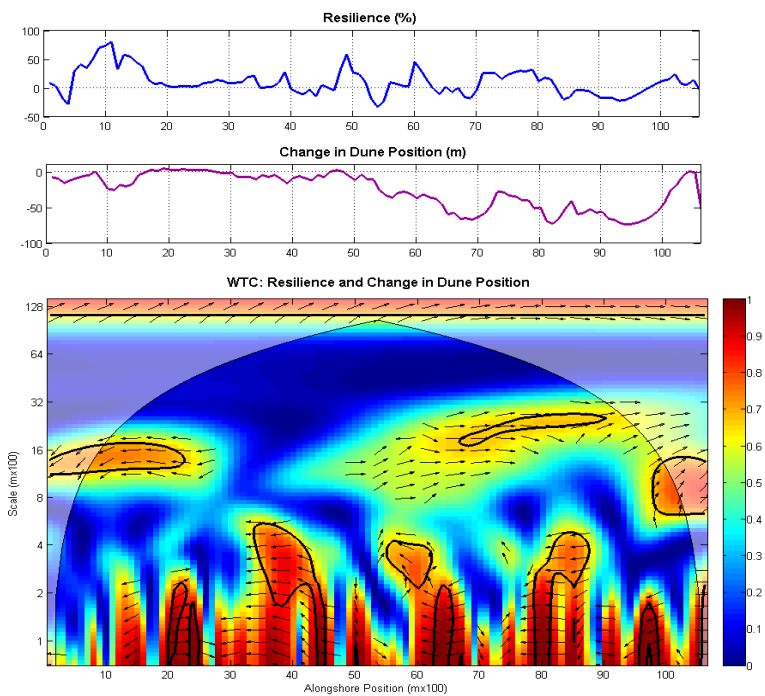
Wavelet coherence and phase angle of resilience and change in shoreline position. Thick black contours represent 95% confidence interval and transparent regions are within the COI. Arrows pointing right are in-phase while arrows pointing left are anti-phase. Arrows pointing up are 90° out of phase where the top panel is south of the middle panel.



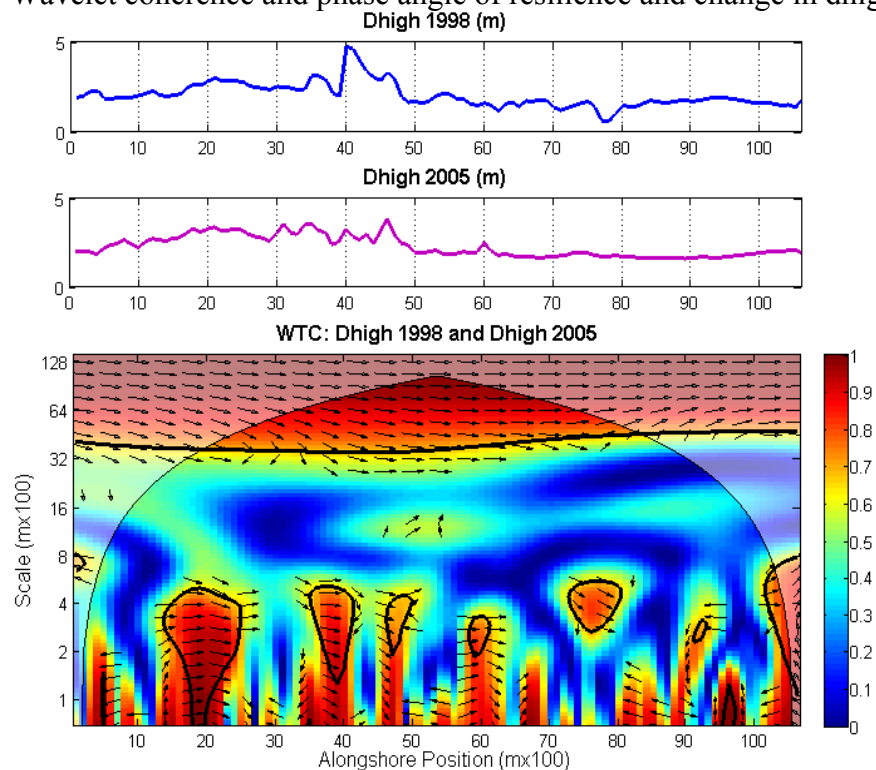
Wavelet coherence and phase angle of resilience and slope in 1998.



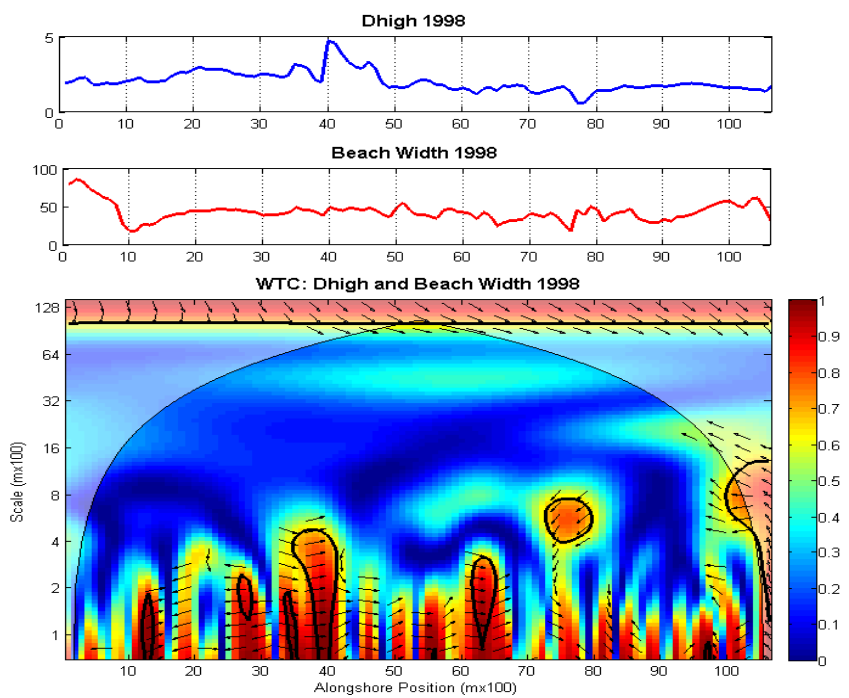
Wavelet coherence and phase angle of resilience and slope in 2005. Thick black contours represent 95% confidence interval and transparent regions are within the COI. Arrows pointing right are in-phase while arrows pointing left are anti-phase. Arrows pointing up are 90° out of phase where the top panel is south of the middle panel.



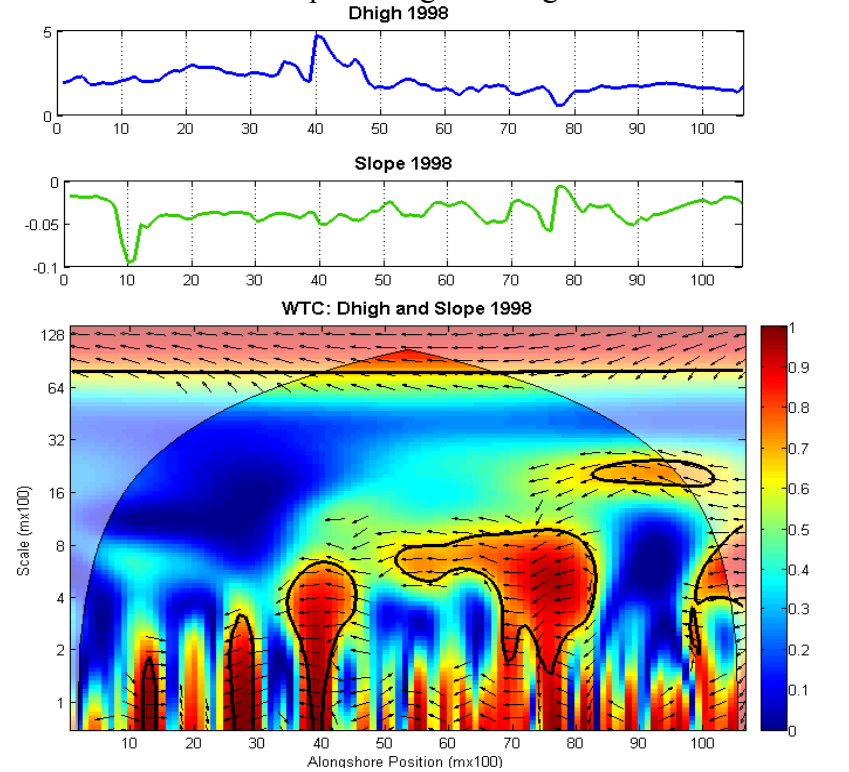
Wavelet coherence and phase angle of resilience and change in dhigh position.



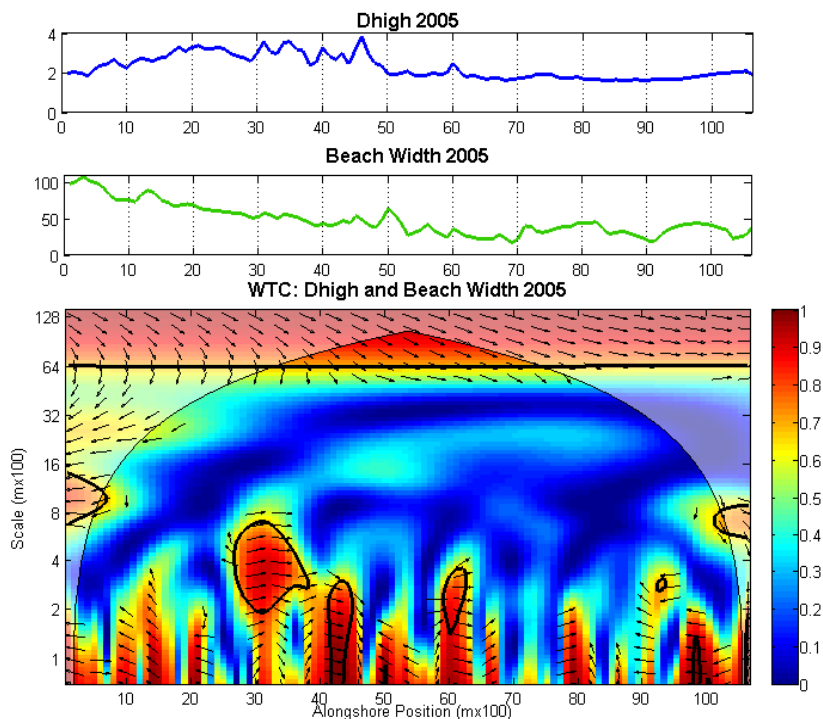
Wavelet coherence and phase angle of dhigh in 1998 and dhigh in 2005. Thick black contours represent 95% confidence interval and transparent regions are within the COI. Arrows pointing right are in-phase while arrows pointing left are anti-phase. Arrows pointing up are 90° out of phase where the top panel is south of the middle panel.



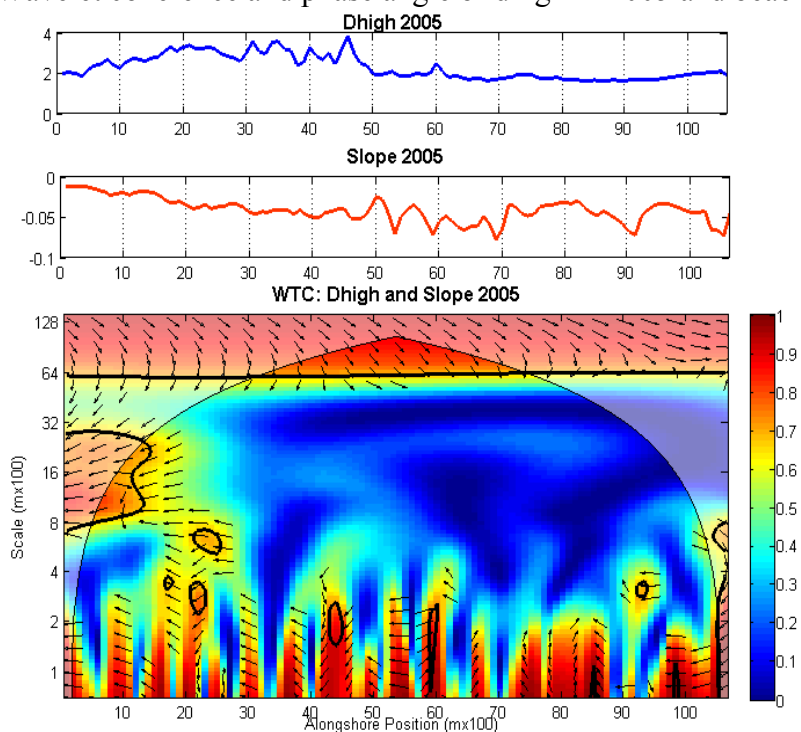
Wavelet coherence and phase angle of dhigh in 1998 and beach width in 1998.



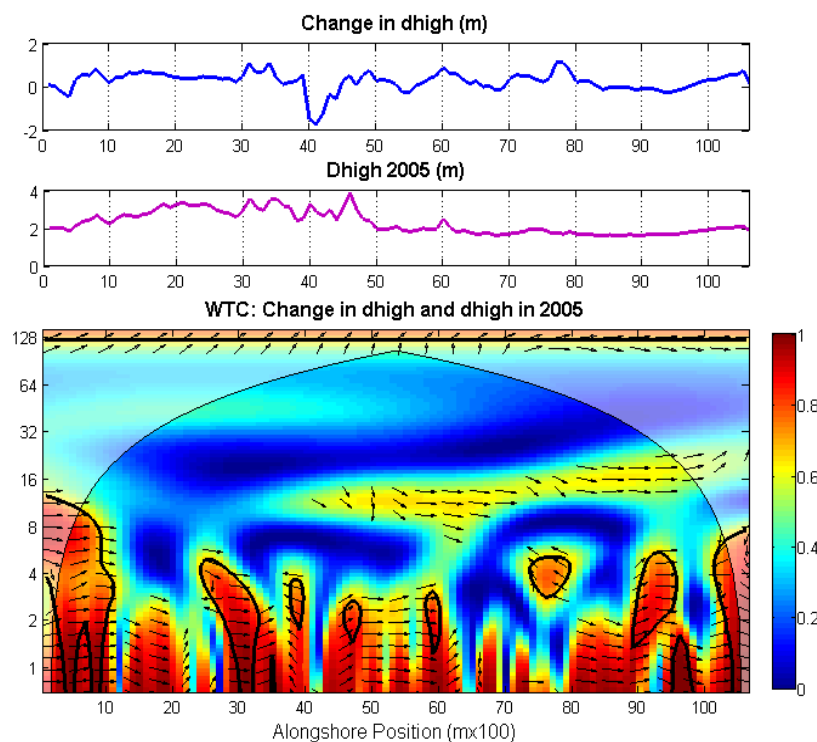
Wavelet coherence and phase angle of dhigh in 1998 and slope in 1998. Thick black contours represent 95% confidence interval and transparent regions are within the COI. Arrows pointing right are in-phase while arrows pointing left are anti-phase. Arrows pointing up are 90° out of phase where the top panel is south of the middle panel.



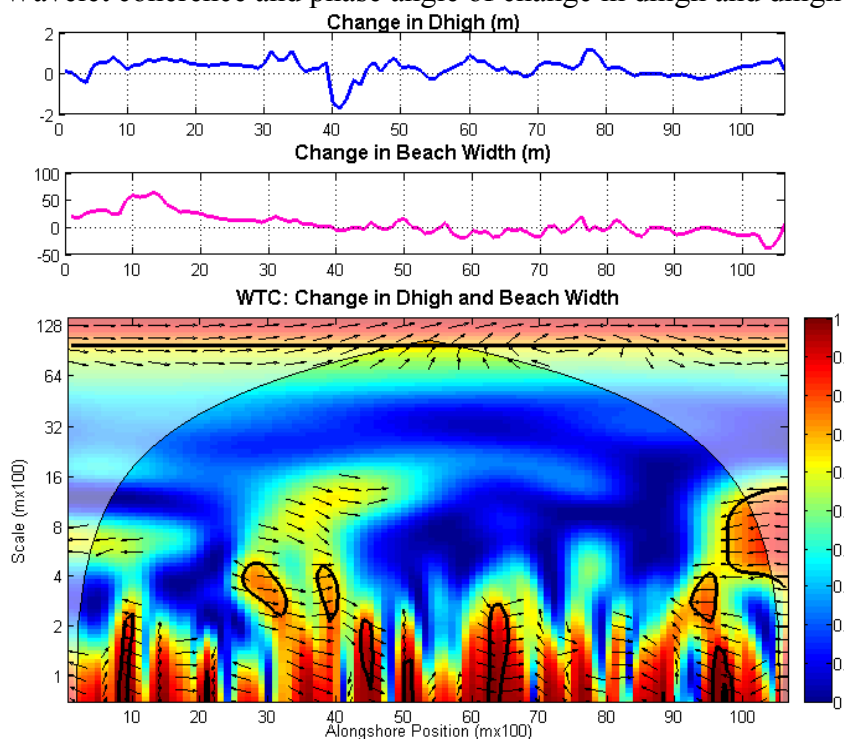
Wavelet coherence and phase angle of dhigh in 2005 and beach width in 2005.



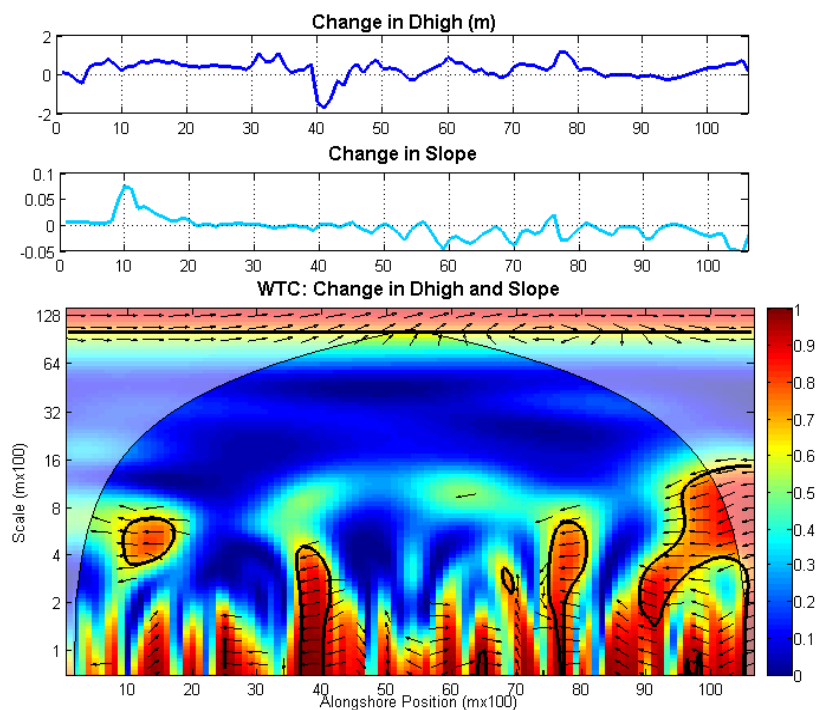
Wavelet coherence and phase angle of dhigh in 2005 and slope in 2005. Thick black contours represent 95% confidence interval and transparent regions are within the COI. Arrows pointing right are in-phase while arrows pointing left are anti-phase. Arrows pointing up are 90° out of phase where the top panel is south of the middle panel.



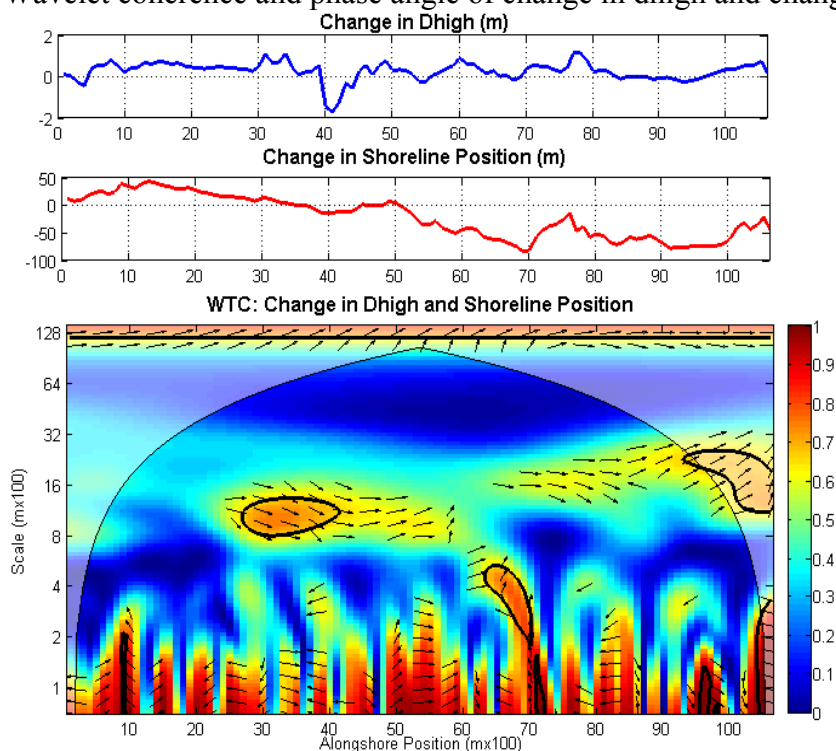
Wavelet coherence and phase angle of change in dhigh and dhigh in 2005.



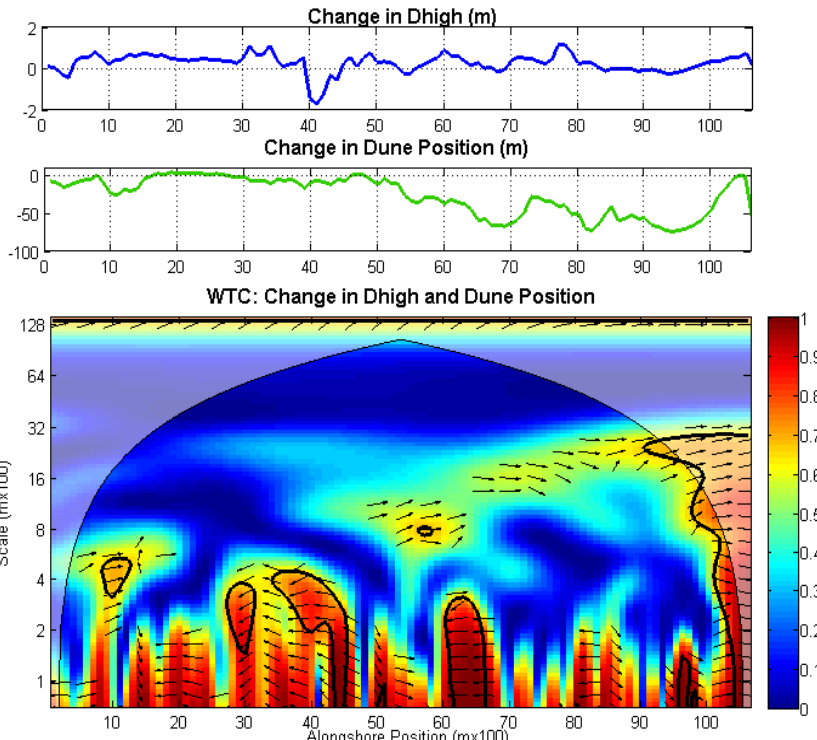
Wavelet coherence and phase angle of change in dhigh and change in beach width. Thick black contours represent 95% confidence interval and transparent regions are within the COI. Arrows pointing right are in-phase while arrows pointing left are anti-phase. Arrows pointing up are 90° out of phase where the top panel is south of the middle panel.



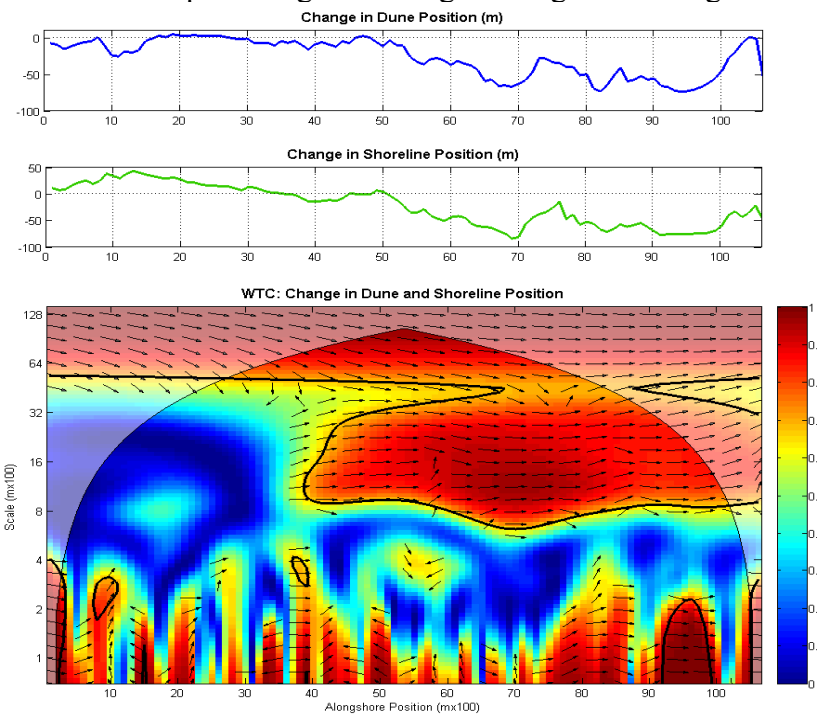
Wavelet coherence and phase angle of change in dhigh and change in slope.



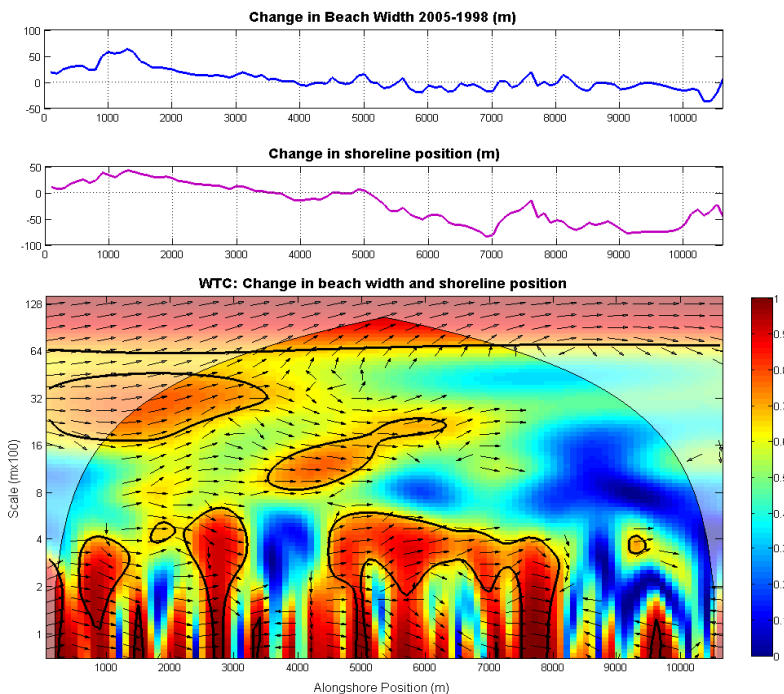
Coherence and phase angle of change in dhigh and change in shoreline position. Thick black contours represent 95% confidence interval and transparent regions are within the COI. Arrows pointing right are in-phase while arrows pointing left are anti-phase. Arrows pointing up are 90° out of phase where the top panel is south of the middle panel.



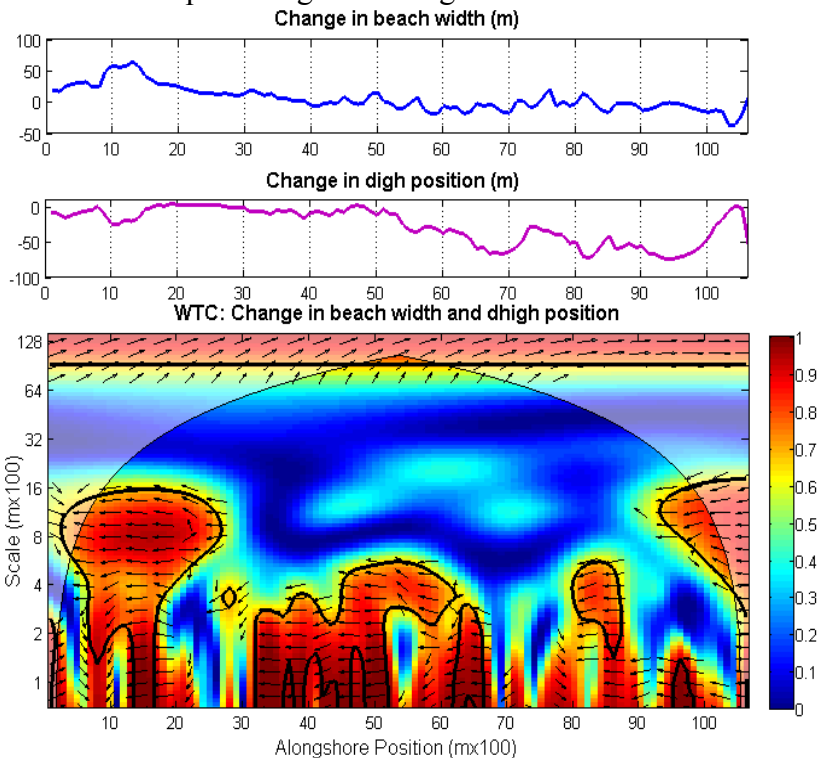
Coherence and phase angle of change in dhigh and change in dhigh position.



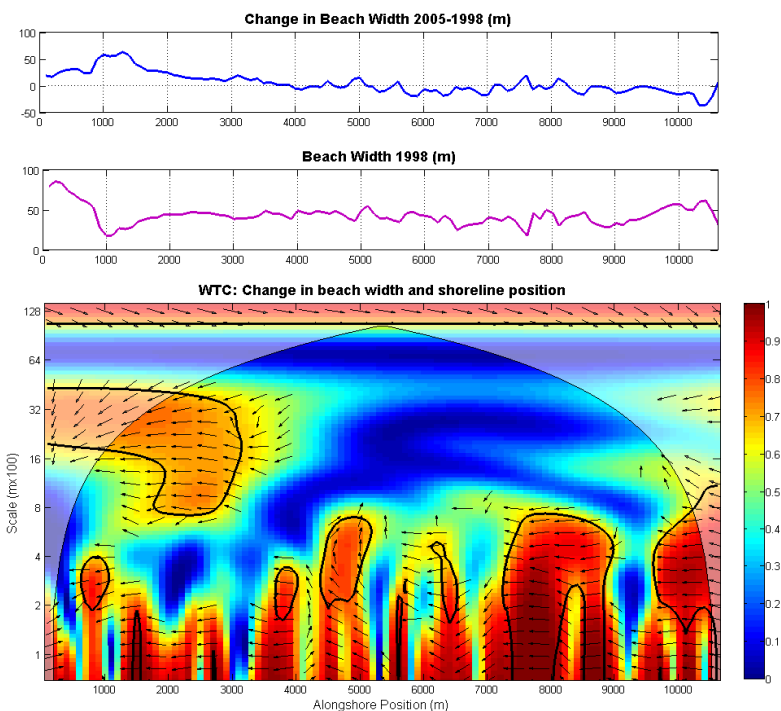
Coherence and phase angle of change in dhigh position and shoreline position. Thick black contours represent 95% confidence interval and transparent regions are within the COI. Arrows pointing right are in-phase while arrows pointing left are anti-phase. Arrows pointing up are 90° out of phase where the top panel is south of the middle panel.



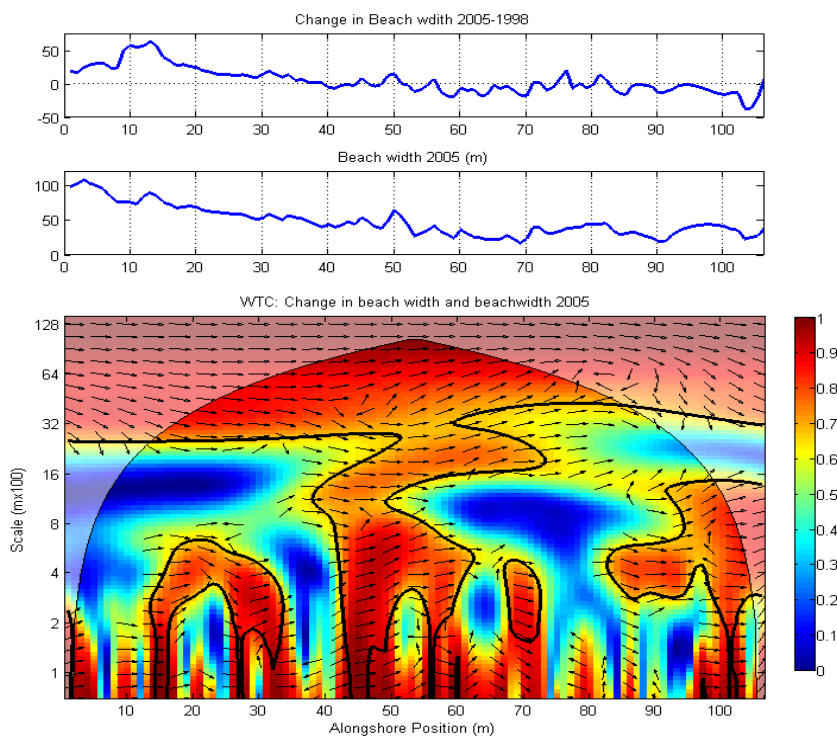
Coherence and phase angle of change in beach width and shoreline position.



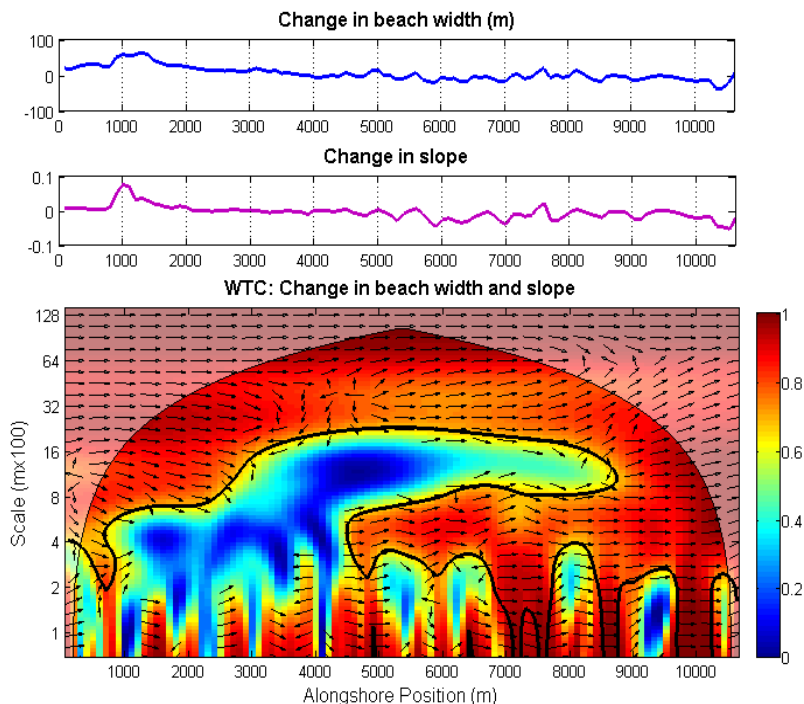
Coherence and phase angle of change in beach width and dhigh position. Thick black contours represent 95% confidence interval and transparent regions are within the COI. Arrows pointing right are in-phase while arrows pointing left are anti-phase. Arrows pointing up are 90° out of phase where the top panel is south of the middle panel.



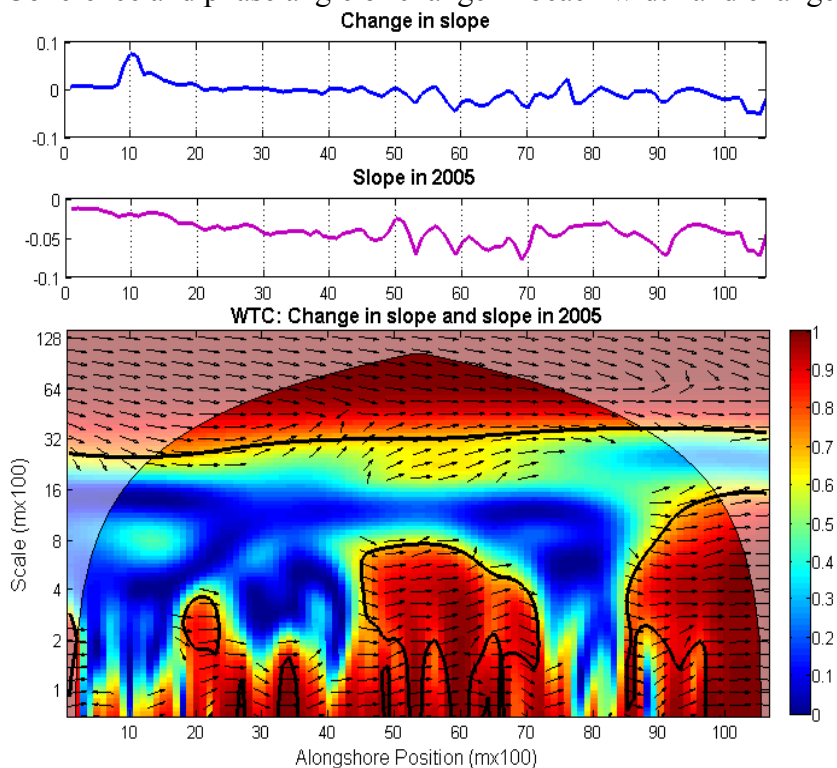
Coherence and phase angle of change in beach width and beach width in 1998.



Coherence and phase angle of change in beach width and beach width in 2005. Thick black contours represent 95% confidence interval and transparent regions are within the COI. Arrows pointing right are in-phase while arrows pointing left are anti-phase. Arrows pointing up are 90° out of phase where the top panel is south of the middle panel.



Coherence and phase angle of change in beach width and change in slope.



Coherence and phase angle of change in slope and slope in 2005. Thick black contours represent 95% confidence interval and transparent regions are within the COI. Arrows pointing right are in-phase while arrows pointing left are anti-phase. Arrows pointing up are 90° out of phase where the top panel is south of the middle panel.